NASA CR-54082
TRW ER-5805

134 p.

FINAL REPORT

SUMMARY REPORT ON ELECTRON BOMBARDMENT ION ENGINE DEVELOPMENT

Prepared for
NATIONAL AERONAUTICS AND SPACE ADMINISTRATION

by

A. C. ECKERT
A. F. BOND
R. J. COERDT
M. W. MUELLER
NEW PRODUCT RESEARCH

FEBRUARY 1964

CONTRACT NAS3-2522

Project Manager
NASA, Lewis Research Center
Spacecraft Technology Division
James A. Wolters

TRW ELECTROMECHANICAL DIVISION
THOMPSON RAMO WOOLDRIDGE INC.
CLEVELAND, OHIO

NASA CR-54082
TRW ER-5805

FINAL REPORT

SUMMARY REPORT ON ELECTRON BOMBARDMENT ION ENGINE DEVELOPMENT

Prepared for
National Aeronautics and Space Administration

by

A. C. Eckert
A. F. Bond
R. J. Coerdt
M. W. Mueller

New Product Research

February 1964

Contract NAS3-2522

Project Manager
NASA, Lewis Research Center
Spacecraft Technology Division
James A. Wolters

TRW ELECTROMECHANICAL DIVISION

ABSTRACT

Experimental and analytical efforts to develop an electron bombardment ion engine having a slit aperture geometry and utilizing permanent magnets are described. Data on engine performance using mercury as a propellant are presented. The performances of several accel-decel extraction system geometries are presented and the dependence of the source performance on the source geometry is discussed. A cathode development program is described and evidence for the occurrence of cathode sputtering is indicated. The results of extended testing of the developed ion engine system are presented. Extraction system lifetime is predicted.

TABLE OF CONTENTS

LIST OF SYMBOLS

A = effective accel channel cross section.

A_c = cross sectional area of mercury vaporizer capillary.

A_m = ammeter.

A_n = anode.

A_R = Richardson's constant.

B = the constant in the equation: $P = P_o\, e^{-B(1/t - 1/T_o)}$ where P is the vapor pressure at temperature T and P_o is the vapor pressure at temperature T_o.

C = cathode.

D = diameter of a circle having the same area as the emitting region of the source.

E_A = average electron energy occurring in a plasma.

e = electronic charge (1.6×10^{-19} coulombs).

F = filament.

I_{Ac} = accel current, ampere.

I_{Dc} = decel current, ampere.

I_S = source current, ampere.

I_{Sc} = screen current, ampere.

I_T = equivalent mercury feed rate, ampere.

I_t = target current, ampere.

j = current density, amperes per unit area.

j_s = emission limited current density from a cathode.

K = Boltzmann's constant.

K_o = correction factor occurring in Child's law.

L = the effective length of the potential well which trap charge exchange ions generated within the well.

M = mass of mercury atom.

M = gram atomic weight.

M_{Hg} = gram atomic weight of mercury.

M_{Ta} = gram atomic weight of tantalum.

N = neutralizer.

N_o = Avagadro's number.

n_o = number rate at which mercury is fed into the vaporizer, atoms/sec.

N_+ = plasma ion density, number of ions per unit volume.

P = perveance.

R = linear erosion rate due to sputtering.

R_A = aspect ratio.

R_{Ta} = linear erosion rate of tantalum.

S = sputtering rate expressed in atoms per ion.

S_{Ta} = sputtering rate of tantalum.

s = position of liquid vapor interface in mercury vaporizer.

T = temperature.

$T(s)$ = temperature at the liquid vapor interface in the mercury vaporizer.

T' = temperature gradient along the length of the capillary of the mercury vaporizer.

t = lifetime of extraction system.

V_{Ac} = accel potential, volt.

V_{Dc} = decel potential, volt.

V_m = voltmeter

V_S = source ionization inefficiency electron volt/ion.

v_n = the most probable thermal speed of a molecule of a gas.

v = potential difference or "voltage".

x = position coordinate in beam direction.

x_o = ion acceleration distance.

List of Symbols (Cont.)

y = ion beam width.

y_o = initial ion beam width.

η_m = propellant utilization.

σ = charge exchange cross section.

τ = characteristic time of the mercury vaporiser system.

ρ = mass density.

ρ_{Hg} = mass density of mercury.

ρ_{Ta} = mass density of tantalum.

ϕ = work function.

LIST OF FIGURES

List of Figures (Cont.)

List of Figures (Cont.)

LIST OF TABLES

1.0 INTRODUCTION AND SUMMARY

The research and development program reported herein has been a logical extension to experimental and theoretical efforts which had been underway at TRW for a duration of nearly four years. To understand fully the logic and necessity for the reported work, it is appropriate briefly to review and summarize the prior efforts.

TRW's activity in the area of electron-bombardment ion engines dates back to the time when virtually the entire activity in the ion engine field was being directed to cesium contact-ionization research. At the time, despite their promise of high propellant efficiencies, these cesium engines were handicapped by operation at low power efficiency. The bombardment engine concept proposed by TRW constituted an approach to the problem which promised increased power efficiency without sacrifice of engine lifetime because of sputtering damage to acceleration electrodes. This approach was postulated on the basis that gas discharge (bombardment) ion sources could be operated over a wide range of ion current density at good power and propellant efficiencies.

In its elementary form, the TRW engine concept consists of a bombardment engine based on a slit aperture geometry. This geometry was chosen because it allowed usable thrust levels to be obtained from a reasonable number of single aperture sources, while simultaneously allowing almost complete freedom in the configuration of the ion accelerating system so as to insure minimum sputtering damage by proper choice of propellant, and by optimizing the geometry in the acceleration region.

The slit aperture geometry, furthermore, favored a single exit aperture per ionization chamber rather than some multiple aperture arrangement. This in turn led to increased design latitude, particularly in acceleration electrode shaping, without sacrificing ion collection efficiency. The result has been a source of high average ion current density per unit of total area subtended by the engine.

The ion source was designed around an axial field electron trap which confines electrons axially by electrostatic forces and laterally by magnetic forces. Electrons from a cathode are injected into the trap and accelerated axially as they approach the anode region. Being constrained from reaching the anodes by a magnetic field, they proceed through the anode region and reflect from the meniscus between the plasma and the ion beam. After reflecting from this surface, the electrons return through the anode channel, and most return again after reflecting from the inner pole sheath, etc. These multiple reflections and traversals of the ionization chamber extend the electron path to sufficient length to give a high probability for an ionizing collision with a gas atom.

The axial field type of trap was chosen because the same electric field which reflects the electrons at the meniscus is effective in sweeping the ions formed in the downstream half of the anode channel out of the exit port into the accelerating region. The same action takes place at the upstream end of the channel, of course, so that ions formed there are swept into the inner pole pieces or into the cathode. The trapping field was asymmetrized somewhat by shaping the inner pole surfaces to favor the downstream focusing.

Before a practical development of this source concept could be undertaken, it was first necessary to establish whether a cathode could be made to operate under the conditions required by the source. The problem was to determine whether a cathode could provide a spatially uniform discharge along the slit. The situation was complicated by the further requirement that the cathode operate space-charge limited. This requirement stemmed from practical considerations such as aging and the possibility of temperature or surface nonuniformities that could prevent the employment of an emission-limited cathode.

Since existing knowledge at the time the source concept was developed was insufficient to answer the cathode question, it was necessary to resort to experiment. This was done by constructing an annular ion source of the design described above, and observing its operation with several types of cathodes. Both pure metal filaments and oxide-coated cathodes were employed and found quite satisfactory when operated space charge limited. This work established the feasibility of the source design and showed good promise for the attainment of high power efficiencies. On the strength of this, NASA provided support for continued development of the source in the form of Contract NAS8-42 (Reference 1).

The first task under the above contract was to investigate electron trapping techniques so that an efficient ionization chamber could be designed. To facilitate experimentation, a one-inch long linear aperture source of flexible design was constructed and used instead of the fairly cumbersome annular slit source described above.

This source featured an electromagnet to provide the requisite magnetic fields which could, of course, be varied in strength. This turned out to be very convenient experimentally, particularly in the early stages of testing. A permanent magnet arrangement was the ultimate goal and was employed later in the program. For purposes of expediency, the initial source work was done using argon as the propellant. As the work progressed and source performance was improved, the

source was modified for operation with mercury, the propellant ultimately selected for use with the source. This choice was based upon a variety of factors, including mercury's ease of handling, storage, metering, and vaporizing, a high mass per particle, and its ability to provide ionizing discharges of high efficiency while maintaining arc voltages compatible with sufficient cathode lifetimes.

The experimental verification of good source performance constituted a large portion of the effort under Contract NAS8-42. The linear slit source mentioned above was employed in extensive experimental studies of electron trapping techniques, and their effect upon ion production (arc power efficiency and propellant utilization). To facilitate this source optimization process, argon propellant and tungsten wire cathodes were used. A variety of internal source geometries were studied; variables included magnetic field strength and shape, anode width and length, cathode slit length and width, source aperture width, etc. The details of this optimization are described in Reference 1, the summary report submitted to NASA under Contract NAS8-42. Briefly stated, this effort resulted in 84 per cent (argon) propellant utilization at an arc input of 450 electron volts per ion.

The next step was the conversion to source operation with mercury. The necessary system changes were made, including the design, fabrication, and installation of porous-plug vaporizer and mercury feed system. Initial testing with mercury showed the necessity for several changes in the details of the source, particularly in the mode of propellant feed to the ionization chamber. The necessary modifications were completed and quite satisfactory source performance was realized using tungsten-filament cathodes. Such cathodes were very convenient to use in experimentation, but had short lives and required too much power for space applications.

The emphasis then was shifted to the development of more suitable cathodes. This effort was centered about the development of a sintered nickel matrix cathode containing commercial barium-strontium oxide emitting compounds. Although this portion of the contractual effort was somewhat limited in scope, matrix cathodes suitable for use in both the linear and (larger) annular source resulted. Much of the initial testing with these cathodes was done in the annular engine, and need not be reviewed since it has been found that an array of linear sources has many advantages over one or more annular sources, particularly from the standpoint of thrust per unit frontal area.

The first tests using one-inch long sources and nickel-matrix cathodes were quite promising but showed a need for more information concerning the behavior of the

electrons emitted. In particular, it was desired to know the electron energy distribution of the electrons coming from the cathode since it was felt that a large fraction of the emitted electrons from the oxide cathodes lost much of their initial energy through inelastic collisions prior to entering the anode region. Experimentation to determine the electron energy distrubution was initiated, and the results obtained were employed to slightly modify the source geometry so as to minimize the electron energy losses. The results were arc power efficiencies of about 450 eV/ion at or near ninety per cent propellant utilization.

At this point the mercury performance of the linear aperture source had been fairly well established and a new linear source, two inches long, was constructed using permanent magnets rather than coils. The idea was to reproduce with permanent magnets the same form and strength of field which had yielded the best results when electromagnets were used. Preliminary testing of this source was conducted near the close of work under NAS8-42, and some outstanding performance was recorded (greater than ninety per cent propellant utilization at a discharge input of only 360 eV/ion), indicating exceptional promise for this type of source.

After the cessation of work under the above contract, a review of the accomplishments, current status, and future potential was made. It was decided that further efforts were desirable and support for such work was afforded under NASA Contract NAS3-2522.

The basic areas of investigation under this contract were to be: (1) engine (source) design, fabrication, and test, including additional cathode development; (2) ion extraction system studies, both experimental and analytical; (3) neutralization studies (experimental); (4) ion engine life tests; and (5) porous diffuser studies (for mercury propellant phase separation). The following sections of this report will discuss in some detail the work performed in each of these area. A brief survey of the progress made in these general areas, however, may be made here.

Source studies were conducted primarily with two engines, each of nominal 5 cm aperture length. A variety of source configurations were studied, including internal geometries and spacings, and magnetic field variations (both strength and shading). Additional cathode development work led to the fabrication and test of improved performance cathodes. Near the end of the program, however, a regression of the cathode performance level was experienced and no direct cause was determined. The requirement of more severe emission characteristics demanded by the design changes experienced near the end of the program may have been the cause of the apparent loss of cathode performance; the presence of an unknown poisoning agent also may have contributed.

Extraction studies were carried out with a variety of accel-decel geometries. Initially these geometries were fitted to sources whose magnetic fields were provided by electromagnets, thus affording experimental latitude in that magnetic field strength could be varied and/or balanced.

The mutual interactions between ion source and extraction system were studied and the effects of various accel-decel geometries and voltages, cathode location, etc. were established. Later extraction studies with a permanent magnet ion source yielded substantially the same low electrode current drains and good beam focusing without a sacrifice in source power or propellant efficiency.

The experimental extraction efforts were supplemented by an analytical (digital computer) effort. The result of this work was the prediction of charge-exchange rates, resulting electrode impingement areas, and a predicted erosion pattern for an extraction geometry similar to that which evolved as a result of the experimentation.

Neutralization efforts succeeded in producing current neutralization, although neutralizer currents typically exceeded the total beam current. Efforts to improve the neutralizer-to-beam coupling were deliberately limited in favor of additional effort in other areas of the program.

The low electrode interceptions obtained as a result of the extraction system studies led to the initiation of life testing of the permanent magnet engine system utilizing a laboratory propellant feed system. Two such life tests were performed. The first, of seventy hours duration, was deliberately terminated when the engine performance had become influenced by aluminum sputtered back from the beam target. The second test proceeded to completion and was terminated after about 10^4 hours of operation. These extended tests showed very little evidence of wear in the critical (focusing) regions of the extraction system and, as will be seen in a subsequent section, have provided experimental evidence in support of the theoretical prediction of long system lifetimes.

Porous diffuser (mercury wetting) tests were conducted over 500 hours; no wetting of a porous graphite diffuser was observed during this time. Such a unit ultimately could be incorporated into a mercury feed system to function as the phase separator.

In the following sections, the progress in each of the above areas will be reported in considerably more detail. The brief survey presented above is intended to serve as a background and to indicate the general areas of effort under the program.

2.0 TECHNICAL DESCRIPTION OF PROGRAM

2.1 Ion Engine Design and Testing

2.1.1 Introduction

The work described in this section initially was concerned with the development of an ion extraction system making use of an ion source which was not of optimum design but which was suitable as a source of ions. It soon became evident, however, that extraction system development could not proceed independently of the source development. Furthermore, it was intended initially that the computer program would lead the way by prescribing suitable geometries for testing. It was soon evident, however, that the experimental program was far more fruitful than the computer program; many geometries resulting from simple theoretical considerations could be tested and evaluated before even one geometry could be inserted into the computer program. It thus turned out that a suitable extraction system geometry was established experimentally, and this geometry subsequently was used in the computer program to determine the charge exchange rate, charge-exchange ion trajectories, and the accel electrode erosion profile.

Early in the program it became evident that the source performance influenced the extraction system performance to a large degree. For example, when using electromagnets, it was determined that the accel electrode interception depends on the value of the magnetic field. This may possibly be explained by conjecturing that the value of the magnetic field affects the properties of the meniscus such that the meniscus becomes less concave at higher magnetic fields. Hence, increased direct interception should occur for higher values of magnetic fields. Minimum interception appears, therefore, to occur for lower values of magnetic fields. However, low magnetic field results in arc characteristics consisting of high values of arc current and low values of arc voltage, a condition which results in inefficient source operation. Thus, it was determined early in the program that the extraction system performance was strongly dependent on the source performance and that the two systems cannot be developed independently. It was at this point of the program that the source and extraction system studies were merged.

Throughout the early portion of this program there existed considerable uncertainty in much of the data due to the uncertainty associated with the feed system employed. The feed system, described in Reference 1, was originally designed to deliver mercury at a rate approximately ten times the rate used in the early portion of this program. The effect of operating at one-tenth of the design flow rate is to multiply the

associated uncertainties by a factor of ten. Hence, the combined error produced by room temperature fluctuation and system time constant could result in relative errors as large as 100 per cent. Not until this problem was recognized and remedial steps were taken to decrease the system time constant and to reduce the effects of room temperature fluctuations was it possible to report data of high reliability. However, the effects of room temperature fluctuation on the feed system had not been completely eliminated at the end of the program; for unusually severe room temperature changes, feed rate variations as much as twenty per cent still were observed. It should be noted, however, that the data considered as reliable was taken during periods in which the temperature fluctuations were minimal.

2.1.2 Program Chronology

The extraction system development program was initiated by attempting to demonstrate the possibility of attaining a flat-to-concave meniscus at the source extraction aperture. The initial testing made use of a one-inch engine which is referred to as the magnetic focusing model; this engine employed a tungsten wire cathode rather than a nickel matrix type. (It had been previously demonstrated that the electron energy distribution in the plasma is the same for each kind of cathode.) The extraction geometry utilized is shown in Figure 1; a simple accel electrode made of carbon was used. Note the asymmetry of the acceleration electrodes due to sag of the supports during preheating of the electrodes. Acceleration electrode preheating was found to be necessary to sufficiently outgas the carbon electrodes such that high voltage operation could be achieved without flashovers. The preheating was accomplished by applying a moderate voltage to the acceleration electrode ($\sim$10 kv) and increasing the beam current until the impingement was obtained inside the accelerating electrode channel. The impingement region was kept at least 0.5 cm downstream of the channel entrance to avoid sputtering back of electrode material on the source. Heating by ion bombardment was continued until the carbon accel electrodes showed a dull red color. After sufficient outgassing the acceleration potential was raised to 16.5 kv at which voltage a flat meniscus and a focused beam were observed.

After successfully demonstrating that the attainment of a flat meniscus was possible, it was decided to modify the facility to enable the operation of an accel-decel system rather than the simple accel used earlier; in addition, neutralization cathodes were installed. Therefore, additional high voltage feed-throughs were installed as well as sufficient additional low voltage feed-throughs for adequate control and metering. A complete ion engine system containing accel and decel

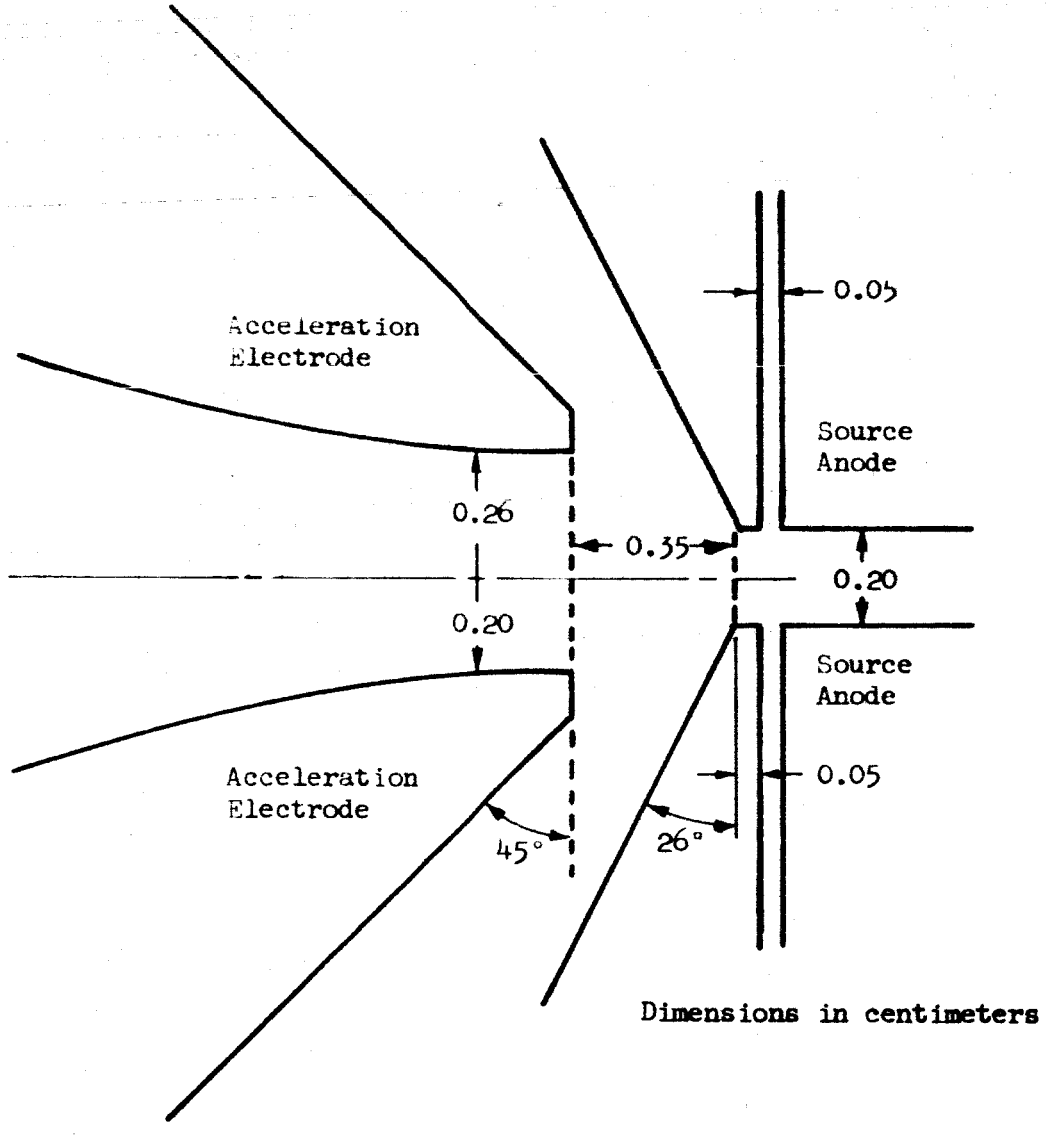

Figure 1

Extraction Electrode Geometry Utilized During Initial Testing of Extraction Systems

electrodes as well as neutralization cathodes was then fabricated and installed. It was expected that this initial accel-decel extraction system would not be optimum; however, the purpose of these initial tests was first to construct an operating system which would provide experience in operating such systems and second to uncover any unexpected problem areas.

A suitable extraction system should have the following characteristics: First, it should be able to extract and focus the desired ion current density such that the direct impingement of the primary ion beam on the acceleration electrode can be made vanishingly small. Second, the geometry of the system should be such that its lifetime as determined by the sputtering rate due to charge exchange is large. Third, the ions should be delivered to the exit of the extraction system with the desired specific impulse and in the form of a parallel beam. The initial accel-decel system was designed to be consistent with the above requirements and is shown in Figure 2. To a first approximation the extraction geometry (the geometry between the accel electrode and the source) was essentially the well-known Pierce geometry for the space-charge flow of a parallel beam from a slit source. The surface angle of the source, however, was 26° instead of the required 22.5° for the ideal Pierce geometry. This angle was increased in an attempt to provide additional focusing because of the possibility of slightly rounded edges on the source meniscus. A typical meniscus shape as observed during operation is shown in Figure 2. Between the acceleration electrodes is a drift region in which the ions drift at essentially constant velocity and the beam expands due to the natural repulsion of the ions. The contour of the inside surfaces of the accel electrode was chosen to follow the profile of the beam. The length of the drift region was chosen to be as long as possible and yet enable the focusing of the accel-decel slit to produce a parallel beam.

The choice of the extraction geometry parameters was guided to a first approximation by three equations (MKS units):

$$v = 4.06 \times 10^5 \, (j/K_o)^{2/3} \, x_o^{4/3} \qquad (1)$$

$$j = N_+ \, e \, (E_A/M)^{1/2} \qquad (2)$$

$$y/y_o = 1 + 2.99 \times 10^6 \, jx^2/v^{3/2} \qquad (3)$$

where v is the minimum potential for extracting the mercury ion current density, j, x_o is the acceleration distance, K_o is a correction factor which is equal to

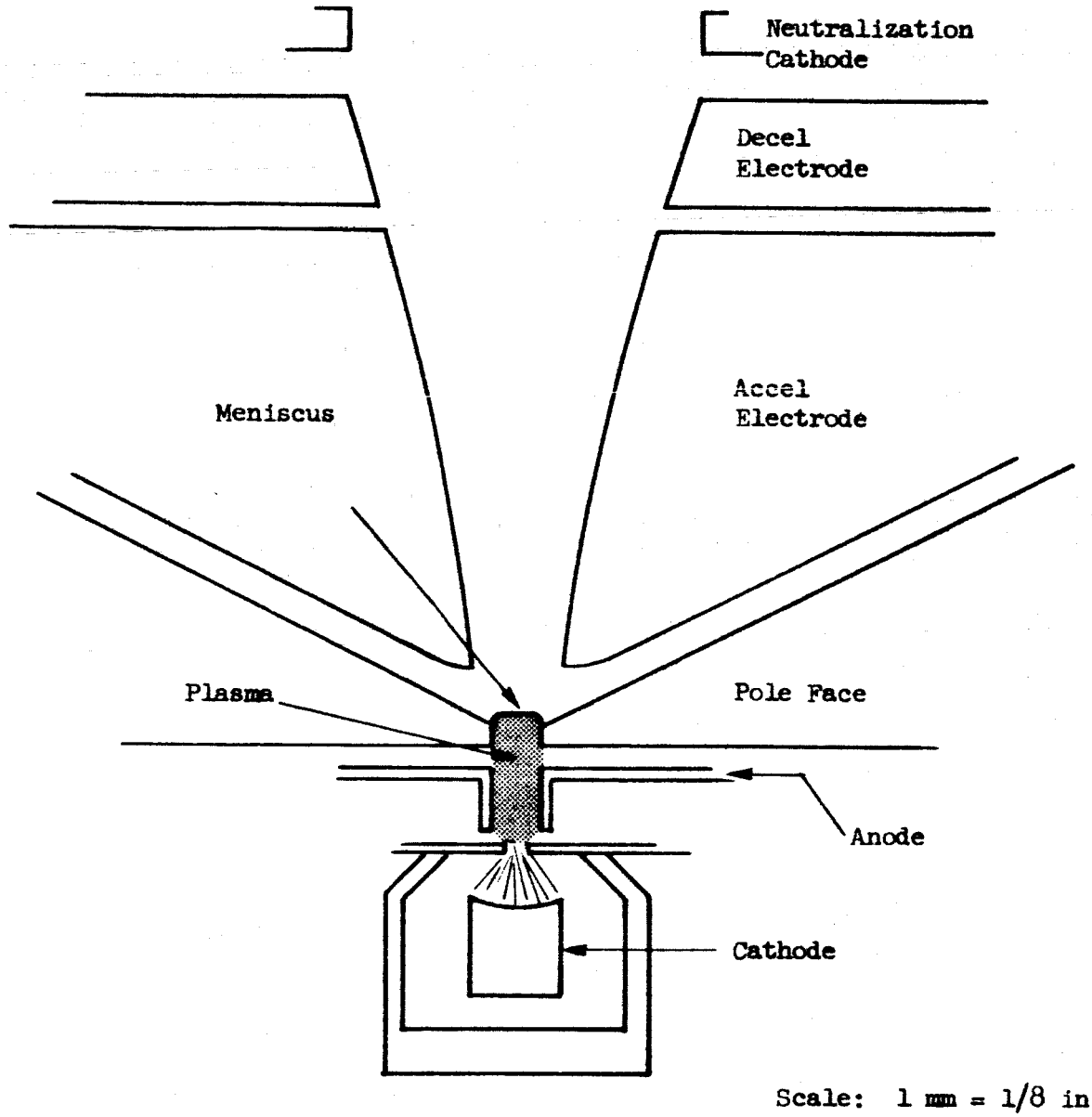

Figure 2

Engine Geometry Used for Initial Extraction System Tests

1 for the idealized Pierce geometry but is less than 1 for other geometries, N_+ is the ion density of the plasma just inside the meniscus, e is the electronic charge, E_A is the average electron energy in the plasma, M is the mass of the mercury atom, y is the width of the ion beam which is initially t_o, and x is the position at which the beam width is y. Equation (1) is Child's law modified by the factor K_o. Since $K_o \leq 1$, it is implied that the extraction efficiency for a specific realistic geometry is less than for the idealized Pierce geometry. Equation (2) is a statement of the maximum ion current density which can be extracted from the plasma through the meniscus. This maximum current density depends on the plasma ion density and the average electron energy inside the plasma. Equation (3) is a statement of the beam blow-up in the drift region between the acceleration electrodes. If it is assumed that the maximum current density as given by Equation (2) is to be extracted, then Equation (1) implies that for low values of extraction potential, the acceleration distance should be small. However, according to Equation (3), a small acceleration potential difference results in a rapid beam blow-up which in turn requires that the length of the acceleration electrode be small if the deceleration electrode is to be able to refocus the beam. For a short acceleration electrode, however, the sputtering rate per unit area due to charge exchange may be excessive. Guided by the above relationships, an extraction electrode 2 cm long and an accel electrode to source distance of 2.2 mm were chosen.

For the first test of the extraction system of Figure 2 the mercury flow rate was set for a current density of 64 ma/cm^2 or 32 ma total beam current for the one-inch source; however, it was found that the source operated poorly at this flow rate yielding a propellant utilization of only 30 per cent. Later tests showed that upon dropping the input mercury flow rate, an increase in propellant utilization was obtained, and for a mercury flow rate of 14.5 ma (29 ma/cm^2) a propellant utilization on the order of 100 per cent was obtained at an arc condition of 710 eV/ion. The necessity of operating at the low current density level of 29 ma/cm^2 was due to the improper positioning of the source cathode in the cathode chamber. The dependence of source operation on cathode position will be discussed later. Table 1 lists the data obtained for this extraction system and Figure 3 shows the circuit schematic for the system.

Note that as the extraction potential was increased above 14 kv the source current increased above 14.5 ma, the value of the mercury input flow rate. It is believed that the observed propellant utilization values in excess of 100 per cent were due to the existence of an uncertainty (which was unknown at the time) in the value of the input mercury feed rate.

A_n - Anode
Ac - Accel Electrode
C - Cathode
Dc - Decel Electrode
F - Filament
N - Neutralizer
S - Source
Sc - Screen
T - Target
V_m - Voltmeter
A_m - Ammeter

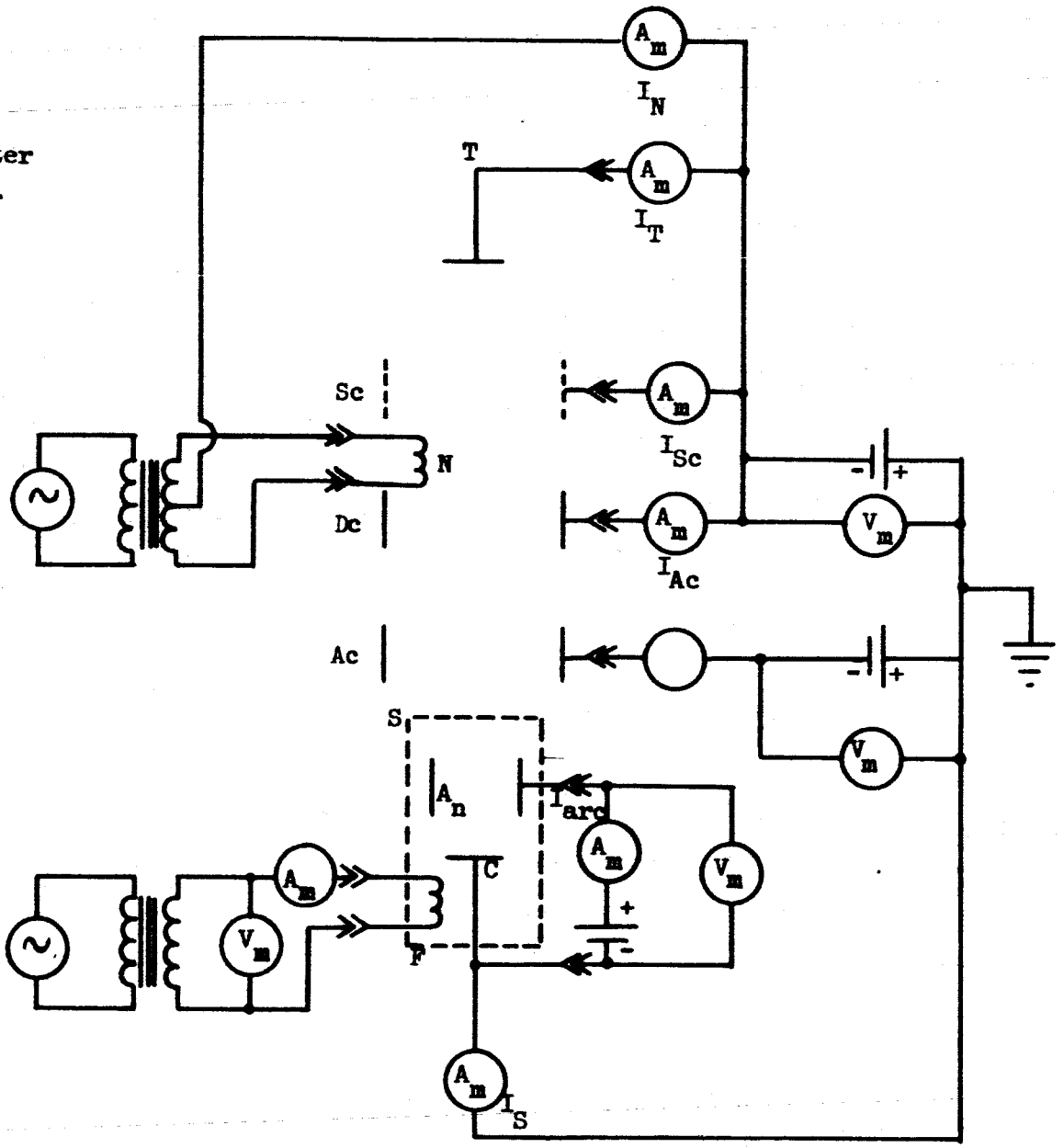

Figure 3

Circuit Schematic for Extraction System Testing

Table 1

Data for Ion Engine Extraction Test No. 4

Accel Current (ma)	4	6	3	2
Target Current (ma)	8.5	12	13	13
Source Current (ma)	14	16	16	17
Neutralizer Current (ma)	1	1	1	1
Arc Current (amp)	0.45	0.60	0.63	0.70
Arc Voltage (volts)	23	21	22	28
Accel Voltage (kv)	14	18	19	19
Decel Voltage (kv)	3	3.3	3.3	3.3
Cathode Temperature (°F)	1550	1580	1680	1680
Filament Current (amp)	8.6	8.6	8.6	8.6
Filament Voltage (volts)	2	2	2	2
Equivalent Mercury Flow (ma)	14.5	14.5	14.5	14.5
Propellant Utilization (%)	96	110	110	117
Ionization Inefficiency (eV/ion)	710	880	950	1350

Limited tests of the neutralization cathodes also were conducted at this time. The neutralization cathodes, which were the simple tungsten wire type, were turned on and they emitted up to 10 ma of current to the beam; a reduction of the target current by the same amount resulted. Thus, current neutralization appeared to be possible at that time.

A further area of investigation was that of meniscus shape. A qualitative description of the observed dependence of meniscus shape on extraction potential is shown in Figure 4. For low accel potentials (< 1 kv) the plasma extends well into the accel electrode region, and all of the beam current impinges directly on the electrode. As the potential is increased (~1 kv) the plasma draws back towards the source, the center region of the plasma changing from pointed to blunt. A still further potential increase (> 10 kv) moves the meniscus back to the source slit, and the meniscus becomes flat although the edges may remain somewhat rounded. At 10 kv the meniscus is flat and a parallel beam is obtained in the acceleration region; in addition, at 10 kv the beam blow-up in the drift region is such that the beam impinges upon the accel electrode. As the accel potential difference is increased, the position of impingement moves deeper into the drift region and for about 14 kv it moves off the back end of the accel electrodes.

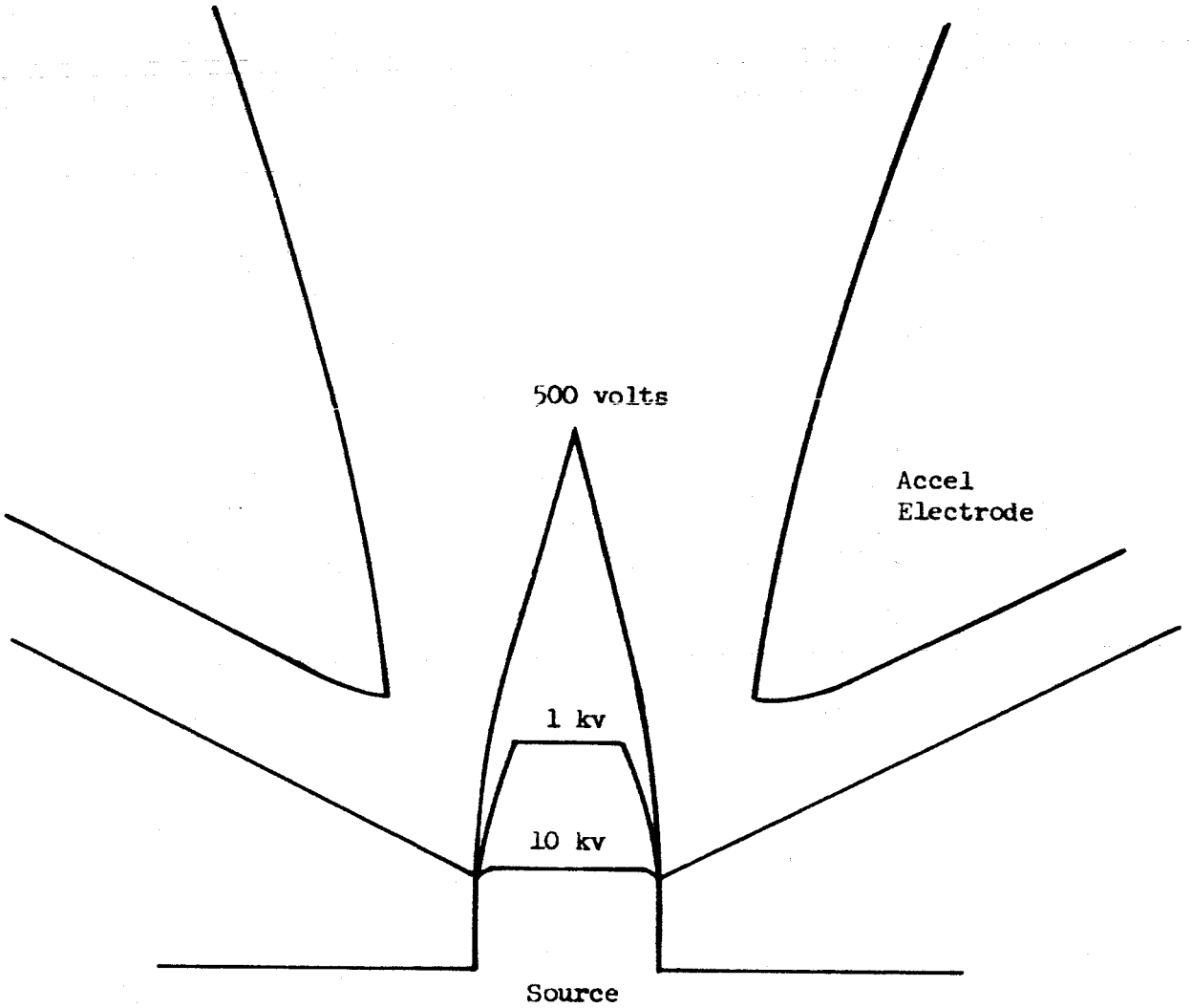

Figure 4

Sketch of the Meniscus Shape for Several Values of Extraction Potential

Equation (3) explicitly shows that the beam blow-up should decrease with increasing potential difference for a constant current density, in agreement with the qualitative description given above.

In this initial investigation of extraction systems qualitative agreement with the simple theory specified by Equations (1) to (3) appeared to exist. Current neutralization appeared to be simply accomplished; however, no information about space-charge neutralization was obtained. Extraction and focusing of an ion beam of density 30 ma/cm^2 had been accomplished; however, some questions about the nature of the current registered by the accel electrode ammeter existed. Was the accel current direct impingement of the beam from the rounded edges of the meniscus, was it scattering of the incident ions by residual gasses in the system (the accel electrode current reduced with reduction of background pressure), or was it current leakage across the insulators or across the gap between the extraction electrode and the source due to a high mercury atom density in this region? A detailed investigation of these possibilities was one of the goals of the following work.

During the course of the extraction studies and during the concurrent source studies it was noted that the operation of the source, especially the current density for optimum source performance, appeared to depend on the position of the cathode in the cathode chamber. Previously the cathode chambers were of minimum size so that the cathode and the cathode shielding filled the cathode region. Hence the position of the cathode did not vary appreciably. However, during later testing the cathode chamber dimensions had been increased to improve accessibility and the bulk of the cathode shielding had decreased because of more efficient radiation shielding. As a result the position of the cathode in the chamber could vary from one test to another even though a reasonable effort was spent in initial cathode location; thus the performance of the source varied from test to test. In order to determine the correlation between cathode position and source pressure (input mercury flow rate), it was necessary to expose the cathode to air between each test in order to change the cathode position. Unfortunately the cathode properties sometimes change when exposed to air and hence no clear-cut correlation was obtained. A cathode assembly which could be moved during source operation was then fabricated, thus enabling the adjustment of the cathode position for optimum source operation at the desired source current density. Subsequent experiments indicated that the cathode-to-cathode slit separation should be held to a minimum.

Because of the outgassing problems associated with the utilization of carbon electrodes it was decided, at this point, to employ metallic electrodes to experimentally

investigate extraction geometries. Since it was readily available and because of its high melting temperature, sheet tantalum was originally used for forming the electrodes. However, it was quickly learned that sheet tantalum 0.040 in. thick tended to sag when heated in this application and thus the extraction system dimensions could not be maintained during testing. Molybdenum 0.040 in. thick was found to be relatively sag free and thus was used. The 0.040 in. thickness provided sufficient rigidity while retaining ease of fabrication. Another problem associated with metallic electrodes immediately became evident; the increased sputtering and increased plating onto the surface of insulating stand-offs resulted in electrical shorting after relatively short periods of operation. The insulator shorting was eliminated, however, by making use of metallic shielding in the form of concentric cylinders, one cylinder attached to each end of the stand-off insulator. With this shielding, engine operation up to 21 kv was possible for sufficient periods.

Several variations of the extraction system geometry were investigated at this point in the program. Common to all geometries tested was a source to acceleration electrode spacing of 2 mm and a separation between the two acceleration electrodes of 3 mm. The variations which were investigated were the length of the acceleration electrode and the angle of the source frontal surface. The acceleration electrode length variation led to a comparison between a measured and theoretical determination of beam perveance; the source angle investigation indicated that for 26° an interception of approximately 20 per cent occurred while for 45° the interception was ten per cent or lower.

The purpose of the extraction system testing during this period was two-fold. The early testing concentrated on determining the aspect ratio and perveance associated with the extraction electrode system. Later testing was directed towards evaluating the system with respect to erosion rate, per cent direct interception by the accel electrode, and overall engine efficiency.

Two important parameters used in describing ion optical systems are the aspect ratio and the perveance. The aspect ratio, R, is defined by the equation

$$R^2 = \left(\frac{D}{x_o}\right)^2$$

where D is the diameter of a circle having the same area as the emitting region of the source, and x_o is the acceleration distance. The perveance, P, is defined by the relation

$$P = I_s / V_{ac}^{3/2}$$

where I_s is the source current and V_{ac} is the acceleration potential difference. The perveance is a scale invariant property of an optical system depending only on the system geometry and ratio of charge to mass of the ion.

During early testing of the extraction systems utilizing molybdenum electrodes, it was observed that the position of the direct beam impingement was readily observable because of the green fluorescence present at the point of impingement. For a constant extraction current the position of impingement depends upon the extraction potential and moves away from the source as the potential increases. It became evident that an investigation of the beam properties may be effected by observing the minimum potential difference required to pass the beam through the accel electrode region. Referring to Figures 5 and 6, it is readily seen that the parabolic beam edge is defined by the accel electrode geometry for the case where the beam edge just grazes the exit end of the accel electrode region. For these tests the currents to the target, screen, and decel electrode were added together and read by one meter since for these tests there was no interest in the division of the current to these regions. The data was taken by observing the position of the accel electrode on which the beam impinged due to the self blow-up of the beam in this region. As the extraction voltage was increased the impingement position was made to move away from the source and finally off of the back end of the electrode. The voltage which took the beam off of the back end of the electrode was recorded and is presented in Table 2. Note that for the same current density the shorter electrode requires lower voltage. In each case the potential difference as a function of beam current was obtained for the condition of beam grazing at the exit end of the accel electrode. For the geometry of Figure 5, the calculated perveance increased almost linearly with beam current while for the geometry of Figure 6 the perveance was found to be essentially constant, as would be normally expected. For comparison, the perveance for each geometry was calculated using the relation for the beam blow-up

$$Y/Y_o = 1 + 3.81 \times 10^6 \frac{P}{R^2} \left(\frac{x}{x_o}\right)^2$$

where for this geometry

$$R^2 = 15.9$$

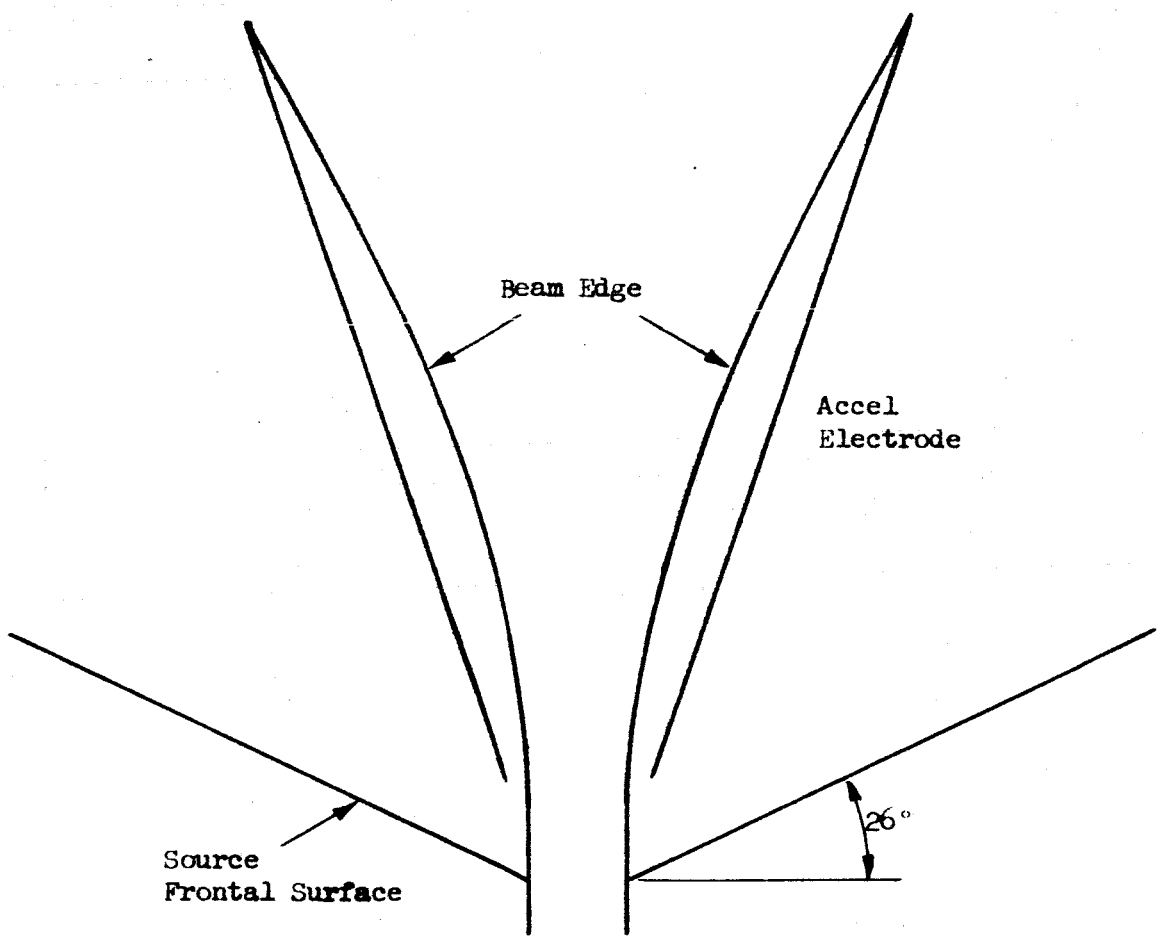

Figure 5

Extraction System Geometry Used to Investigate Beam Profiles. The Perveance Determined by the Indicated Beam Edge is 4.1×10^{-9} MKS Units for an Aspect Ratio of 15.9.

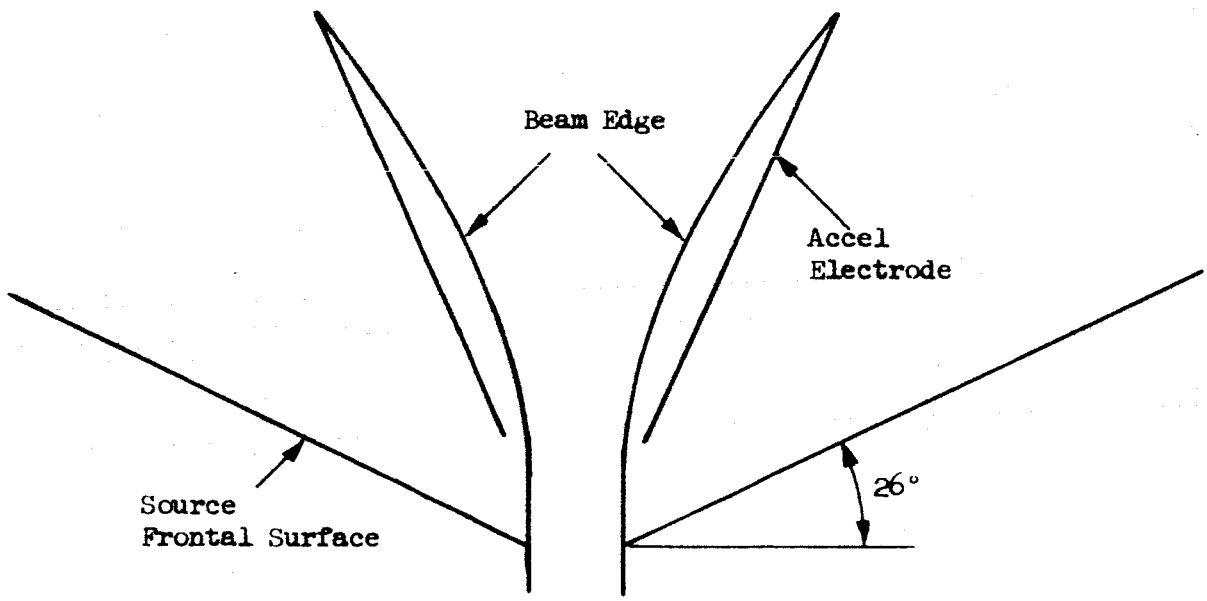

Figure 6

Extraction System Geometry Used to Investigate Beam Profiles. The Perveance Determined by the Indicated Beam Edge is 9.6×10^{-9} for an Aspect Ratio of 15.9.

Table 2

Data Obtained from the Beam Profile Investigation.

Source Current (ma)	Target Current (ma)	Decel Current (ma)	Accel Voltage (kv)	Decel Voltage (kv)	Perveance x 10^9 (amp/(volt)$^{3/2}$)	Percent Interception (%)	Vacuum Pressure (10^{-6} torr)
			Geometry of Figure 5				
10	7.5	2.5	15.5	2.5	5.2	25	10
15	11.5	4	17.4	2.5	6.5	26	?
20	13.5	6	18	2.5	8.3	30	?
25	16	9	19	2.5	9.5	36	6
30	20	11	23	2.5	10.6	36	9
			Geometry of Figure 6				
10	8	2	11.5	2.5	8.1	20	4
15	12	2	11.8	2.5	11.7	13	?
20	15	4.5	14.4	2.5	11.6	22	?
25	18	6	17	2.5	11.3	24	?
28	18	10	21	2.5	9.4	35	3

The perveance values expressed in MKS units were found to be 4.1×10^{-9} and 9.6×10^{-9} for the geometries of Figures 5 and 6 respectively. The perveance values calculated by the two methods indicated apparent good agreement for Figure 6 but for Figure 5 the measured perveance was high. The high values were possibly due to the high background pressure 6×10^{-6} to 10×10^{-6} which prevailed during the experimentation and which produced excessive scattering resulting in an apparent increase of the beam spread for the geometry of Figure 5. On the other hand while testing the geometry of Figure 6 a background pressure in the range 3×10^{-6} to 4×10^{-6} torr reduced the scattering to a negligible level. This information about the effect of background pressure level has led to the conclusion that during future testing the system pressure should be maintained below 5×10^{-6} torr in order to perform meaningful determinations of interception ratios.

The initial accel electrode testing indicated the importance of background pressure and illustrated the degree to which Equations (1) to (3) predicted the performance of the general geometries used. Subsequently, effort was directed to testing a sequence of accel-decel designs. The first design tested is that shown in Figure 7; data obtained in testing this configuration is presented in Table 3. The source used in this testing was one-inch long and made use of a tungsten cathode. The circuit diagram of the metering circuits is presented in Figure 3. The engine power efficiency for each case was computed from the equation

$$\text{Power Efficiency} = \frac{V_{dc}\, I_t}{V_{Dc}\,(I_t + I_{Sc} + I_{Dc}) + V_{Ac}\, I_{Ac} + V_S\, I_S}$$

where V_S is the source ionization inefficiency expressed in eV/ion. The data of Table 3 were taken during three different test periods which are referred to by the numbers 1, 2, and 3 appearing as the first integer in the row marked Data Set No. The second number, appearing behind the decimal point, is the data set obtained during the particular test period. The best performance may be noted to have occurred during test period 1 where the interception levels are between 5 and 10 per cent at 20 ma/cm^2, up to 8 and 13 at 60 ma/cm^2. The engine efficiencies defined previously for test period 1 vary from 67 per cent at 20 ma/cm^2 down to 43 per cent at 60 ma/cm^2 and tend to increase with decreasing accel/decel voltage ratio. Test periods 2 and 3 do not display as favorable performance levels as does test period 1. This may well be an indication of the criticality of electrode positioning since all three geometries were made "identical". Note the data under columns 3.9, 3.11, and 3.15. For these conditions the source efficiencies were 150, 168, and 167 eV/ion respectively for utilizations of 50, 67, and

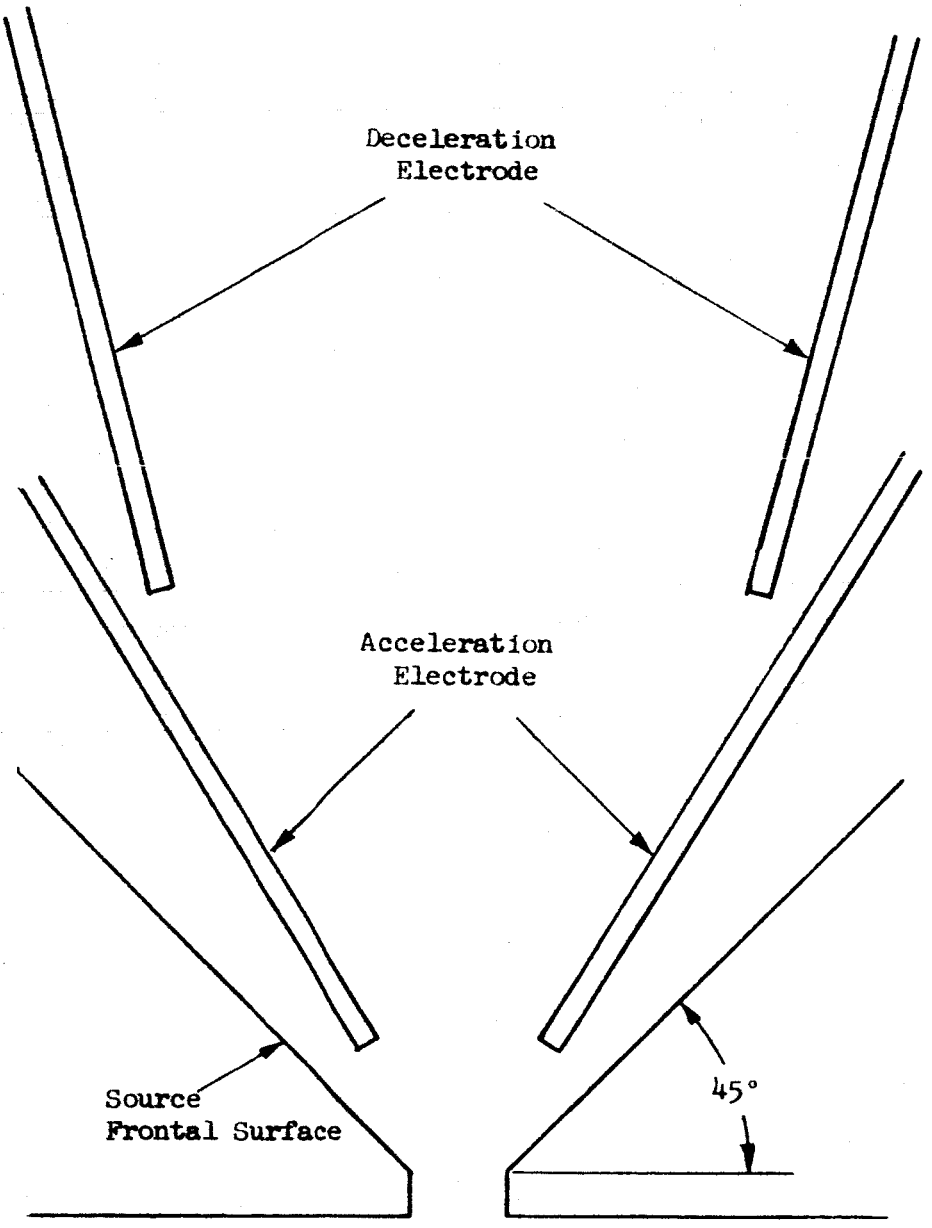

Scale: 1/4 in = 1 mm

Figure 7

Extraction System Geometry, Design No. 6

TABLE 3

DATA OBTAINED DURING EXTENSIVE TESTING OF EXTRACTION SYSTEM DESIGN NO. 6

Data Set No.	1.2	1.7	2.1	2.2	2.3	2.5	3.5	3.6	3.7	1.3	1.16	2.4	2.6	3.8	3.9	3.10
Mercury Flow Rate,ma	36.6	36.6	37.2	37.2	58	38	30	30	30	36.6	36.6	38.0	38	30	30	30
Source Current,ma	10	10	10	10	10	10	10	10	10	15	15	15	15	15	15	15
Target Current,ma	5.5	8	5.8	7.1	5.8	6.5	6.5	6.5	6.5	8.0	10.5	10.0	9.5	8.5	8.5	7.9
Accel Current,ma	1.0	0.5	1.5	1.2	1.0	0.8	1.2	1.0	0.8	2.0	0.5	0.9	1.0	1.2	1.3	2
Decel Current,ma	3.0	2	2.0	1.5	3.0	2.0	2.3	2.5	2.6	3.0	4.0	3.5	4.0	5	4.5	4.5
Screen Current,ma	1.0	0.5	0.5	0	0	0	0	0	0	2.0	0.5	0	1.0	0	0	0
Total,ma	10.5	11.0	9.8	9.8	9.8	9.3	10.0	10.0	9.9	15	15.5	14.4	15.5	14.7	14.3	15.4
Accel Voltage,kv	11.0	11.5	12.5	12.5	9.0	12.5	14	12.9	12.5	14.5	12.6	12.8	13.4	15.5	15.1	15.0
Decel Voltage,kv	2.7	5.6	2.7	5.1	5.1	3.9	3	4.5	6	2.6	5.5	5.0	4.4	6	4.5	3.0
Specific impulse,sec	5200	7500	5200	7140	7140	6250	5480	6700	7750	5100	7410	7160	6630	7740	6710	5470
Engine Efficiency,%	38	67	48	51	48	51	43	53	60	32	62	60	52	50	47	33
Accel/Decel ratio	4.08	2.05	4.64	2.45	1.76	3.2	4.66	2.87	2.08	5.6	2.3	2.5	3.0	2.6	3.3	5.0
Interception,%	10	5	15	12	10	8	12	10	8	13	3.3	6	6.7	8	8.7	13.3
Current Density ma/cm^2	20	20	20	20	20	20	20	20	20	30	30	30	30	30	30	30
Ionization inefficiency, eV/ion	198	252	160	209	280	144	162	153	153	217	310	240	167	157	150	150
Propellant Utilization,%	27	27	26.9	26.9	26.3	26.3	33	33	33	41	41	39.5	39.5	50	50	50
Vacuum Pressure,(10^{-6}torr)		2	3	3	3.5	3	1	1	1	3.4	2.4	6	3.4	1	2	2

TABLE 3 (CONTINUED)

Data Set No.	1.1	1.4	1.15	2.7	2.8	3.11	3.12	3.13	1.5	1.14	2.9	3.14	3.15	3.16
Mercury Flow Rate, ma	36.6	36.6	36.6	38	38	30	30	30	36.6	36.6	36.2	30	30	30
Source Current, ma	20	20	20	20	20	20	20	20	25	25	25	25	25	25
Target Current, ma	10	10	12.8	12	12	9.5	11	10.5	12	17.5	15.5	13	12	11
Accel Current, ma	2	2	0.5	1.2	1.2	2.5	1.8	1.8	3	1	1.5	2.8	3.5	4.8
Decel Current, ma	5	5	6	5.0	6.0	3	6.2	6.7	7	6	6.0	9	8.5	7.5
Screen Current, ma	2	2	0.5	1.0	1.0	0	0	0	3	1	1.5	0	0	1.2
Total, ma	19	19	19.8	19.2	20.2	16.0	19.0	19.0	25	25.5	24.5	24.8	24.0	24.5
Accel Voltage, kv	16.5	16.7	13.5	15.2	15.2	17.5	17.2	17.0	18	17	18.2	19.5	19.2	19.6
Decel Voltage, kv	2.5	2.5	5.4	4.3	4.3	3	4.5	6	24	5.2	4.1	6	4.5	3.0
Specific Impulse, sec	5000	5000	7350	6630	6630	5480	6700	7740	4900	7210	6400	7740	6700	5480
Engine Efficiency, %	28	28	58	49	49	?	44	46	25	56	46	25	33	21
Accel/Decel Ratio	6.6	6.7	2.5	3.5	3.5	5.8	3.8	2.8	7.5	3.4	4.4	3.2	4.3	6.5
Interception, %	10	10	2.5	6	6	12.5	9	9	12	4	6	11.2	14	19
Current Density, ma/cm^2	40	40	40	40	40	40	40	40	50	50	50	50	50	50
Ionization Inefficiency eV/ion	225	255	386	472	287	168	162	168	288	660	616	167	167	167
Propellant Utilization, %	55	55	55	52.6	52.6	67	67	67	68	68	69.2	82	82	82
Vacuum Pressure, (10^{-6} torr)	4.8	4.4	2.6	3.4	3.5	2 ?	2 ?	2 ?	5.0	3.6	4.5	1	2	2 ?

TABLE 3 (CONTINUED)

Data Set No.	1.9	2.10	3.17	3.18	3.19	2.11	2.13	3.20	3.21	3.22
Mercury Flow Rate, ma	36.6	36.2	30	30	30	36.2	36.2	35	35	35
Source Current, ma	30	30	30	30	30	35	35	35	35	35
Target Current, ma	11.5	17.4	12	14	15	16.8	17.6	15	14.5	12.5
Accel Current, ma	4	2.4	8.5	5	4.2	4.9	4.1	7.5	9	10.5
Decel Current, ma	10	7.0	7	9.5	10	9.0	9.0	10	10	8
Screen Current, ma	4	2.0	2	.5	0.2	4	4.0	1	1	1
Total, ma	29.5	28.8	29.5	29.0	29.4	34.7	34.7	33.5	34.5	32
Accel Voltage, kv	18.5	19.1	20	20	20	21.2	21.2	19.5	19.8	20
Decel Voltage, kv	2.2	4.0	3	4.5	5.6	4.0	4.0	5.7	4.5	3
Specifice Impulse, sec	4690	6320	5480	6700	7500	6320	6320	7540	6700	5480
Engine Efficiency, %	18	43	15	30	35	29	32	28	22	13
Accel/Decel Ratio	8.4	4.8	7.7	4.5	3.6	5.3	5.3	3.4	4.4	6.7
Interception, %	13.3	8.3	28.4	16.7	14	14	11.7	21.4	25.7	30.0
Current Density, ma/cm^2	60	60	60	60	60	70	70	70	70	70
Ionization Inefficiency, (eV/ion)	410	340	197	194	194	333	364	206	206	206
Propellant Utilization	82	83	100	100	100	96.6	96.6	100	100	100
Vacuum Pressure, (10^{-6} torr)	3.6	5	2	2	2	7	7	2	2	3

82 per cent and current densities of 30, 40, and 50 ma/cm^2. Thus, very efficient source operation was experienced during these runs; however, low engine efficiency was experienced, i.e., 47 to 33 per cent. This low engine efficiency was due to the low percentage of source current which arrived at the target even though the interception ratio (ratio of accel current to source current) was low. A relatively large decel interception was the problem.

The effort was then directed towards increasing the percentage of the through beam by consideration of the accel-decel geometry; in this manner it was expected that the focusing would be improved by testing a series of extraction geometries. The abridged data of the testing during this period is shown in Table 4. Design No. 9 as shown in Figure 8 was studied early in this period and is a modification of the geometry of Design No. 6, shown in Figure 7. As compared to Design No. 6 the accel electrode of Design No. 9 is shorter in order to reduce the accel electrode impingement due to beam blow-up in accel electrode region; furthermore, the decel electrode is placed behind the accel electrode. The purpose for such positioning of the decel electrode was two-fold. First the separation between the decel electrode was increased to reduce the direct impingement, and second, the overlap behind the accel electrode was expected to catch ions which enter the accel-decel electrode gap. In previous designs having no overlap, ions which entered this region struck the back side of the accel electrode as evidenced by the luminescent spot at the impingement position. With the decel electrode thus positioned the back side bombardment of the accel electrode was eliminated and the current to the decel electrode was greatly reduced. Associated with this geometry there was, however, the possibility of poor beam focusing because of the remote position of the decel electrode.

To provide better focusing the geometry was modified to yield Design No. 10 as shown in Figure 9. In this design the accel and decel electrodes are again in line. The exit side of the accel electrode region was widened to reduce impingement due to beam blow-up in the accel region; a second reason was to reduce the chance that ions could get into the accel-decel gap and thus result in accel electrode back side impingement. For this geometry the accel electrode impingement was between 1 and 3 per cent at 20 ma (40 ma/cm^2) and was between 3 and 5 per cent at 30 ma (60 ma/cm^2).

The final geometric variation examined in this period, Design No. 11, is shown in Figure 10. In this case the accel and decel electrode configuration was the same as in Design No. 10 but the geometry of the source extraction slit was modified in accordance with the data reported in Reference 2. The source slit geometry of

TABLE 4

PERFORMANCE DATA OF EXTRACTION SYSTEM DESIGN NOS. 9, 10, AND 11

Data Set No.	9.8	9.10	10.5	10.9	10.11	12.19	12.22	13.13	14.38
Design No.	9	9	9	9	9	10	10	11	11
Mercury Flow Rate, ma	29	29	33.2	31.8	31.8	33.2	33.2	40	40
Source Flow Rate, ma	30	30	30	30	30	30	30	30	30
Target Current, ma	26.2	26.5	26	29.6	28.8	28.2	29.8	24	27
Accel Current, ma	2.8	2.75	2.1	1.1	1.4	0.88	0.63	1.2	1.0
Decel Current, ma	1	1	1	0.5	1	0.40	0.40	4	0.8
Screen Current, ma	1.5	2	1.5	1	1	1.6	1.4	1.8	2
Accel Voltage, kv	18.6	18.5	19.4	19.4	17.6	16.6	15.4	13.2	15
Decel Voltage, kv	7.7	7.6	7.6	9.1	8.1	8.0	9.2	8.0	8.0
Specifice Impulse, sec	8760	8720	8720	9540	8960	8940	9590	8940	8940
Engine Efficiency, %	59	59	59	70	66	57	63	57	62
Accel/Decel Ratio	2.42	2.44	2.55	2.13	2.17	2.07	1.67	1.65	1.87
Interception, %	9.3	9.2	7.0	13.7	4.7	2.9	2.1	4.0	3.3
Current Density, ma/cm^2	60	60	60	60	60	60	60	60	60
Ionization Inefficiency (eV/ion)	320	270	540	530	470	1000	1000	280	900
Propellant Utilization,%	103	103	90.4	94.4	94.4	90.4	90.4	75	75
Vacuum Pressure (10^{-6} torr)	9.8	8.9	8.0	9.6	10	9.8	8.5	5	19

TABLE 4 (CONTINUED)

Data Set No.	9.17	9.18	9.19	10.1	10.3	10.14	10.15	10.18	10.22	12.7	12.15	13.15	13.18
Design No.	9	9	9	9	9	9	9	9	9	9	9	9	9
Mercury Flow Rate, ma	36.1	36.1	36.1	33.2	33.2	33	33	30.5	31.4	40	33.2	40	40
Source Current, ma	20	20	20	20	20	20	20	20	20	20	20	20	20
Target Current, ma	18.9	16.4	19.2	20	18	18.5	15	20	19.9	19.1	19.3	17.5	15.2
Accel Current, ma	0.55	0.85	0.30	0.4	1.2	0.5	1.3	0.3	0.4	0.20	0.50	0.75	0.38
Decel Current, ma	0	1.0	0	0	0	0	0	0	0	0.35	0.2	1.0	1.2
Screen Current, ma	1	1.5	0.5	0	1	1	2.5	0.2	0	0.40	0.45	0.6	2
Accel Voltage, kv	16.2	14.9	13.9	14.1	15.1	13	13.2	14.1	13.3	11	13.5	9.6	9.0
Decel Voltage, kv	7.6	5.8	8.0	9	7.7	8	2.7	8.2	8.0	8.1	7.9	8	8.0
Specific Impulse, sec	8710	7620	8940	9490	8770	8940	5200	9050	8940	8960	8890	8940	8940
Engine Efficiency, %	55	45	61	55	47	65	38	64	64	57	56	59	56
Accel/Decel Ratio	2.13	2.56	1.74	1.57	1.96	1.63	4.89	1.72	1.66	1.36	1.71	1.20	1.12
Interception, %	2.75	4.2	1.5	2.0	6.0	2.5	6.5	1.5	2.0	1.0	2.5	3.8	1.9
Current Density, (ma/cm^2)	40	40	40	40	40	40	40	40	40	40	40	40	40
Ionization Inefficiency, (eV/ion)	1230	1195	623	724	319	240	265	904	780	676	524	420	243
Propellant Utilization, %	57	57	57	60	60	60.5	60.5	65.5	63.6	50	60.4	50	50
Vacuum Pressure, (10^{-6} torr)	6.2	7.4	5.8	10	5.6	4.8	?	6.5	4.1	5	4.8	4	3

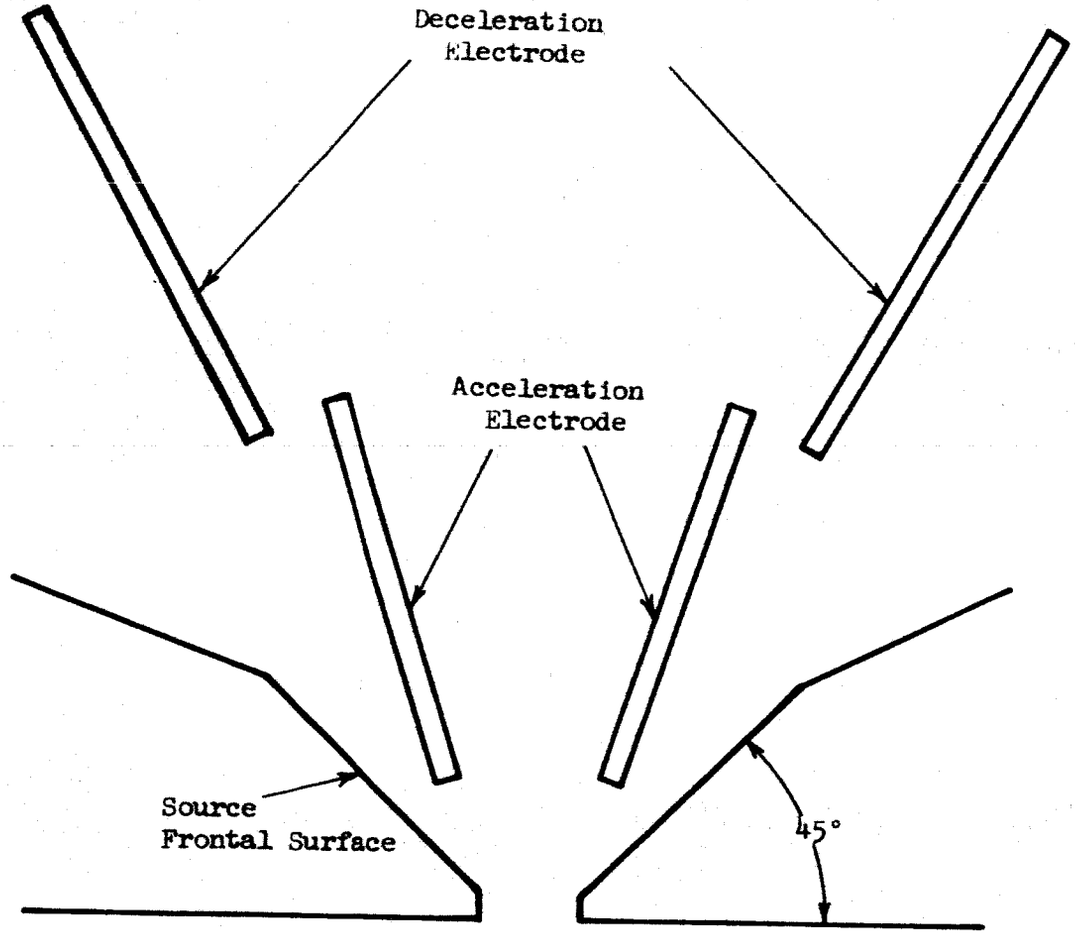

Scale: 1/4 in. = 1 mm

Figure 8

Extraction System Geometry, Design No. 9

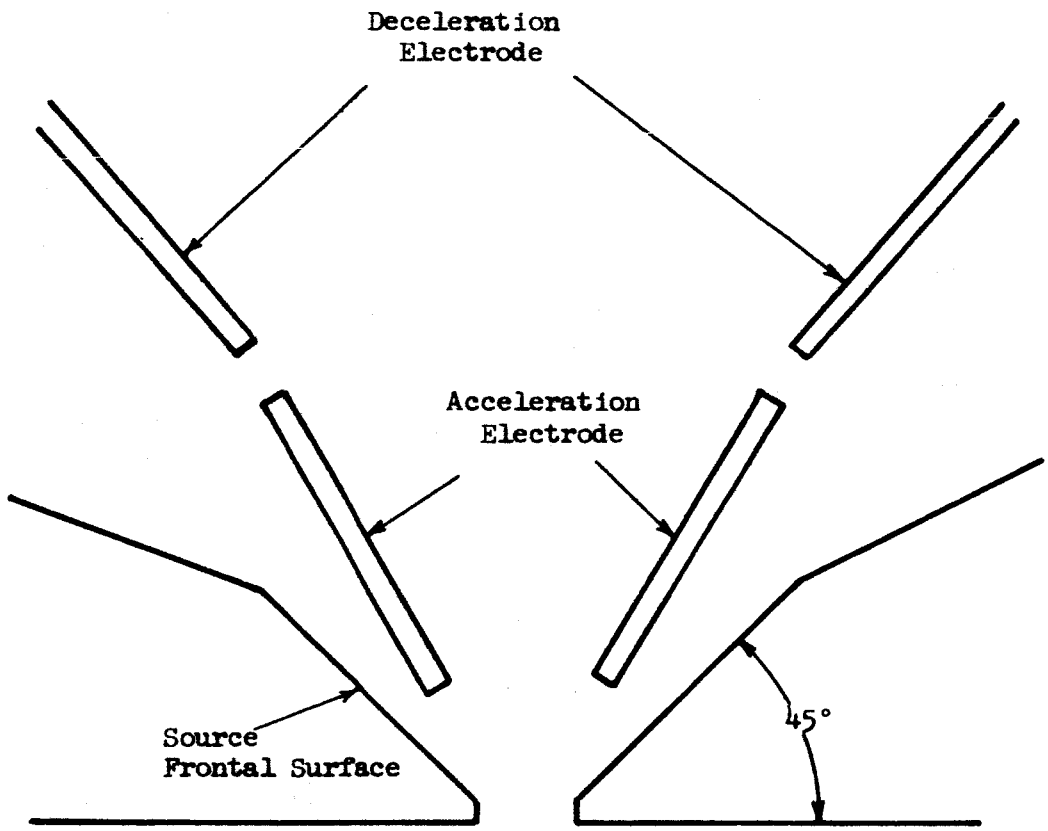

Scale: 1/4 in. = 1 mm

Figure 9

Extraction System Geometry, Design No. 10

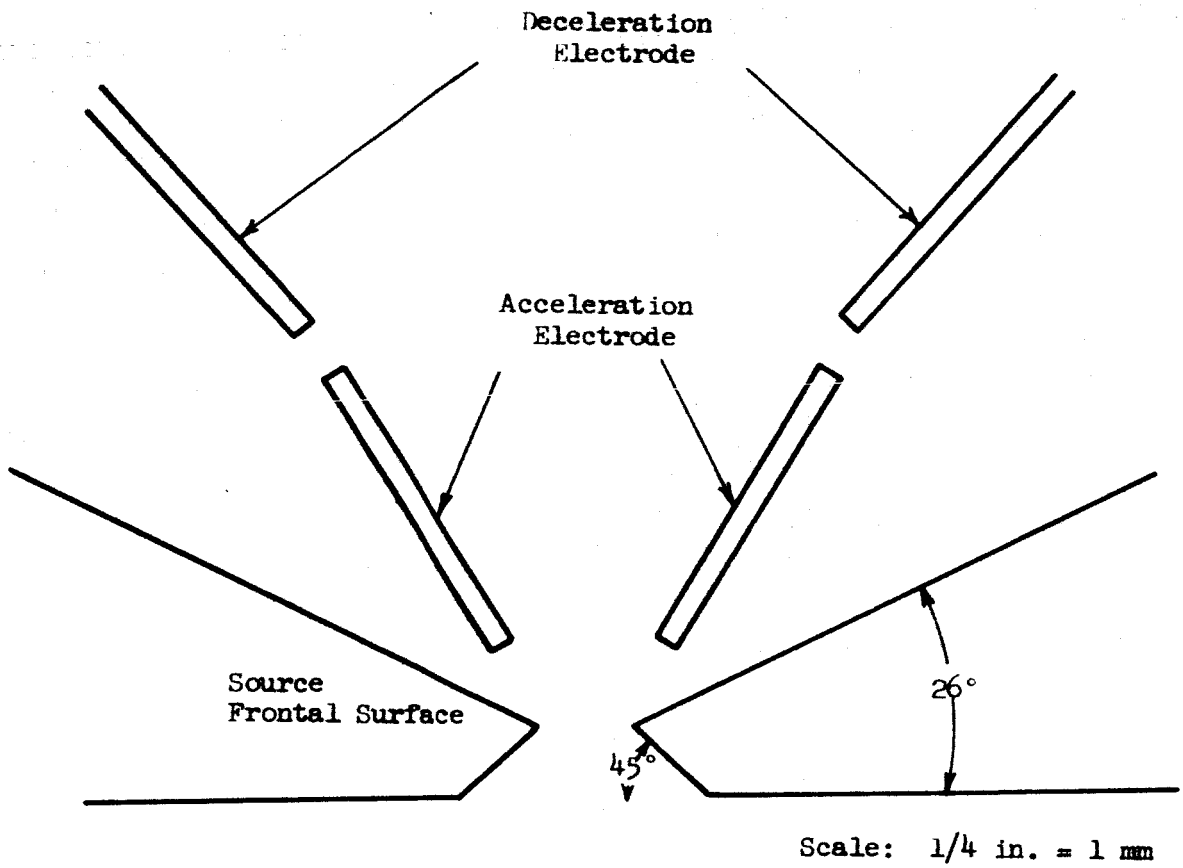

Figure 10

Extraction System Geometry, Design No. 11

of Design No. 11 appeared to produce less interception than for the previously employed source slit geometries although the data at this point was not definitive since the interception at 60 ma/cm^2 is less for Design No. 11 than for Design No. 10 but the data at 40 ma/cm^2 is not conclusive. It was decided that further testing would be necessary before definite conclusions could be drawn.

At this point in the program, it was believed that the accel-source spacing needed optimizing. Thus a means of varying the distance between the source slit and extraction electrode during engine operation was fabricated. The results obtained using the movable system are given in Figure 11, where the accel interception as a function of extraction voltage is shown for several accel electrode-source separations. The extracted current for these curves was 30 ma (60 ma/cm^2) and the minimum interception obtained was approximately 1 ma, thus the minimum interception level was approximately three per cent. The interception increases from 3.3 per cent to 5.3 per cent as the separation is increased from 1.0 mm to 2 mm. The above data was obtained using Design No. 11 with the exception that the source-accel electrode spacing was variable. Note that the optimum spacing for this geometry is determined to be 1 mm.

The total accel interception now had been decreased to a level where the next logical step appeared to be one of gaining knowledge of erosion patterns. Therefore, the extraction geometry reported as Design No. 11 was used at this point to determine the erosion pattern associated with such an extraction system. The test lasted for a duration of 30 hours and was terminated by the breaking of a stand-off insulator. The resulting erosion pattern is shown in Figure 12 and the typical operating conditions are given in Table 5. Study of the erosion pattern revealed that relatively little sputtering occurred at the focusing edge of the accel electrode; in fact, almost negligible sputtering occurred farther forward than the eroded line which is evident in Figure 12. It was presumed that this line resulted from the focusing of the charge exchange ions formed in the acceleration region. Beyond this line the sputtering appeared to be distributed uniformly over the surface except for several shallow longitudinal lines; these lines carried over onto the decel electrode, where they were much deeper. It was presumed that the decel electrode interception was due to beam blow-up and that the occurrence of the longitudinal crevices indicated beam nonuniformity.

During the 30 hour run the currents intercepted by both electrodes were about equal; hence it might be anticipated that the electrodes would have comparable erosion rates

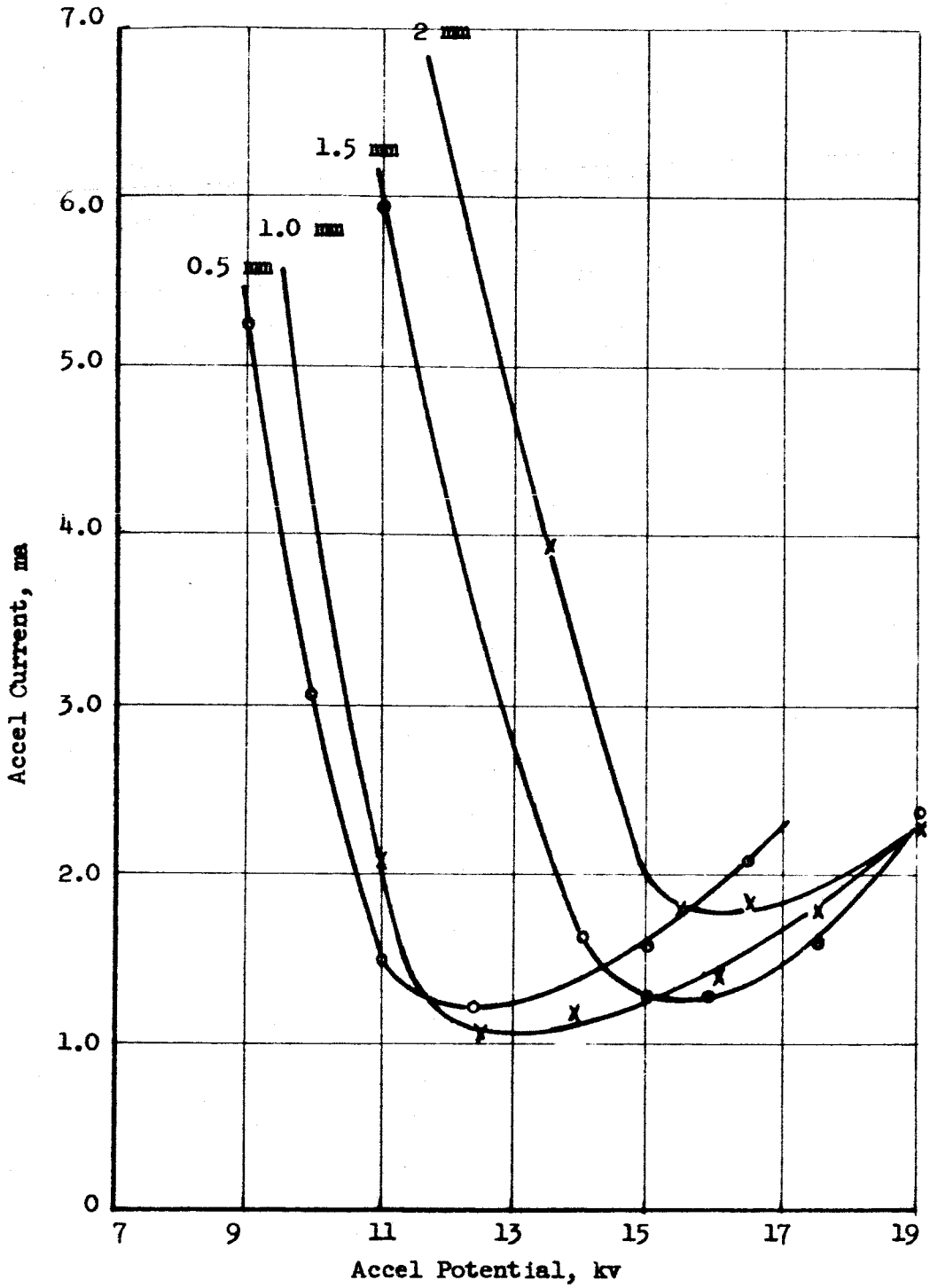

Figure 11

Accel Electrode Interception Current vs. Accel Potential for Several Values of Accel Electrode - Source Separations at a Beam Current of 30 ma (60 ma/cm^2). (Design No. 11).

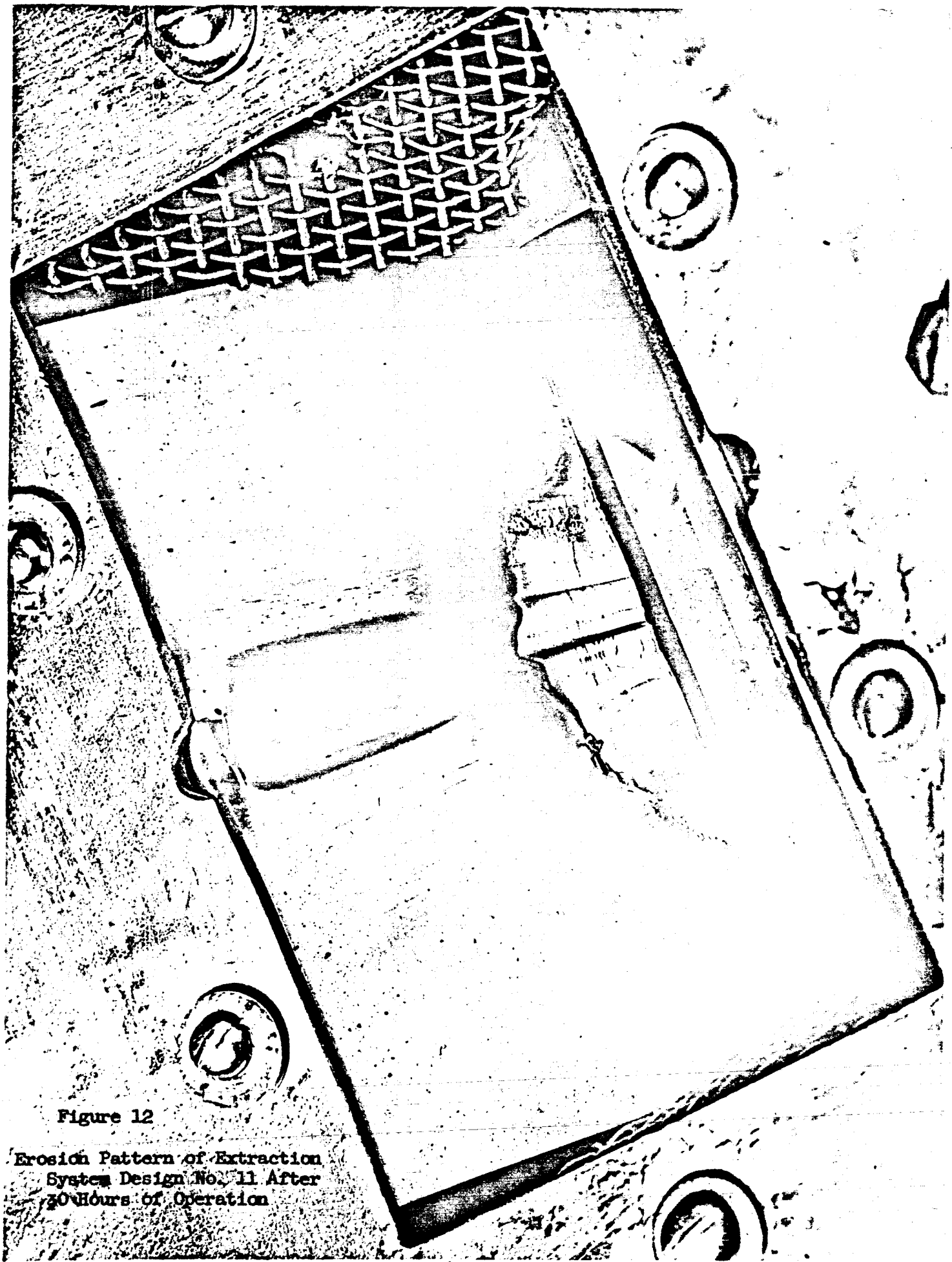

Figure 12

Erosion Pattern of Extraction System Design No. 11 After 30 Hours of Operation

Table 5

Operating Conditions that Existed During the Study of Extraction System Design No. 11

Mercury Feed Rate, ma	34.0
Source Current, ma	30.0
Target Current, ma	27.5
Accel Current, ma	1.0
Decel Current, ma	0.7
Screen Current, ma	1.8
Accel Voltage, kv	14.2
Decel Voltage, kv	8.0
Arc Current, amp	1.03
Arc Voltage, volts	26.0
Filament Current, amp	6.5
Filament Voltage, volts	13.5
Ionization Inefficiency, eV/ion	894.0
Propellant Utilization, %	88.0
Power Efficiency, %	63.5
Rocket Efficiency, %	55.9
Accel Interception, %	3.3
Pressure, (10^{-6} torr)	7.0

if the ions incident on each electrode have comparable energies. The observed erosion, however, indicated that the decel electrode was eroded two to three times as much as the accel electrode. This difference may have been because the ions that struck the decel electrode had higher kinetic energy than those which impinged upon the accel electrode, or if the ion energies to each electrode were the same, then the sputtering rates of the two electrodes may have been different. The accel electrode was made of tantalum and the decel electrode of molybdenum. According to the results of G. K. Wehner (Reference 3) the sputtering rates of Ta and Mo are comparable in the range of ion energy from 150 to 500 eV, the Ta rate being about ten per cent higher. If this relationship can be extrapolated to higher ion energies then the observed difference in total sputtering of the two electrodes must have been due to a difference in incident ion energy and not to different sputtering rates. These arguments led to the conclusion that the decel electrode current was due to beam blow up resulting in the incident ions having about 8 kev of kinetic energy while the accel electrode current is due primarily

to charge exchange since this is the only way that the incident ions can have a resultant kinetic energy less than 8 kev. In order to support the above conclusion an approximate calculation of the percent accel electrode interception due to charge exchange was performed making use of the equation

$$\frac{I_{Ac}}{I_B} = (1 - \eta_m) \frac{I_T}{e} \left(\frac{\sigma}{v_n}\right) \left(\frac{L}{A}\right) \qquad (4)$$

where I_{Ac} = charge exchange current to the accel electrode

I_B = ion source current

η_m = propellant utilization

I_T = mercury feed rate in amp equivalent

σ = charge exchange cross section

v_n = the most probable thermal velocity of a molecule of a gas

L = the width of the potential well in which the charge exchange ions are produced and trapped resulting in a current to the accel electrode.

A = effective accel channel cross section

e = electronic charge

For a mercury feed rate of 34 ma, a propellant utilization of 88 per cent, a charge exchange cross-section equal to 62×10^{-16} cm^2, (Reference 4) a neutral gas temperature of 530°K, and a potential well width of 1.5 cm, the charge exchange current relative to the beam current was calculated to be 2.2 per cent, a value comparable to the measured value of 3.3 per cent shown in Table 5. Hence, there was no detectable contradiction in assuming that the measured accel electrode current was predominantly charge exchange.

Further support of this assumption was obtained from the observation that the accel electrode current reduces as the accel/decel ratio is reduced (i.e., by holding the accel potential constant and reducing the accel-decel potential difference). This operation is in the direction of reducing the depth and the width of the potential well, resulting in a reduction of L of Equation (4).

The current to the decel electrode probably was due to beam blow-up which could not be compensated for by the focusing action of the accel-decel slit. It was

concluded that the reduction of this current could be accomplished through the reduction of the length of the accel electrode. This would have two effects. The first would be to reduce the width and divergence of the beam upon entering the accel-decel gap. The decel electrodes could then be more closely spaced and could result in stronger focusing, presenting the possibility of compensating for the beam blow-up. The second effect would be a reduction of the quantity, L, in Equation (4). Hence the charge-exchange current would be reduced.

The contour of the decel erosion indicated a beam nonuniformity which was composed of two parts, one which was smoothly varying resulting in maximum current density in the geometric center of the beam and the other which was localized producing the crevices which are evident in Figure 12. It was concluded that the smoothly varying portion was due to end effects or to distribution of the incoming mercury vapor. In order to investigate these factors a two inch electromagnetic engine was constructed.

Incorporated in this two-inch engine was the ability to vary the position of the cathode relative to the cathode slit, the ability to vary the distance between the accel electrode and the source, and a means of directing the input mercury vapor into the source cathode chamber, into the source anode chamber, or dividing it into any proportion between the two chambers. It was early determined, in support of previous data, that best engine performance was obtained when all of the mercury vapor was directed into the anode chamber.

Typical performance data of the two-inch electromagnetic engine is indicated in Table 6, and the source ionization inefficiency versus propellant utilization for this engine is given in Figure 13. Figure 14 shows the extraction geometry used. In order to investigate the nature of the current to the accel electrode a measurement of the accel current as a function of propellant utilization was made, maintaining the accel and decel potentials at 15 kv and 8 kv respectively; the input mercury flow rate was constant at 66.5 ma. Figure 15 provides a plot of the data points in the form of percent accel electrode interception versus $(1 - \eta_m)$, where the propellant utilization was varied by adjusting the arc conditions at constant mercury flow rate. It is evident from the plot that the data points can be fitted to a good approximation by a straight line if the points in the vicinity of 80 to 90 per cent utilization are excluded. Recalling Equation (4) it is seen that if the width of the potential well is independent of or a very weak function of the current density then the percent interception is a linear function of $(1 - \eta_m)$ and the experimental points should fit a straight line. The observed deviation

Table 6

Typical Performance Data of the

Two Inch Electromagnetic Engine During the Testing of 10/4/63.

Mercury Feed Rate, ma	66.5	66.5	66.5
Source Current, ma	60.0	55.0	50.0
Accel Current, ma	1.0	0.90	0.89
Target Current, ma	62.0	59.0	53.0
Decel Current, ma	1.7	1.0	0.50
Accel Voltage, kv	15.0	15.0	15.0
Decel Voltage, kv	8.0	8.0	8.0
Arc Current, amp	1.8	1.7	1.4
Arc Voltage, volt	23.5	23.0	21.0
Filament Current, amp	4.6	4.6	4.6
Filament Voltage, volt	7.25	7.25	7.25
Filament Temperature, °F	1780.	1760.	1745.
Source Efficiency, eV/ion	705.0	711.0	588.0
Propellant Utilization, %	90.2	82.7	75.2
Power Efficiency, %	83.2	84.0	84.0
Overall Efficiency, %	75.1	69.6	63.2
Accel Interception, %	1.67	1.64	1.78
Decel Interception, %	2.84	1.82	1.00
Specific Impulse, sec.	8940.	8940.	8940.
Vaporizer Temperature, °C	238.	238.	238.
Pressure, (10^{-6} torr)	6.0	6.0	6.0

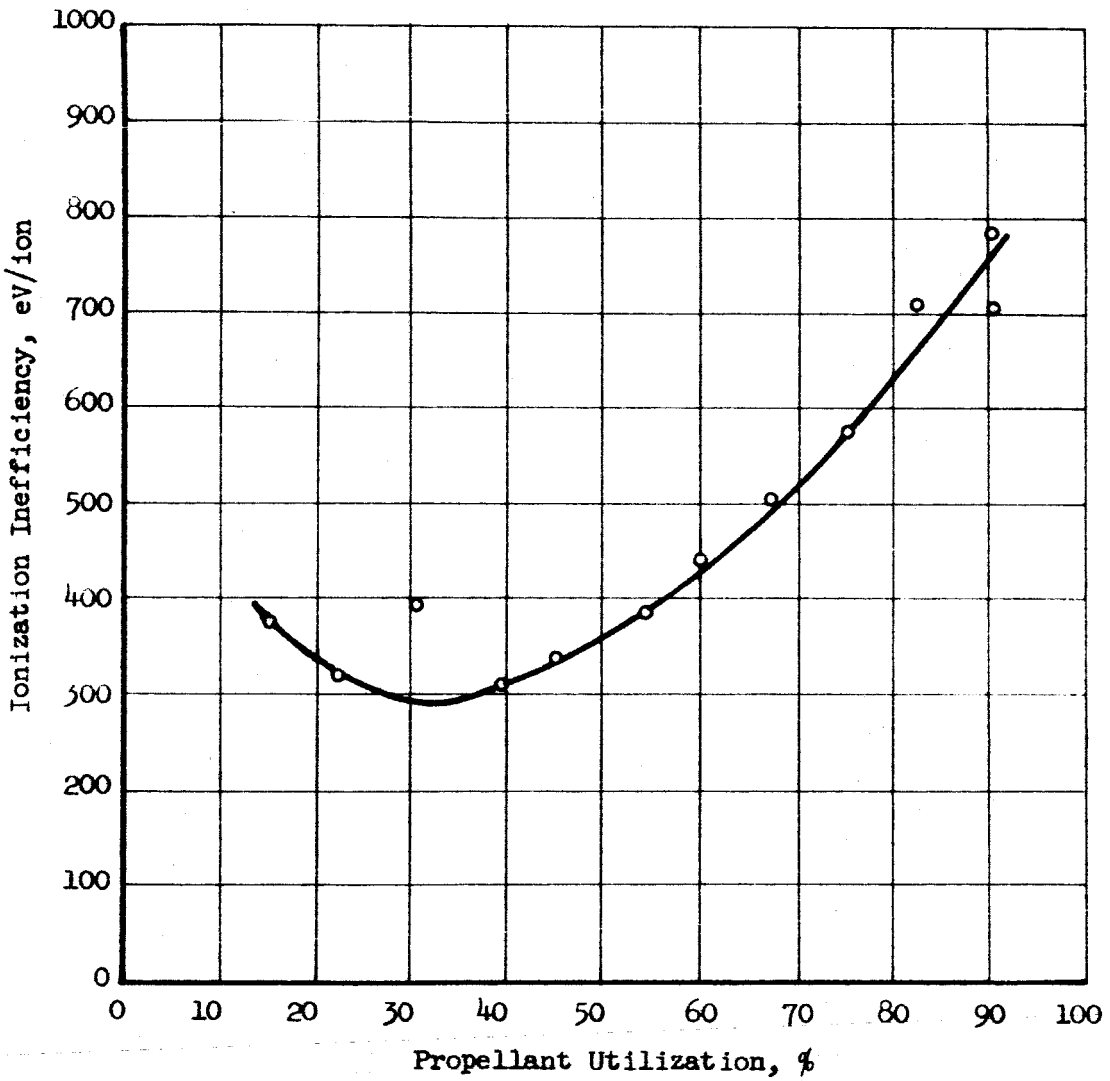

Figure 13

Ionization Inefficiency vs. Propellant Utilization
for the Two-Inch Electromagnetic Engine

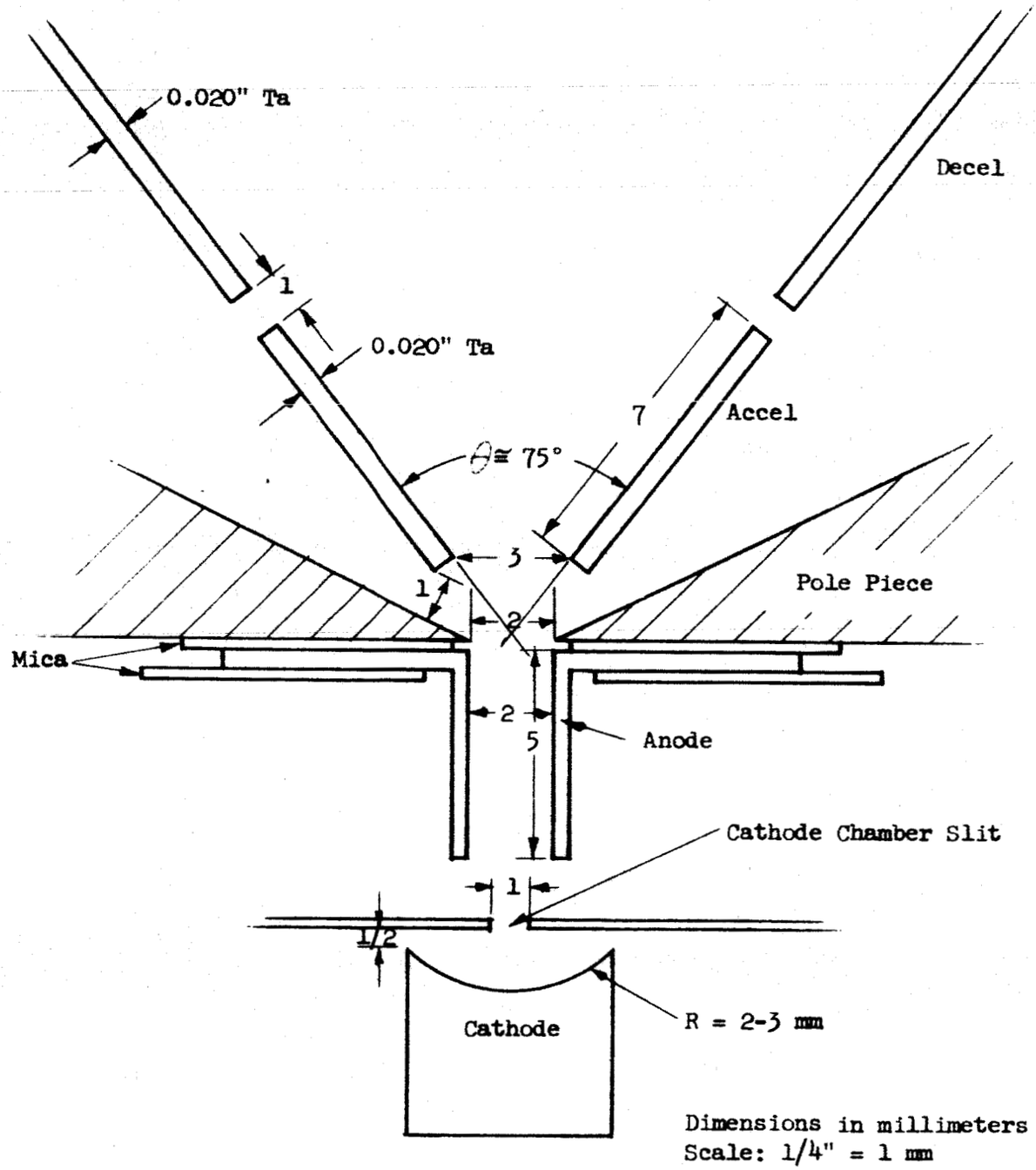

Figure 14

Geometry of the Two-Inch Electromagnetic Engine

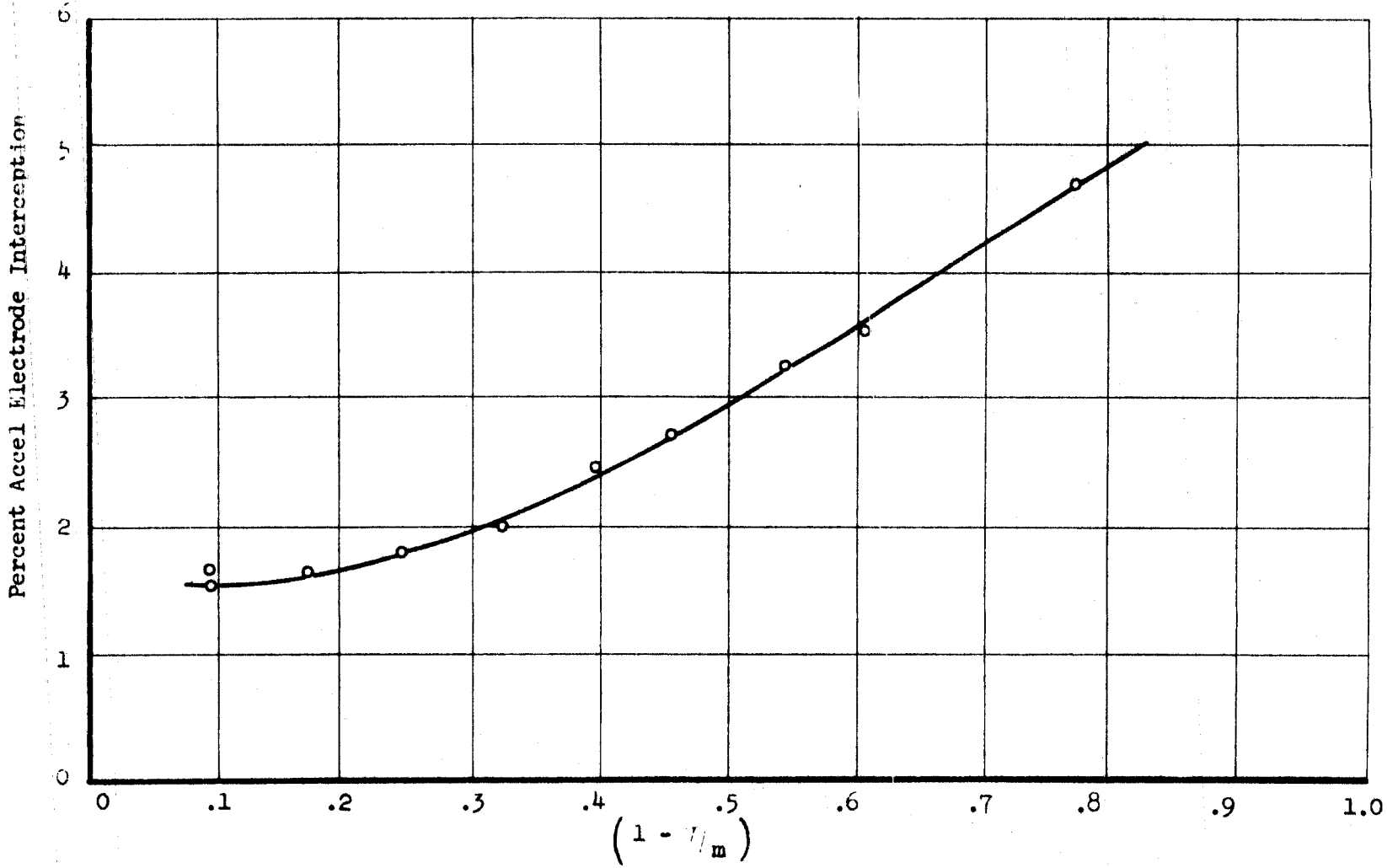

Figure 15

Percent Accel Electrode Interception vs. $(1 - V/V_m)$ for the Two Inch Electromagnetic Engine

from the linear dependence was probably due to two effects. The first was that the width of the potential well in reality is a function of the current density and hence the propellant utilization. This dependence showed up as a deviation from linearity at low current density. The deviation at the high propellant utilization end was probably due to a combination of direct impingement and charge exchange, resulting from the residual mercury background. [This set of data was taken when the accel and decel voltages arbitrarily were set for minimum interception of a 50 ma beam (75 per cent utilization). Lower minimum interception would have been obtained if the accel voltages had been optimized for 60 ma (90 per cent utilization)].

The data reported in Table 6 was obtained making use of a new fast response vaporizer described in Appendix 4. Previous vaporizers, using a porous plug rather than a single capillary, had observed response times on the order of hours at the feed rates employed in the present experiments; observed response times on the order of seconds were obtained with the new design. Previous vaporizer designs, therefore, required long waiting periods to insure the establishment of equilibrium conditions in the vaporizer. With the new vaporizer the waiting periods were on the order of minutes. The new vaporizer design resulted in a considerable saving of time and increased the reliability of the feed rate measurements by enabling the immediate observation of flow rate variations due to external disturbances (room temperature fluctuations) of the feed system. In addition to decreasing the response time of the vaporizer the uncertainties produced by room temperature variations were reduced by jacketing the mercury feed line by a tube through which tap water flowed. It is believed with these improvements that feed rate measurements were possible to within an uncertainty of four per cent providing the room temperature held reasonably constant.

At this point in the program the understanding of the interception currents was that the current to the accel electrode was due to charge exchange alone, while the current to the decel electrode was due to direct interception resulting from natural beam spread. Thus, it was concluded that reducing the beam spread or shortening the length of the decel electrode should result in decreased decel current while the accel current could be reduced by reducing the charge-exchange rate.

Considering first the decel electrode interception, it was observed that without neutralization the beam spread at a constant current density depended on the decel voltage in the following way. As the decel voltage approaches the accel voltage the beam spread reduces. Thus, the higher the specific impulse the less the impingement on the decel electrode. Since the impingement due to beam spread occurred at the downstream end of the decel electrode there appeared to be the

possibility of reducing the impingement by simply removing this portion of the electrode. When this was tried, however, it became immediately obvious that this was not an acceptable solution to reducing the decel impingement. For this case the beam spread became so excessive that some beam was lost to the external vacuum chamber. Furthermore, the loss of thrust associated with such a highly divergent beam would be unacceptable. It was thus concluded that the most meaningful way of reducing the decel electrode impingement would be to neutralize the beam before appreciable beam spread takes place. It was then decided to try to neutralize making use of oxide cathodes which emitted through a slot in the decel electrode. The decision to use oxide cathodes was based on the desire to visually observe the beam profile during neutralization; the light associated with the usage of tungsten cathodes would have completely obscured the beam luminescence. The extraction geometry utilized is shown in Figure 14 with the addition of an oxide neutralization cathode mounted behind a slot located one centimeter downstream from the accel-decel gap. For this geometry the coupling to the beam was poor, the main portion of the current emitted by the neutralizer cathode going back to the source rather than to the beam. The electron current to the source did not have to go between the accel electrodes but rather went around the accel electrodes avoiding the potential hill that existed between them. In order to improve the coupling, tungsten wire cathodes were placed close to the accel-decel gap and close enough to the beam that grazing occurred. For this case, current neutralization was achieved. However, the neutralizer emission current was greater than the beam current; some of the excess current went back to the source by some path around the accel electrodes, some was lost to the external vacuum chamber, and some went to the decel electrode.

At this point, it was decided to redesign the extraction system to reduce the neutralizer current to the source in addition to incroporating other improvements. Among these was a change from tantalum sheet metal to solid stainless steel electrodes in an attempt to rigidize the system and eliminate the possibility of thermal warpage.

The use of stainless steel rather than tungsten or tantalum for solid electrodes was dictated by both a cost and machinability standpoint. Carbon, which is the best material from the sputtering standpoint, was not used at this time because of the associated outgassing problems. The new design included halving the length of the accel electrode to reduce the charge-exchange rate in the accel potential well; in addition the length of the decel electrode was reduced by approximately a factor of ten in order to introduce the neutralization before the beam experienced appreciable blow-up. In addition to changing the extraction geometry, the source

geometry was changed according to the then existing theory on the source performance. This theory indicated that for an oxide cathode the cathode slit width should be larger than required for operation with a tungsten-wire cathode; this theory was shown later to be erroneous. The testing of the stainless steel extraction system suffered delay because of excessive arcing which eventually led to the build up of conducting whiskers which shorted out the extraction electrodes or the source anode. This excessive arcing was traced to the utilization of a braze in joining the accel electrodes to their supporting structure.

The performance of the engine consisting of the magnetic focusing source utilizing a solid stainless steel extraction system was determined after the braze joint was eliminated. The geometry of the engine is shown in Figure 16. The feed system employed during the performance determination displayed a maximum periodic variation of seven per cent (Appendix 4) but was kept below five per cent by taking data at the proper angular position of the gear drive. Early in the testing of this engine, it was found that good extraction conditions were obtained for accel voltages from 15 to 17 kv, decel voltage at 8 kv, and current densities in the range of 50 to 70 ma/cm^2. However, after some arcing had occurred it was found that the accel voltage required increased to 19 to 20 kv for minimum interception at the same current density. Since one of the main purposes of the test was to investigate source performance using a well-calibrated and stable feed system, it was decided to continue the test although due to the arcing damage to the accel electrodes the performance of the extraction system would not be optimum. Figures 17 and 18 show the data on source efficiency and propellant utilization so obtained. Also shown is the arc voltage which is in the thirty volt range for propellant utilizations above 90 per cent. In this voltage range it is possible to have approximately seven per cent double ionization according to N. L. Milder (Reference 4). This double ionization rate was measured in the Kaufman type ion engine and, therefore, may not necessarily have the effect of yielding a measured value of propellant utilization which is higher than the actual value. Double ionization, which appears to be possible for arc voltages above 20 volts, together with an uncertainty in the feed rate on the order of four per cent can explain the attainment of utilization values as high as 105 per cent. From Figures 17 and 18 it is seen that approximately 650 eV/ion arc power is required to obtain a measured utilization of 95 per cent. Taking into account the possibility of double ionization reduces this utilization to 88 per cent if a seven per cent correction is applicable to this engine. The determination of the appropriate correction must await measurement of the double ionization rate by means of an e/m analysis of the beam.

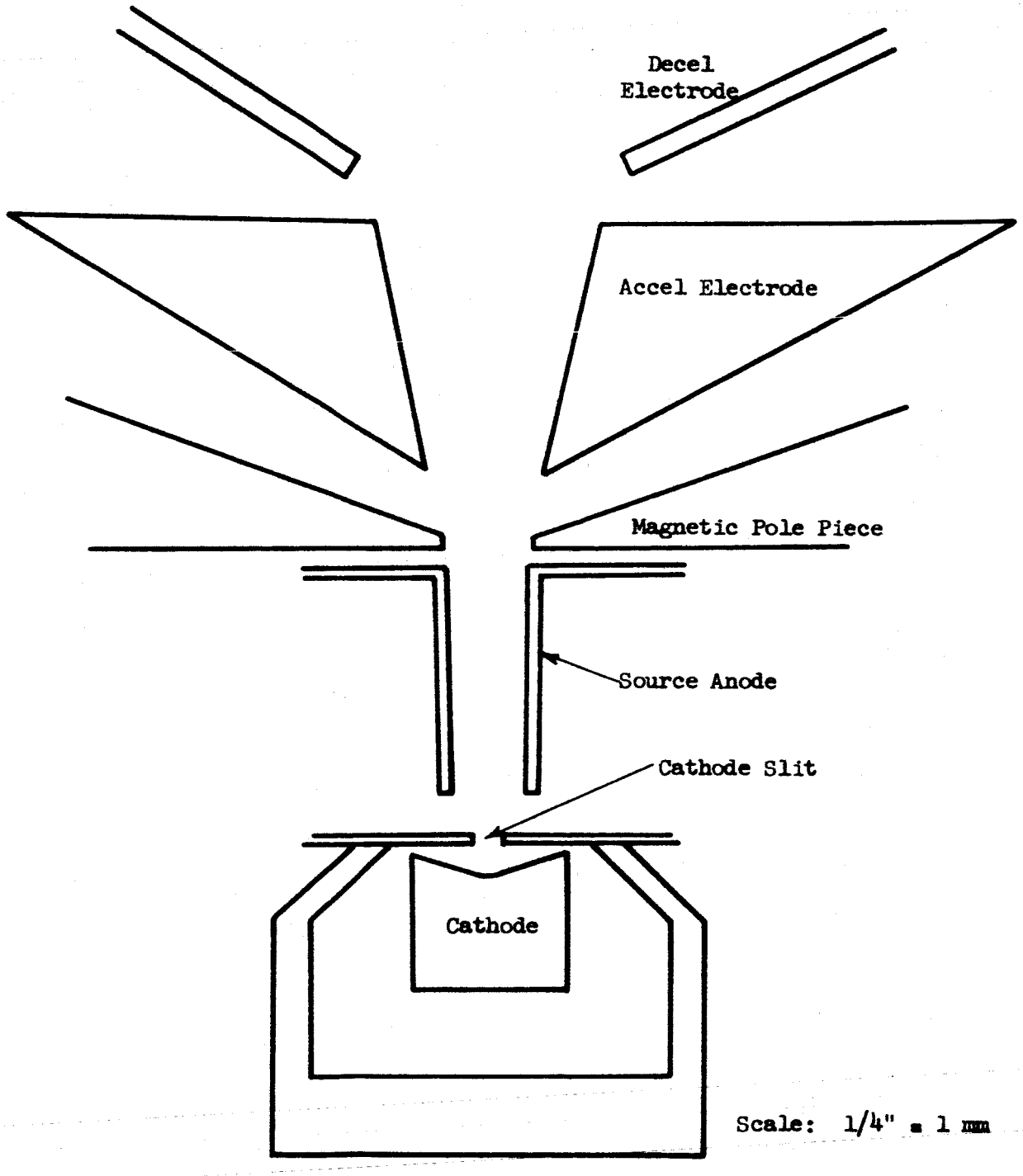

Figure 16

Geometry of the Stainless Steel Extraction System and the Magnetic Focusing Source

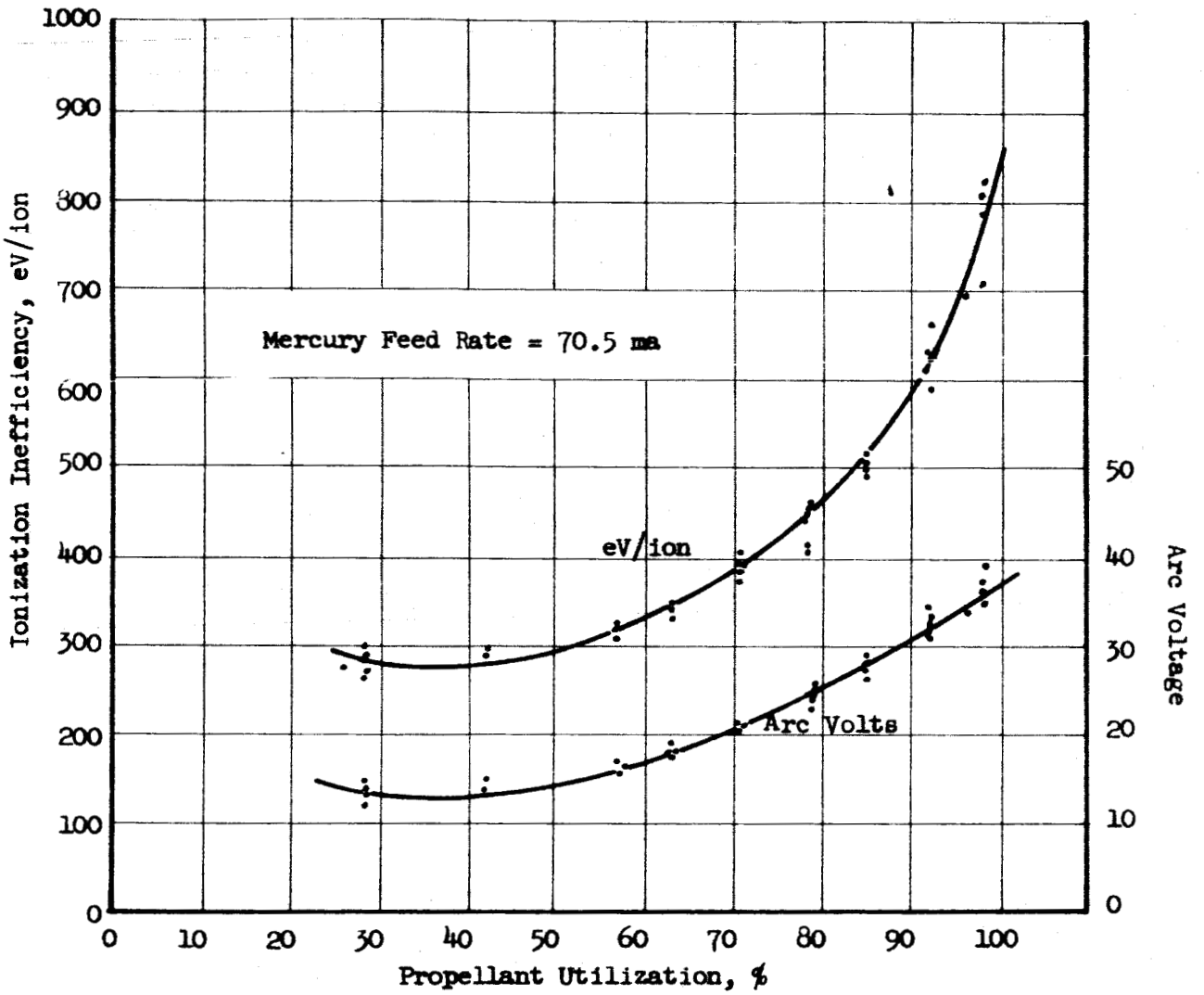

Figure 17

Ionization Inefficiency and Arc Voltage vs. Propellant Utilization for a Mercury Feed Rate of 70.5 ma.

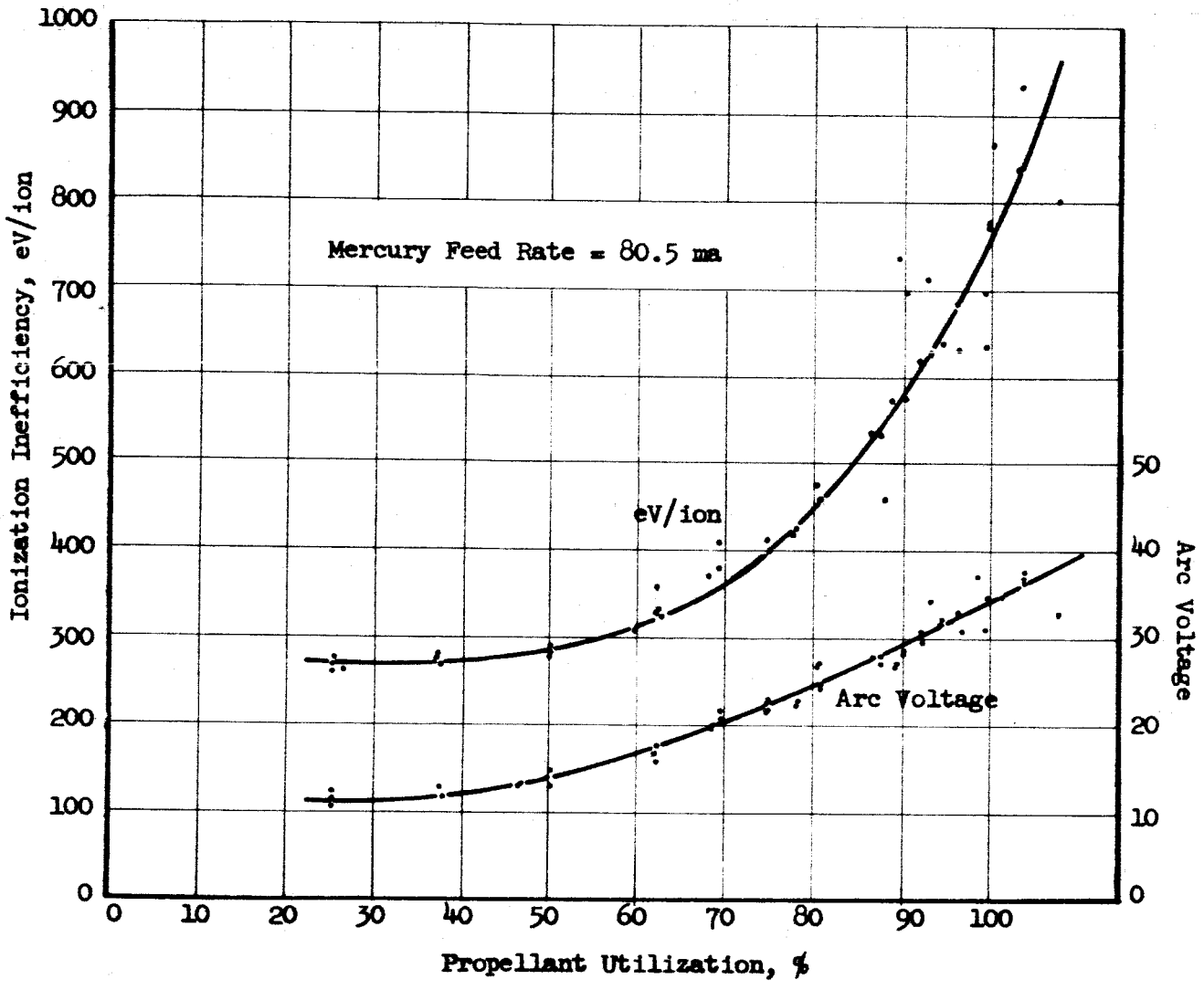

Figure 18

Ionization Inefficiency and Arc Voltage vs. Propellant Utilization for a Mercury Feed Rate of 80.5 ma.

Figures 19 and 20 show the engine power efficiency, excluding the electromagnet power, as a function of propellant utilization for two different mercury flow rates. For both flow rates the power efficiency shows a maximum value of about 78 per cent in the 80 to 85 per cent utilization range. It is anticipated that the maximum efficiency can be increased and moved to higher utilization values by operating with an extraction system that has not been damaged by arcing. It was found after termination of the testing that arcing had melted a portion of the accel electrode and that the reshaping of the electrode resulting from solidification of the melted material had produced a constriction of the accel channel. Thus, in order to focus through the narrowed channel, higher accel voltages were required. Since 19.5 kv represents a safe upper limit above which considerable arcing is encountered, it was found for 19.5 kv of accel voltage that minimum accel interception occurred at 85 per cent utilization for 70.5 ma equivalent mercury flow and at 80 per cent for 80.5 ma Hg flow. For higher utilization, the increased beam spreading results in higher interception values. Figures 21 and 22 present the accel interception versus propellant utilization for the two flow rates. The increased interception in the 90 per cent range was due not to charge exchange but to beam expansion resulting in direct impingement occurring at the exit end of the accel channel. Because of the location of the direct impingement, it is anticipated that any resulting secondary electrons did not go back to the source, but rather went to the decel electrode. Hence, these electrons, if present, did not result in an erroneously high measurement of propellant utilization. For utilization values below that for minimum interception, Figures 21 and 22 display the linear dependence as was predicted by assuming that the measured accel electrode current was due only to charge exchange occurring in the potential well of the accel electrode.

As a check on the internal consistency of the current measurement to the various electrodes a plot of the total current detected at the extraction system electrodes, the calorimeter, and the shield was determined as a function of the measured current from the source; this plot is shown in Figure 23. It is seen that the maximum deviations were less than three per cent which is within the accuracy of the meters.

It was decided at this time not to use stainless steel in future fabrication of extraction systems because of its relatively low melting temperature. It was believed by appropriately shaping tantalum sheet metal, that sufficient rigidity could be obtained. Thus, because of the relatively high melting temperature of tantalum accidental arcing would not produce the severe changes of geometry as were experienced using stainless steel.

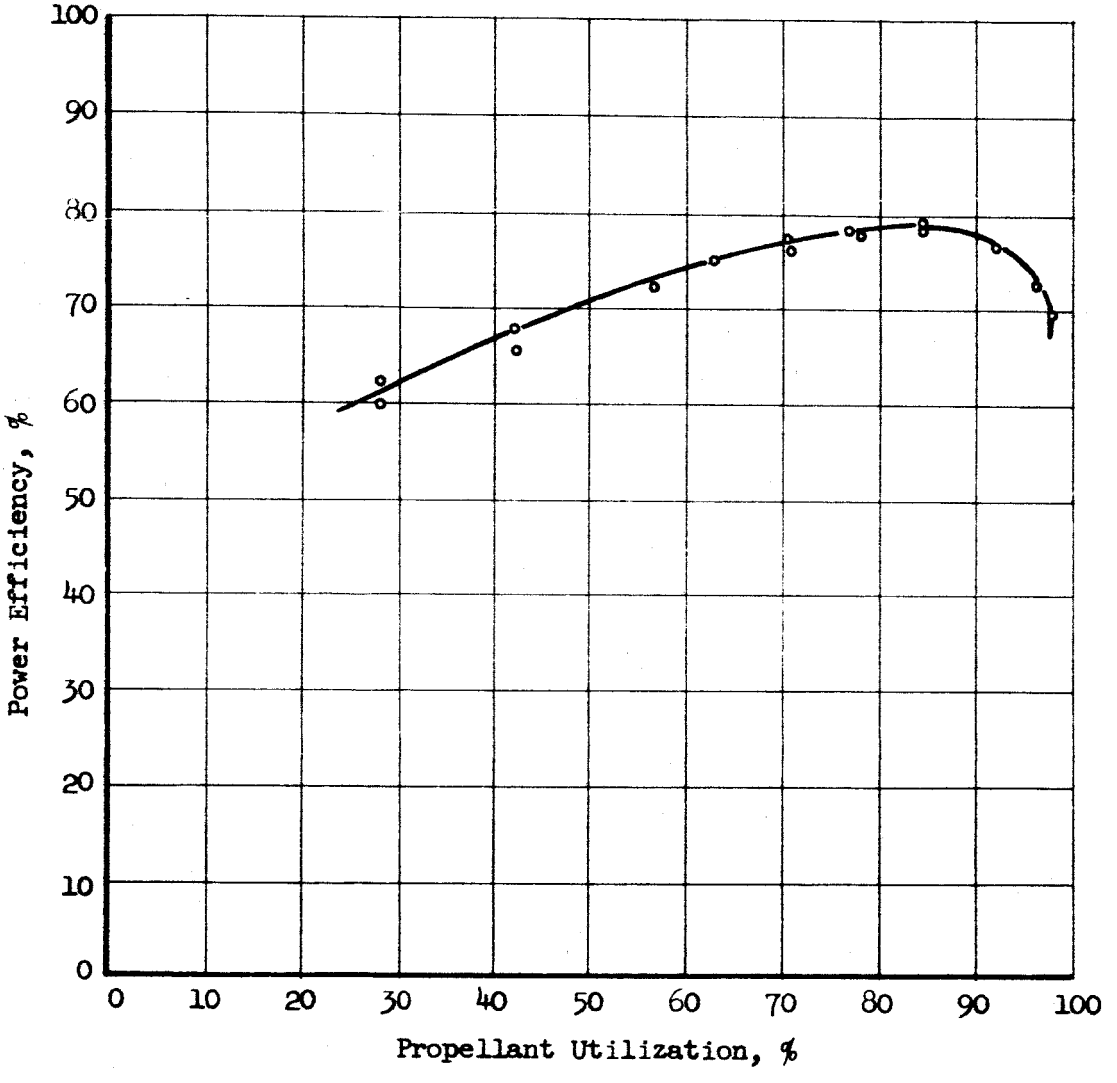

Figure 19

Engine Power Efficiency vs. Utilization for a Mercury Feed Rate of 70.5 ma Equivalent

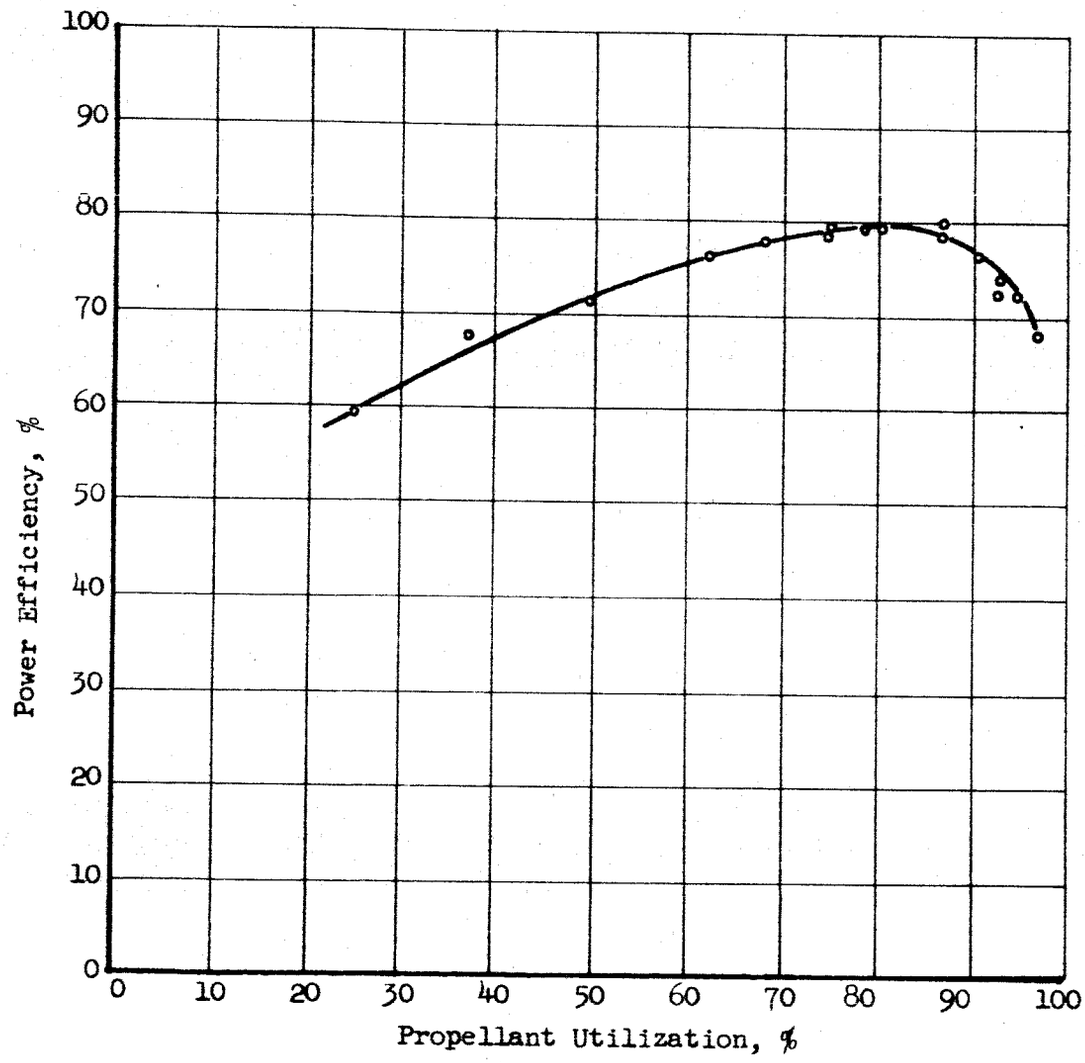

Figure 20

Engine Power Efficiency vs. Propellant Utilization
for a Mercury Feed Rate of 80.5 ma Equivalent

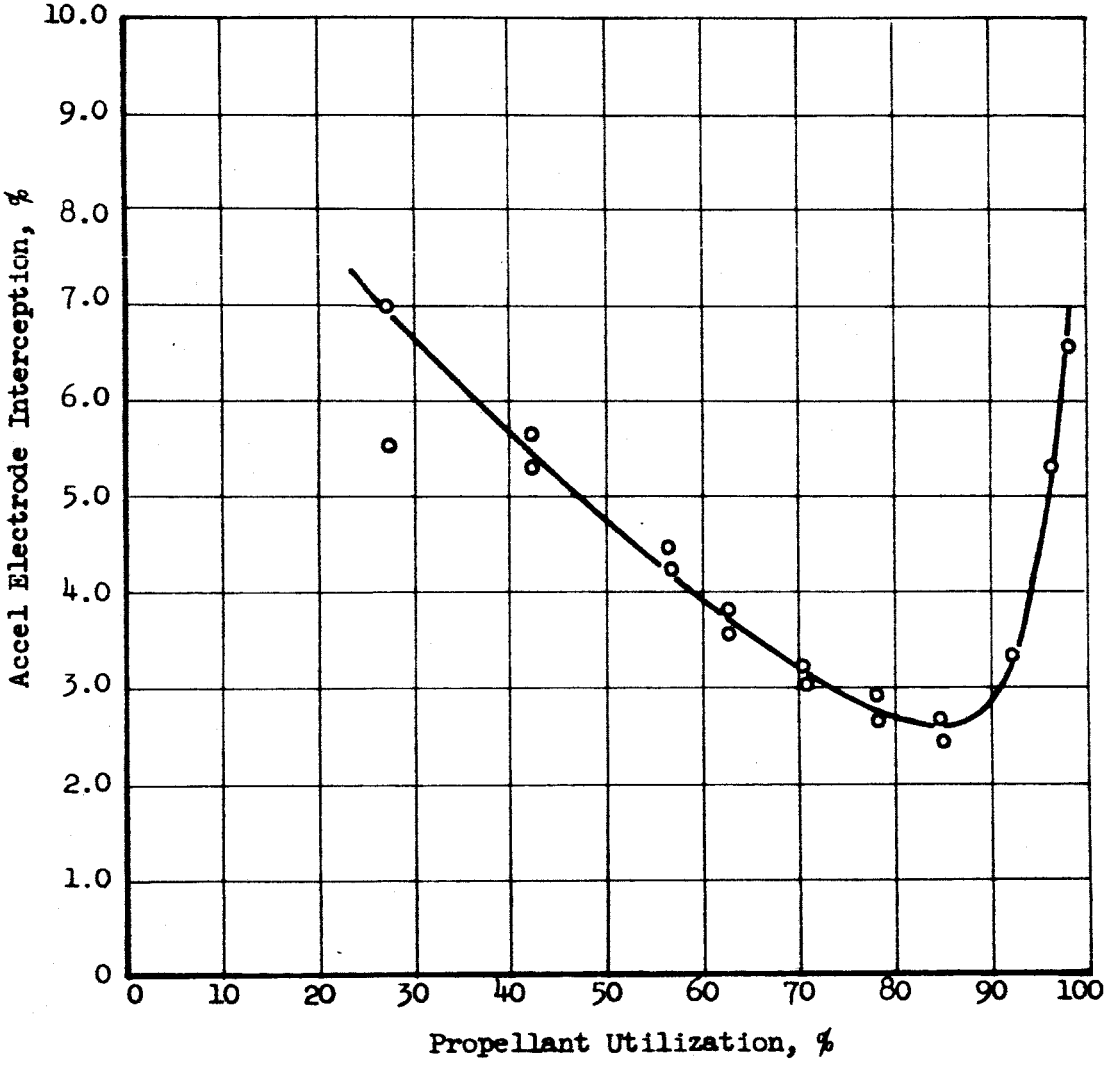

Figure 21

Accel Electrode Interception vs. Propellant Utilization for a Mercury Feed Rate of 70.5 ma Equivalent

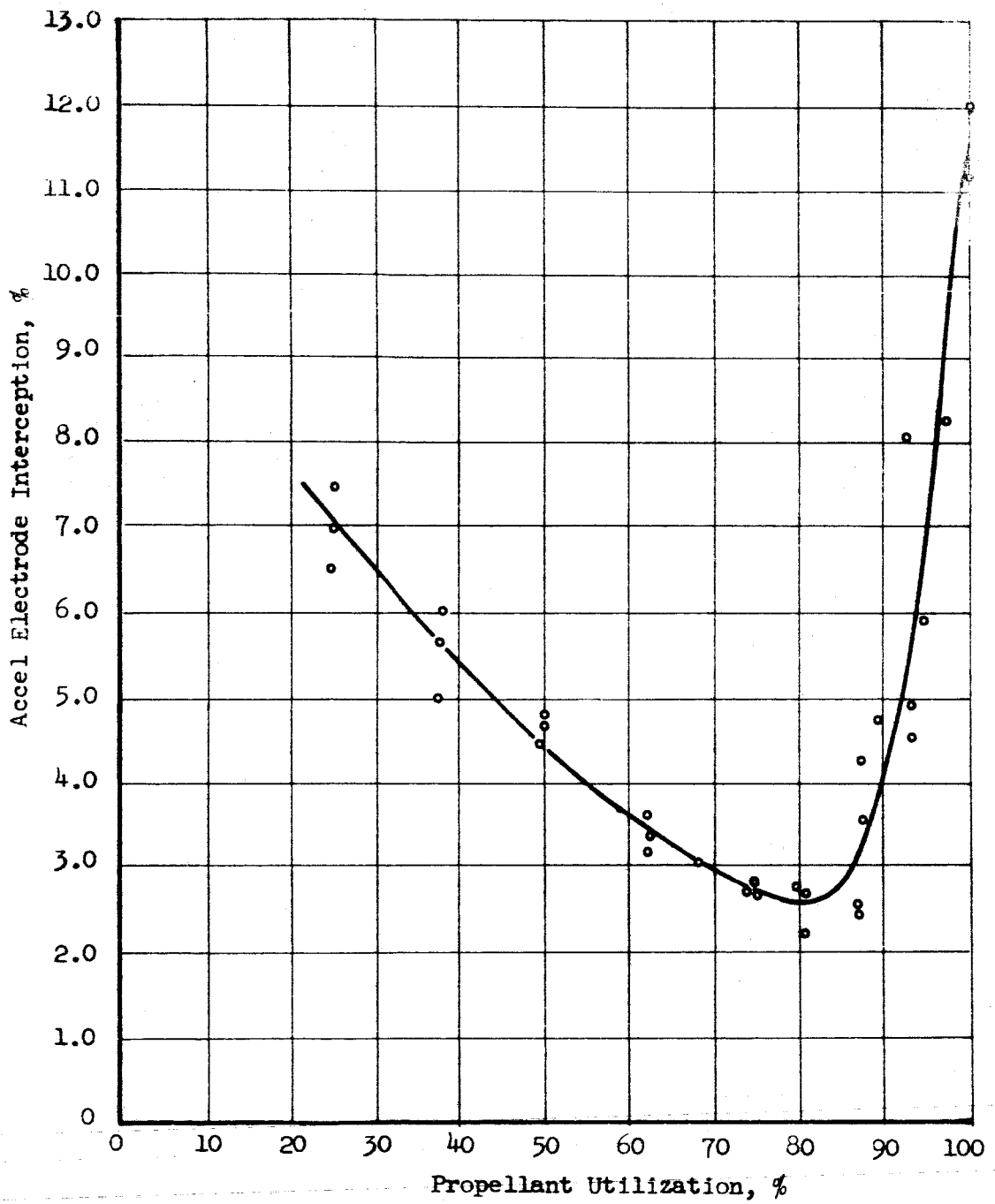

Figure 22

Accel Electrode Interception vs. Propellant Utilization for a Mercury Feed Rate of 80.5 ma Equivalent

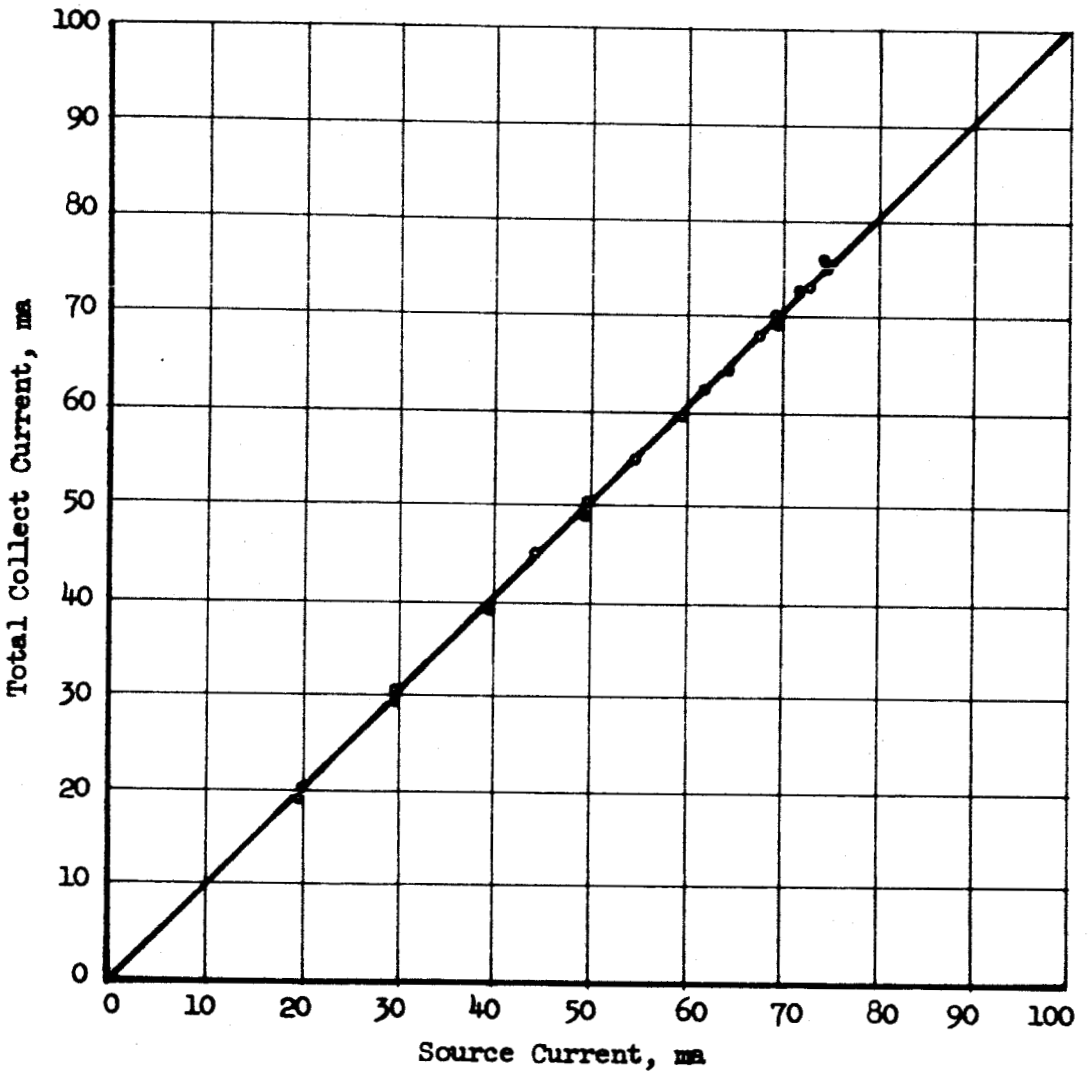

Figure 23

Source Current vs. Total Collected Current

Having obtained favorable engine performance utilizating electromagnets it was decided, in accordance with contractual obligations, to convert the magnetic focusing electromagnet engine to permanent magnet operation. The performance of the magnetic focusing permanent magnet engine is displayed in Figures 24 and 25. It is seen from the figures that for 90 per cent propellant utilization, the arc ionization efficiency is 625 eV/ion, the arc voltage is 36 volts, and the rocket efficiency is 66 per cent for a specific impulse of 8950 seconds. It is thus seen that the conversion to permanent magnet operation involves no fundamental difficulties and yields performance characteristics similar to those obtainable utilizing electromagnets.

At this point in the program some significant results were being obtained in the source development portion of the effort. Because of the implications of these results with respect to the overall engine development, it is appropriate that these results should be mentioned here.

Throughout the program, effort has been expended on investigating the performance properties of a permanent magnet source based on the electrostatic focusing design depicted in Figure 26. This is the source which displayed the favorable characteristics which were reported in Reference 1. Early in the present program, it was also believed that this source displayed excellent performance characteristics; however, the good performance was not reliably repeatable. Subsequently, after converting to a fast response vaporizer and accurately calibrating the positive displacement feed system it was found that the source as it existed was limited in propellant utilization to the range of 60 to 70 per cent depending on the feed rate. From past experience (Reference 1) such performance was indicative of the migration of low energy electrons directly to the anode without acquiring sufficient kinetic energy for ionization. The relative number of such low kinetic energy electrons was found to depend on the width of the cathode slit relative to the anode chamber width. The source performance for several values of cathode slit width, therefore, was determined and is presented in Figure 27. It is seen that as the cathode slit width is reduced from 2 mm to 0.7 mm, the performance of the source improves considerably. The anode chamber width was maintained at 2 mm.

It is evident that the narrow slit width yields the most efficient performance; however, cathode performance requirements become rather severe in that as the slit width is reduced the effective cathode emission area is also reduced. Higher emission current densities are, therefore, required necessitating increased cathode

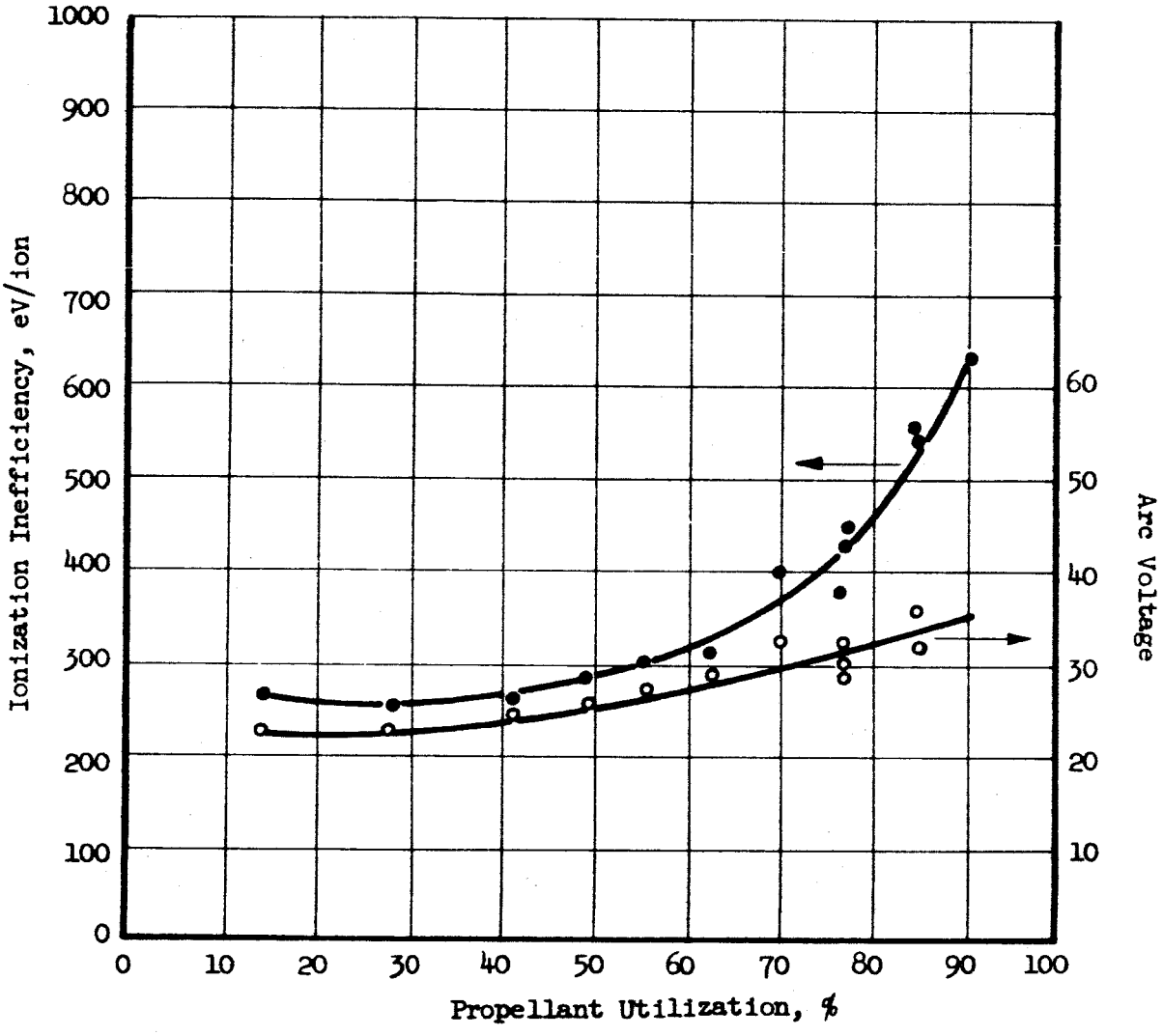

Figure 24

Ionization Inefficiency and Arc Voltage vs. Propellant Utilization for a Source Having a 2 mm Anode-Chamber Width

◦ 2 mm anode width

C 3 mm anode - power efficiency

□ 3 mm anode - rocket efficiency

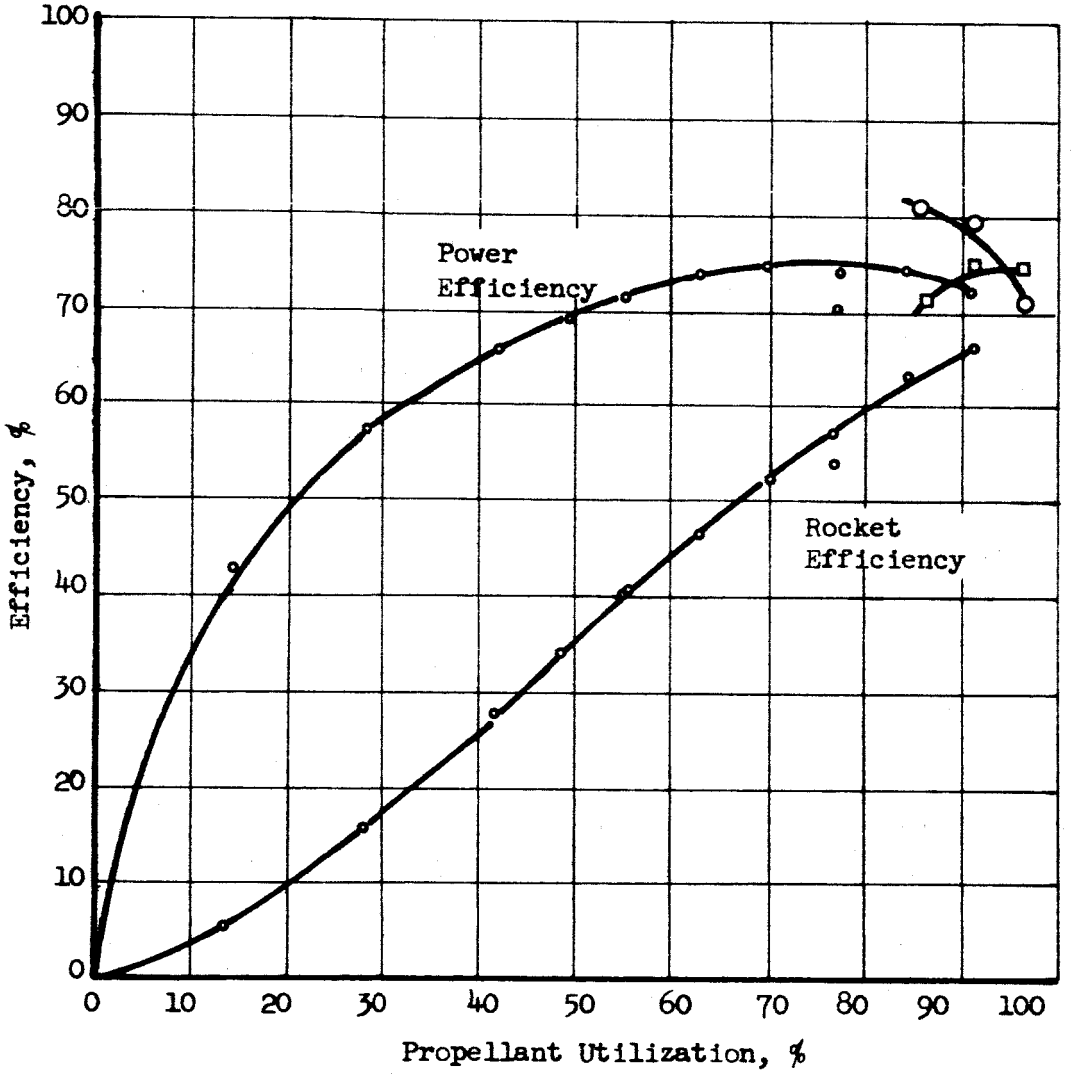

Figure 25

Power Efficiency and Rocket Efficiency vs. Propellant Utilization for a Source Having an Anode Chamber Width of 2 mm. Also Shown for Comparison are the Limited Data Points for a 3 mm Chamber Width.

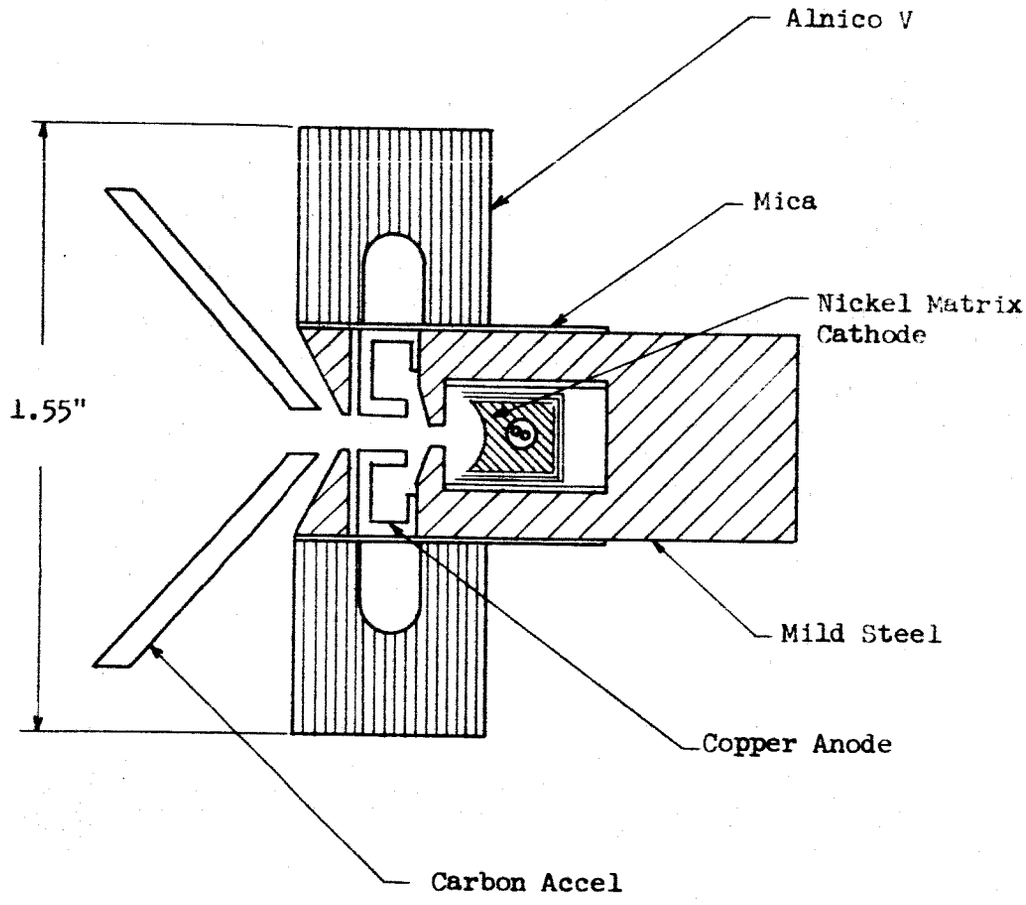

Figure 26

Cross Section of the Permanent Magnet Source which Utilizes Electrostatic Focusing to Direct Electrons to the Center of the Arc Chamber.

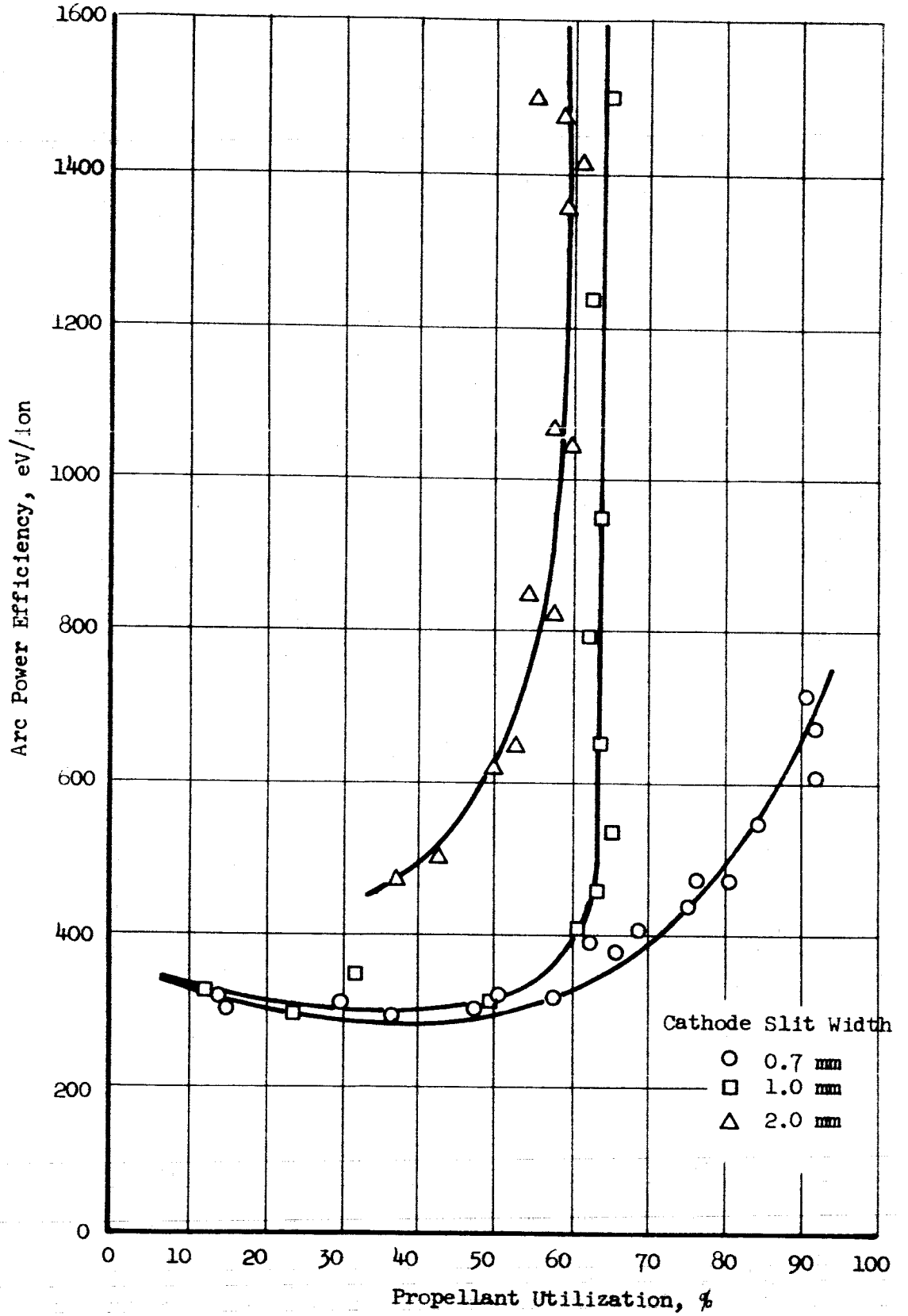

Figure 27

Performance of the Electrostatic Focusing Source for Several Values of Cathode Slit Width

temperature with the associated additional power loss. This situation may be avoided to some extent by scaling the engine to a large size, maintaining a suitable ratio for the anode chamber width to the cathode slit width. Preliminary thoughts concerning the effect of such scaling revealed that no fundamental obstacles should be encountered. It was anticipated that the total beam current would remain the same and since the frontal area depends primarily on the magnet size and not on the exit slit width, the thrust per unit area should not change appreciably. The reduction of current density should, however, reduce the charge-exchange rate. Thus, not only would the cathode lifetime be increased, but in addition, an increase in accel electrode lifetime should be realized.

The performance of the scaled-up engine is indicated in Figures 25 and 28. Comparing this performance with that indicated in Figure 24 for the engine having a 2-mm anode region width, it is seen that a significant improvement in engine performance resulted from scaling up the engine width. Not only was the rocket efficiency increased from 66 per cent to 72.5 per cent but the accel electrode interception at 90 per cent was also reduced from 2.5 per cent to 1.5 per cent, (see Figure 29) the arc voltage was reduced from 36 to 30 volts, and the cathode temperature (for the same cathode in both cases) was reduced from 2000^{+}°F down to the range 1750 to 1850°F. A substantial increase in lifetime, therefore, should be realized. This is the engine which was used in the life testing, the concluding portions of the program.

2.1.3 Computer Solutions

In the period preceding the start of this contract a computer program to aid in the design and analysis of the ion acceleration system had been written to run on the IBM 7070 at the Data Processing Center of TRW Equipment Group. This was begun under Contract NAS8-42. During the course of the present contract the computer program was modified and debugged. Due to symmetry, an acceleration system of the linear types under study is fully defined by its cross section perpendicular to the long direction of the source slit. For numerical representation in the computer and for computation, there is superimposed on the cross section a grid of mesh lines intersecting each other at mesh points; the computer stores and operates upon values of electrostatic potential and charge density corresponding to the locations of mesh points in the defining cross section. The computer program is more fully described in Appendix 1 of this report.

Computer runs were carried out for two electrode configurations. One configuration, used for checking out the program, was a source-accel geometry with the

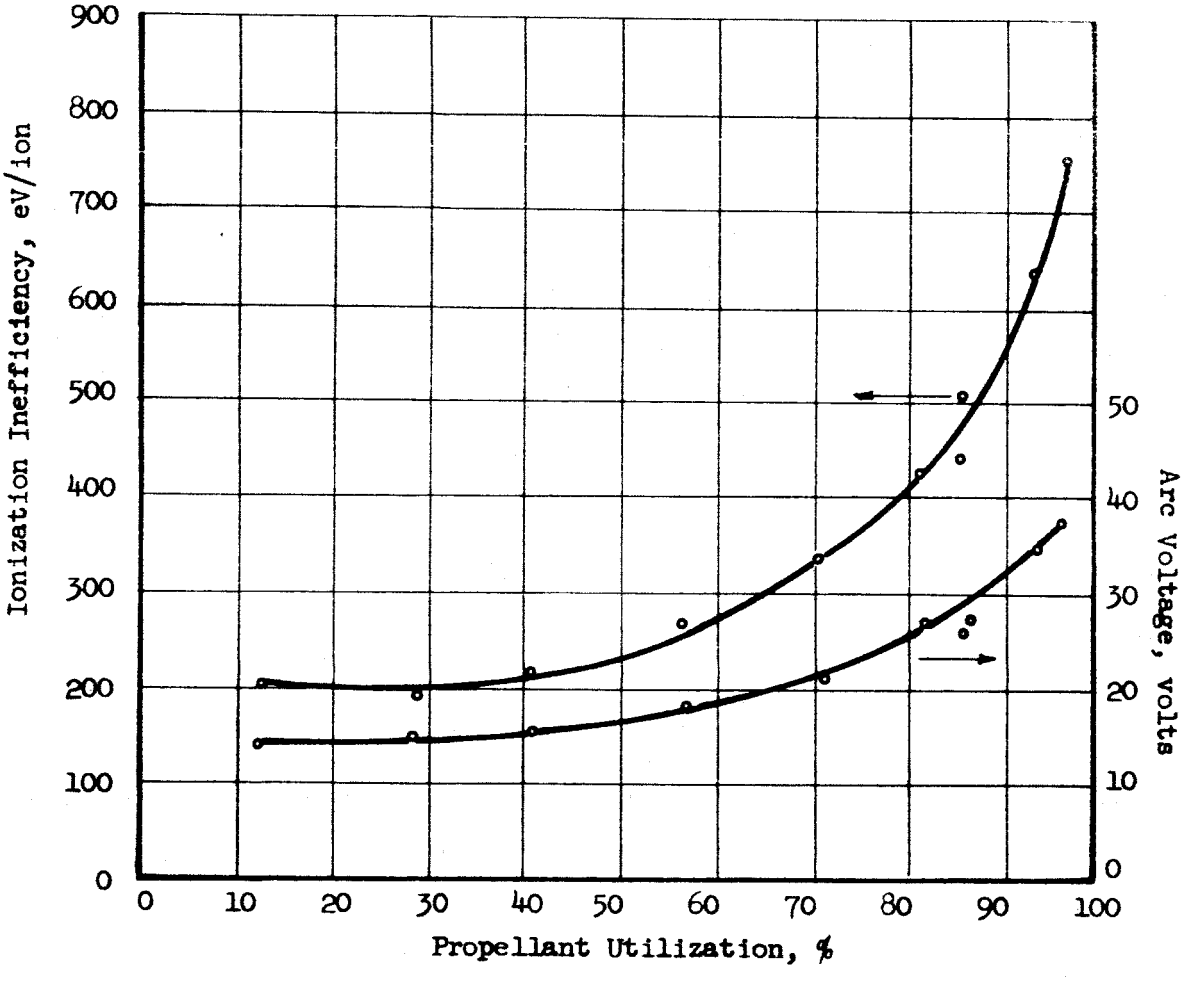

Figure 28

Ionization Inefficiency and Arc Voltage vs. Propellant Utilization for a Source Having an Anode Chamber Width of 3 mm.

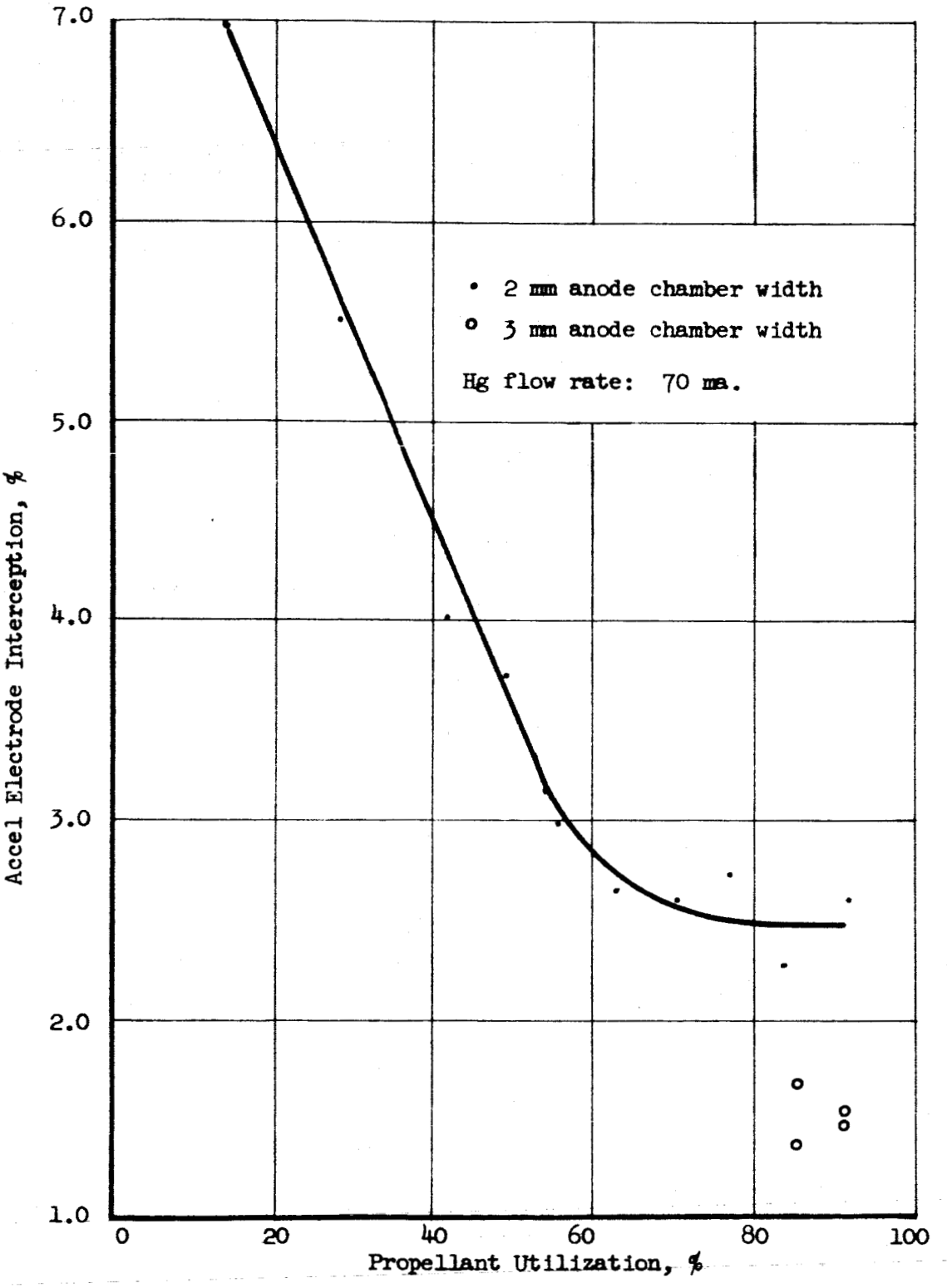

Figure 29

Percent Accel Electrode Interception vs. Propellant Utilization for the 2 mm Anode Chamber Width. Also Shown is the Limited Data for the 3 mm Anode Chamber Width.

plasma-ion interface (the meniscus) represented by a straight line across the opening in the source. A pair of decel electrodes was included in the second configuration, and a concave meniscus was assumed. This configuration was suggested by experimental results which were then available and is illustrated in Figure 30. Two cases were evaluated using the computer. One was for an accel electrode voltage of -10,000 volts and a decel electrode voltage of -2,500 volts relative to the source; the other was for an accel voltage of -15,000 volts and a decel voltage of -7,500 volts. The solutions for these two cases are treated in the paragraphs below.

Case I (-10, -2.5 kv). The final solution that was obtained by the computer for the configuration of Figure 30 when the accel and decel potentials were set, respectively, at 10 and 2.5 kilovolts negative with respect to the source is probably the best solution to have been reached up to the present, in the sense that the computed beam shape and meniscus shape approached most closely those that would physically occur with the assumed conditions of beam current, electrode configuration, and electrode voltage. Earlier computer runs had solved accurately the flat meniscus case and cases of other meniscus shapes, but the flat meniscus solutions do not give strong enough focusing to represent properly a beam emerging from a slit; the runs with curved meniscus shapes had previously assumed, as input, a flat distribution of current along the width of the source slit.

The computed beam and meniscus shapes for the -10, -2.5 kv solution are presented in Figure 31. The ion beam focuses somewhat and then spreads widely at this low accelerating voltage. At the downstream end, the accel channel is almost completely filled by the beam, which then impinges on the decel electrodes. The lack of conformity of the beam to the channel was anticipated, since the channel contour (a parabola) had been established with a 15 kilovolt accelerating potential difference in mind. For 10 kilovolts the accel channel should be shortened and re-contoured. The computed meniscus shape is shown as a rough succession of line segments because the computer was programmed only to determine the meniscus position to within one mesh length (the distance between adjacent mesh points). Analysis of the trajectories of beam ions in the computer output for this solution indicates that the roughness of the computed meniscus had only a small effect on the beam shape, causing it to spread more widely than it should.

One objective of this computer run was to study the effect of the decelerating electrode in bringing about refocusing of the ion beam. Study of the beam ion trajectories shows a very slight, insignificant refocusing effect. Only about

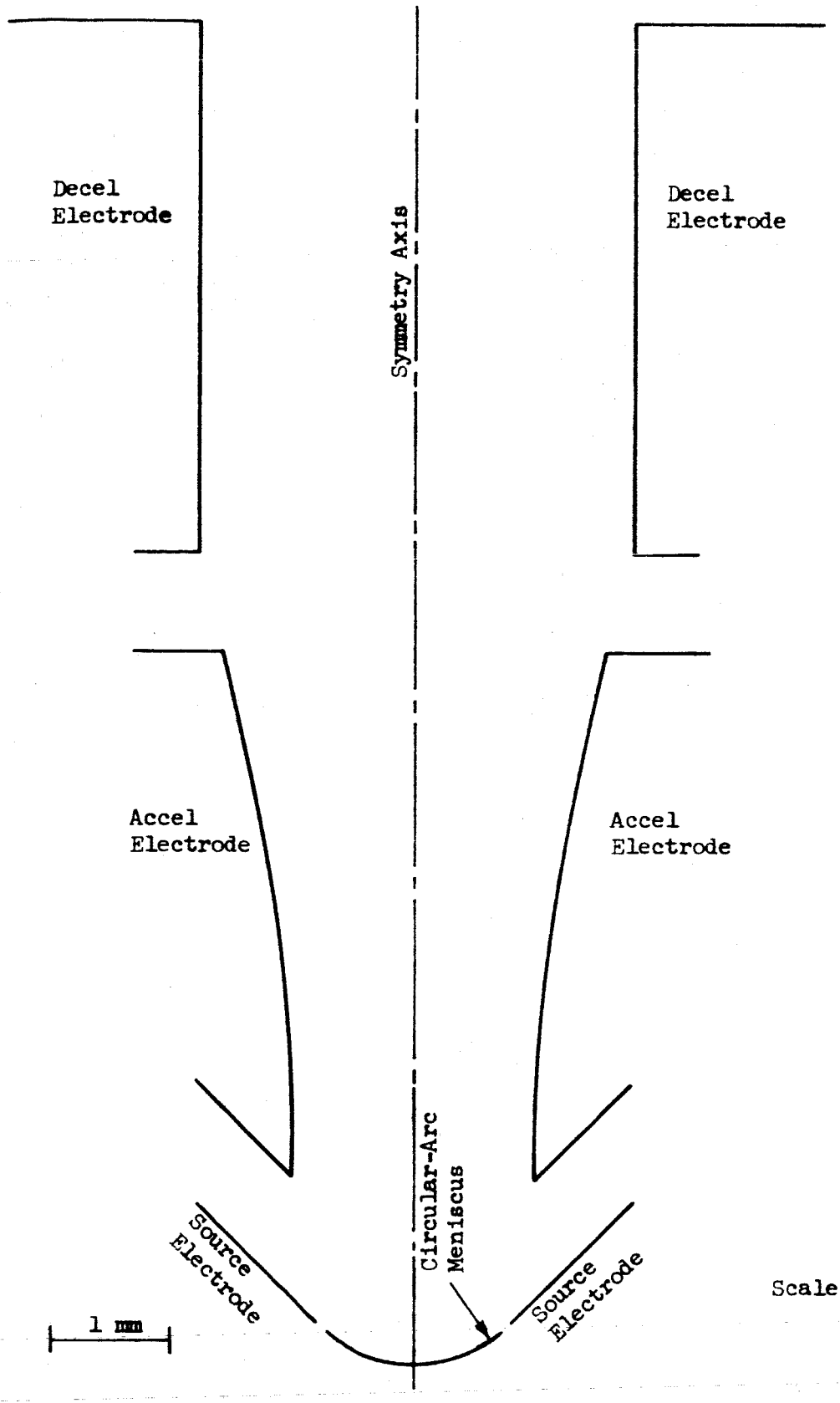

Scale: 3/4" = 1 mm

Figure 30

Cross Section of Electrode Configuration for Computer Evaluation

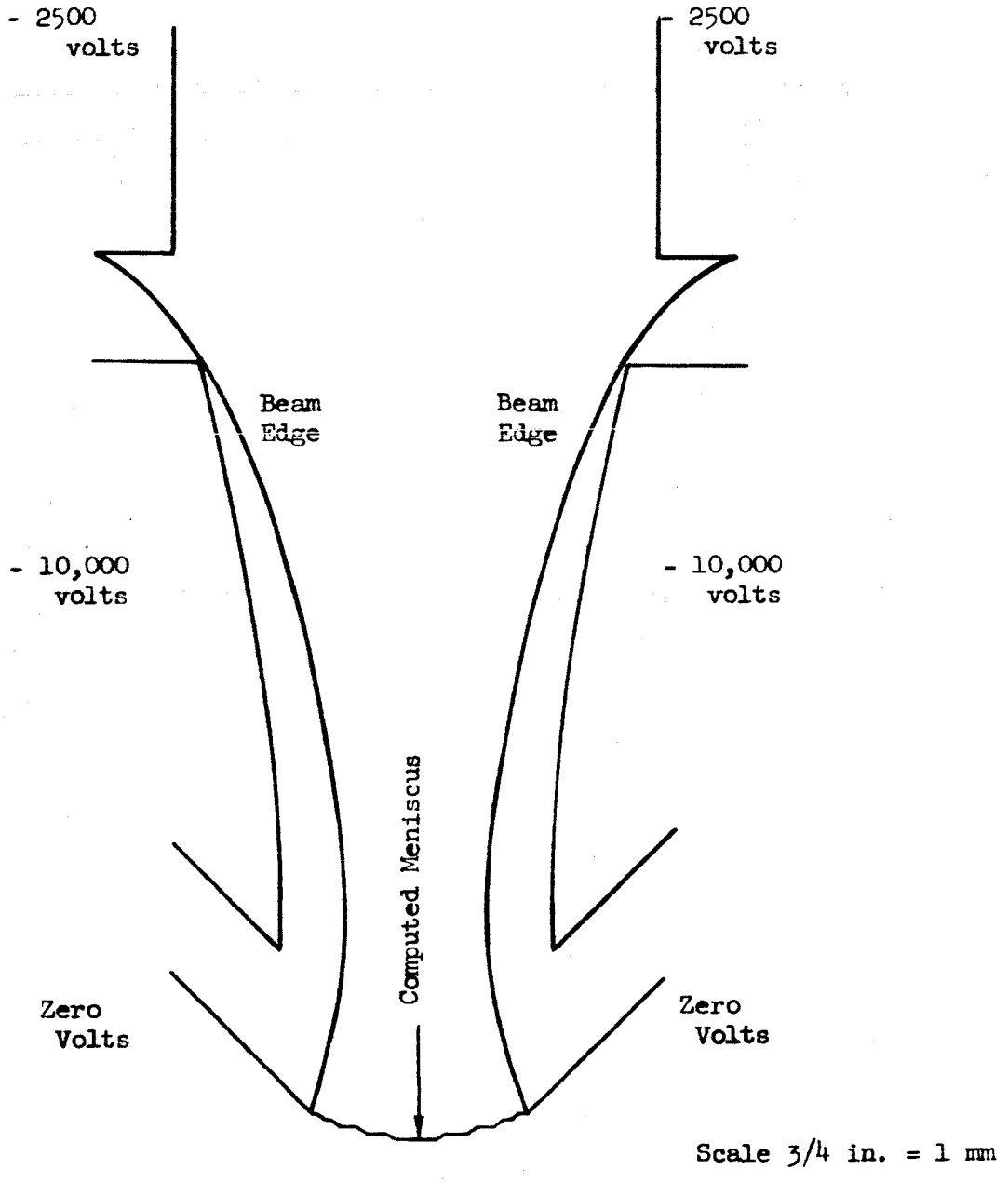

Figure 31

Computer Solution for Case I

40 per cent of the beam current reached the downstream end of the decel channel, the remainder being intercepted. The conclusion can be drawn that the decel electrodes ought to be made as short as possible. The function of the accel-decel gap is primarily not to refocus the beam but to prevent backstreaming of electrons from the neutralizer into the source.

A number of charge-exchange ion trajectories were generated by the computer for this solution, employing a selected set of creation locations (i.e., points from which the trajectories start). No sputtering erosion rates were calculated for this case; nevertheless, it was observed that the tips of the accel electrodes, where the precise shape and position are most critical, receive a very small proportion of the total number of charge-exchange ions that are formed. This observation was borne out by the more complete erosion studies for Case II.

Case II (-15, -7.5 kv). The final solution reached when the accel and decel potentials were set, respectively, at 15 and 7.5 kilovolts negative with respect to the source displays strong focusing. This is illustrated in Figure 32. It is apparent that the accel electrodes could safely be brought considerably closer together without encountering direct beam impingement.

This solution exhibits also one effect of the roughness in the computed meniscus shape. The steep outer slopes of the central convexity caused certain beam ion trajectories in the computed solution to diverge more than the other trajectories, and the beam shape was significantly affected as a consequence. If the convex portion of the meniscus had been smoother (and there is even some doubt that it should be there at all), then the diverging portion of the beam would have been narrower, and it might have passed cleanly through the decel channel.

The extent to which the beam is refocused by the decel electrodes is barely visible in Figure 32, and bears out the remarks made for Case I; the change in angle due to refocusing in this case is not more than about one degree.

For Case II, after a selected set of charge-exchange ion trajectories on the computer was generated, a calculation of the relative erosion rates along several portions of the accel electrodes was carried out. The channel face of an accel electrode was partitioned into four segments, and the inter-electrode regions were correspondingly partitioned in such a way that charge exchange ions created in any sub-region would land somewhere on the corresponding segment. Figure 33 shows the manner of partitioning the accel electrodes into segments; also shown are the major regions in the ion beam where charge-exchange ions are created that

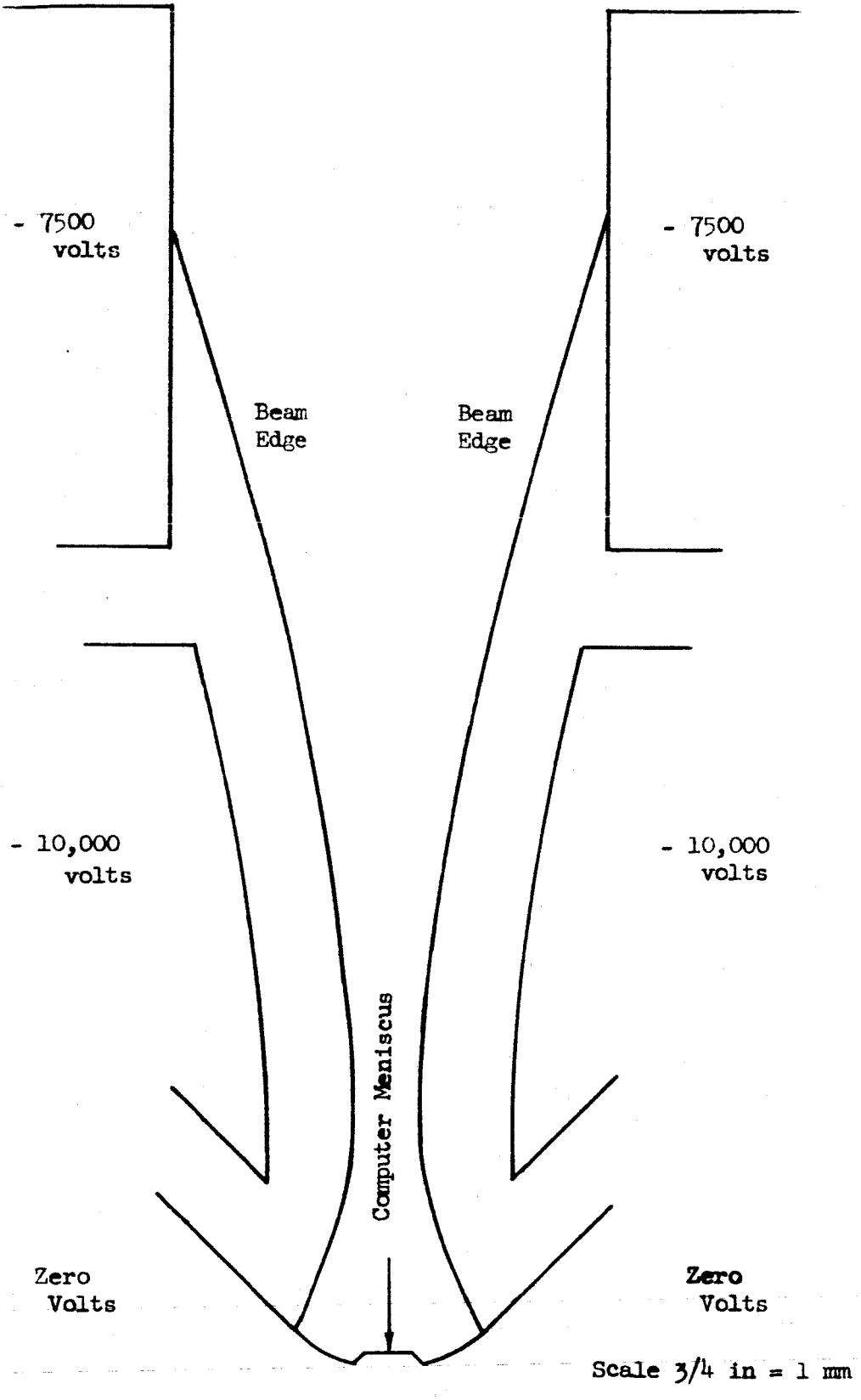

Figure 32

Computer Solution for Case II

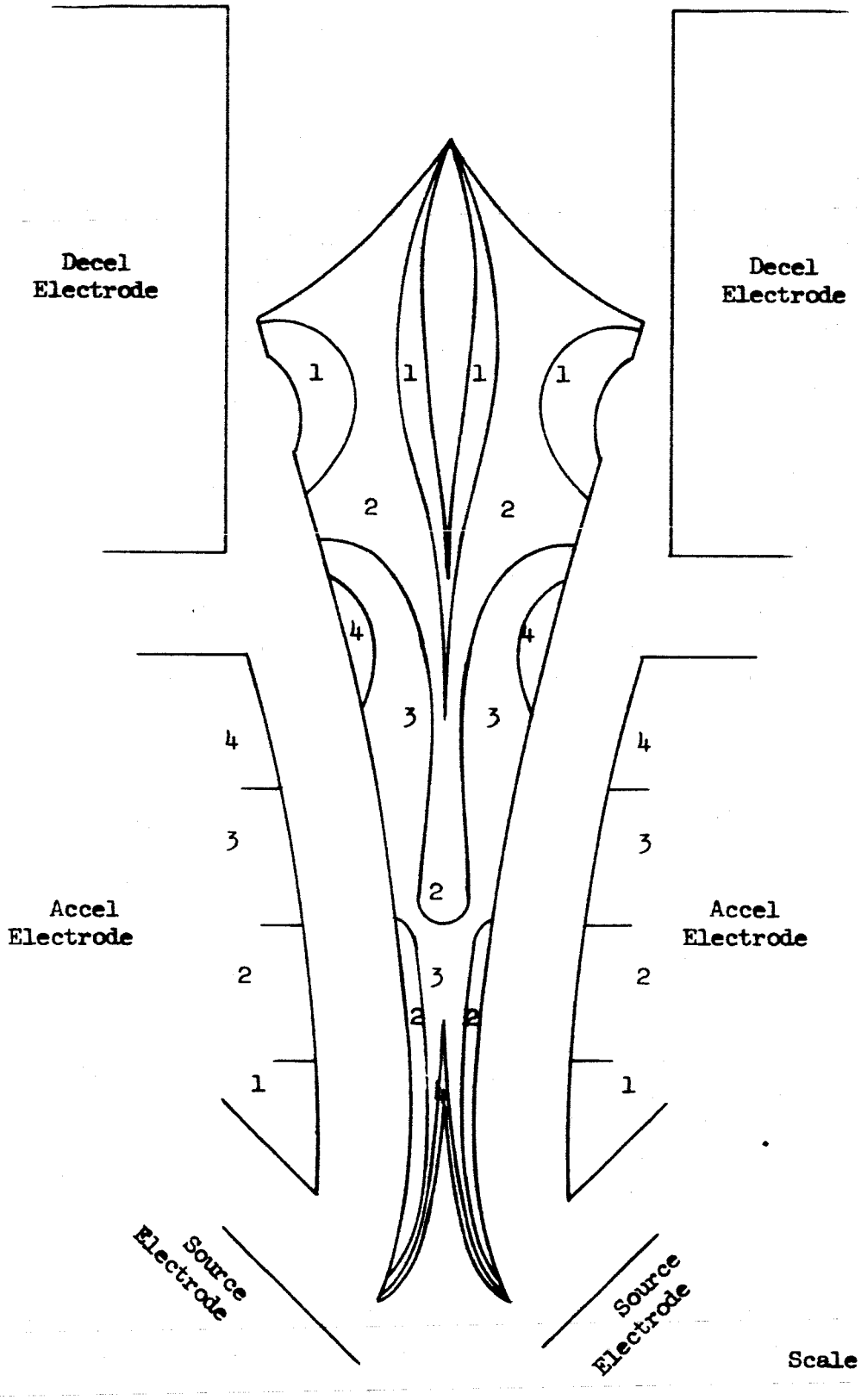

Figure 33

Major Regions of Ion Beam Contributing
to Accel Electrode Sputtering
Through Charge Exchange Ion Generation

cause erosion on the accel segments. The correspondence between the sub-regions and the segments is given by the numbering in the illustration with the additional remark that none of the charge-exchange ions created in the numbered sub-regions cross the symmetry axis.

The sputtering erosion rates based on the partitions described above included only the sputtering due to charge-exchange ions. A more complete treatment would have included the effect of charge-exchange neutral atoms (which before the charge exchange collision were beam ions). In a long accel channel these neutrals may increase the erosion rate on the downstream segments of the electrodes.

The calculation yielded these results:

Accel Segment	Relative Rate of Erosion
1	16%
2	45%
3	25%
4	14%

As these results show, the erosion rate is greatest near the middle of the channel (perhaps peaking about one-third of the way from the electrode tips). Since the precise contour in the most affected segments is not important in shaping the ion beam, a possible way of spreading this sputtering damage over a larger area is to hollow out this portion of each accel electrode; such a procedure could have the further benefit of allowing many of the sputtered atoms to recondense within the hollowed-out portion.

2.2 Source Studies

2.2.1 Introduction

Throughout the course of the program two source designs were under investigation. One design referred to as the magnetic focusing source was used primarily to study extraction phenomena. The magnetic field for this source was provided by electromagnets throughout most of the program; conversion of this source to permanent magnet operation was accomplished prior to life testing. The other design referred to as the electrostatic focusing source has been used for the study of the permanent magnet source. Until late in the program, the performance of the two sources was vastly different with the magnetic focusing design generally displaying superior charcteristics. Previous to the commencement of this

contract effort, it was believed that the performance of the two sources was about the same with the electrostatic focusing source being somewhat superior. The final status is that the two sources again display approximately the same performance; however, the magnetic focusing engine appears to be slightly superior. The efforts necessary to lead up to this status were many; the main ones were as follows:

1. Determining the influence of the cathode slit width and selecting the optimum value.
2. Determining that all appropriate components of the source are maintained at a sufficiently high ambient temperature to insure that no mercury condensation results in a reduction of net mercury feed rate and later, if the ambient temperature increases, provides an additional mercury feed yielding the possibility of greater than 100 per cent propellant utilization.
3. Improving the design of the mercury vaporizer to decrease its response time from hours down to seconds thus enabling the establishment of equilibrium conditions within minutes after changing the mercury feed rate and also enabling the immediate observation of flow rate variations due to external disturbances of the feed system.
4. Observing and reducing the variations in the feed rate due to imperfect mechanical alignment and room temperature fluctuations.
5. Improving the cathode performance such that reliable operation over a range of temperatures can be obtained for many days of engine testing.
6. Determining the effect of cathode position and selecting the optimum position.

2.2.2 Source Chronology

The initial source studies were directed towards determining the characteristics of the 5-cm long permanent magnet source established late in the effort under Contract NAS8-42. The cross-section of this source is shown in Figure 26. Initial studies were considerably impeded due to a cathode heating problem encountered when going from a one-inch to a two-inch length of cathode. The problem due to the increase in necessary heater power was that the required filament temperature limited the filament lifetime to less than ten minutes. Two measures were taken at that time. The first was to improve the thermal contact between the heater and the cathode by utilizing swaged heaters. For expediency and experimental flexibility the heaters previous to this time were made from two-hole Al_2O_3 tubing through which was threaded a tungsten wire filament. Since

the wire size was usually less than the hole size poor thermal contact was inherent in this design. The second measure was to improve the cathode shielding or insulation. It was found in a source mock up that by placing thick layers of Al_2O_3 powder between the nickel foil heat shields of the cathode that the conductive loss through the shielding was considerably reduced. However, this design was not suitable in the source itself because of the difficulty in outgassing the powder layers between the radiation shields. The use of the Al_2O_3 powder was, therefore, terminated. The improved thermal contact provided by the swaged heaters, however, sufficiently reduced the filament temperature (in spite of the poor cathode shielding) to allow the daily operation of the cathode for as long as one week.

The characteristics of the two-inch permanent magnet engine obtained early in the program are shown in Figure 34. This early performance data, however, had large uncertainties associated with it. Particularly, the uncertainties with respect to the mercury feed rate may have been as high as 100 per cent although at that time the magnitude of this uncertainty was not known.

At this point, it became evident that the cathodes which had been developed were not as reliable as anticipated. Earlier, upon switching from the use of double carbonate to the use of triple carbonate as the emission mix material, both 20 per cent by weight in the nickel matrix cathode, a drop in the necessary cathode temperature from 1850°F down to 1600°F was experienced. It was, therefore, prematurely concluded that the attainment of suitable operating characteristics had been achieved. However, later cathode material, fabricated in the same way, turned out to have poor emission properties. Because of the importance of dependable cathode performance on the significant testing of the source and the extraction system it was decided to delay the source testing and make a concentrated attack on the cathode problem. A detailed discussion of the cathode development program may be found in Section 2.3.

The source study was resumed after a delay of approximately five months, during which time the cathode development program had yielded improved cathode performance and study of the mercury feed system had resulted in design modification leading to a system of short response time having a reduced sensitivity to room temperature fluctuations (see Appendix 4). The performance of the permanent magnet engine which utilizes electrostatic focusing had not been well established until this time in the program and the unexpected results were that the source displayed considerably poorer utilization and efficiency than expected. It was found that the propellant utilization limited to values less than 100 per cent,

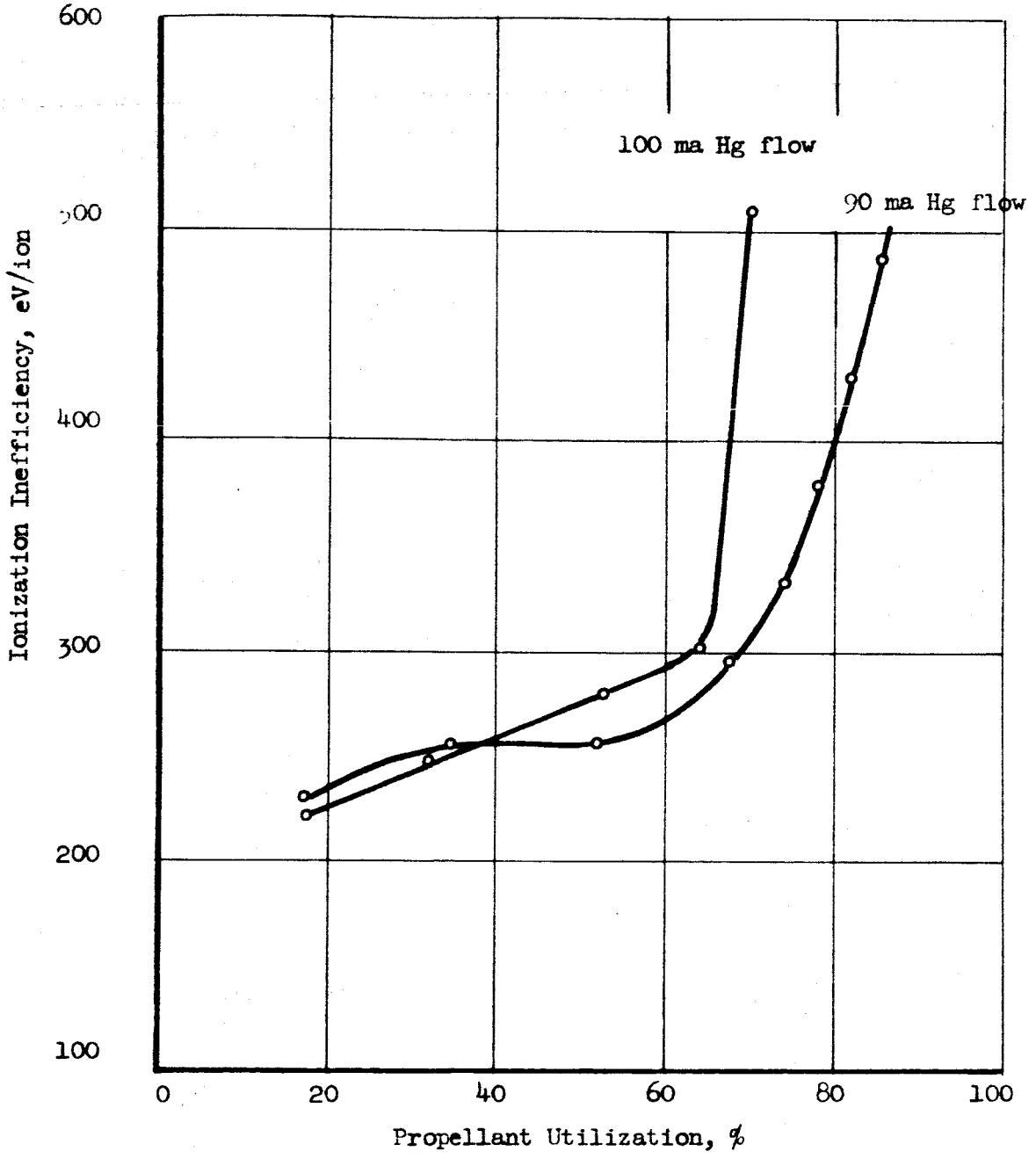

Figure 34

Ionization Inefficiency vs. Propellant Utilization

the limiting value depending on the mercury flow rate. This type of performance was indicative of either excessive scattering of electrons resulting in a poor electron energy distribution or poor electron trapping in the anode region due either to improper magnetic field strength or the presence of transverse electric fields resulting from excessive charge density. In order to determine the effect of increasing the trapping efficiency by increasing the magnetic field strength, the source was modified to accept a permanent magnet which provided a 40 per cent increase in the field strength. For this increased field, no significant improvement of the source was observed.

It was, therefore, concluded that the limiting utilization was most likely due to an unfavorable electron energy distribution. Past experience had revealed that the relative number of low energy electrons was affected by the size of the cathode slit width relative to the anode chamber width. An investigation of the dependence of the source performance on the relative size of the cathode slit width was then undertaken. The results of this investigation have already been shown in Figure 27. It is seen there that marked improvement of the source performance is realized as the cathode slit width is reduced from 2 mm down to 0.7 mm, the anode chamber width being held at 2 mm.

Although the reduction of the cathode slit width improved the source performance with respect to increasing the propellant utilization and the ionization efficiency, it was found to adversely affect the arc characteristics and the cathode requirements because of the reduction of the effective cathode area requiring an increase in emission current density. The increased emission density was achieved by increasing the cathode temperature or operating at higher arc voltages. Both of these alternatives, however, tend to reduce the cathode lifetime, the increased voltage leading to increased sputtering and the elevated temperature leading to increased evaporation. In addition, the higher arc voltage increased the probability of producing double ionization. Because of a practical upper limit of 2000°F to the cathode temperature, based on the amount of power that can be transferred by the existing cathode heaters and based on the evaporation rate of nickel which exceeds that of the emitting material, it was found that the arc voltages of 30 volts or more were necessary in order to achieve propellant utilization values in the 90 per cent range. Thus, the cost of improving the source performance was an increased sputtering rate and the possibility of an increased double ionization rate. There existed, however, a possibility of avoiding this situation by scaling the engine to a size consistent with lower cathode temperature, and

lower arc voltage, i.e., requiring lower emission current densities. This scaling was in the direction of increasing the dimension of the engine relative to the cathode dimension.

Scaling up of the source was performed for the magnetic focusing source in conjunction with the engine testing portion of the program; the electrostatic focusing source was not scaled up because of a change in program emphasis which occurred at that time. The sequence of events was that the information concerning the pertinent geometric ratio obtained from testing the electrostatic focusing source was applied to the magnetic focusing source because this was the source which was being operated in a total engine (source plus extraction system). At this point in the program the emphasis was being directed towards total engine performance, while research leading to component (source alone) optimization was being deemphasized. There also existed the belief that component optimization without regard to the interaction of the component to the system may not lead to system optimization. Thus, at this point of time, the source development portion of the program merged with the engine development portion. Since the engine system which existed at this point included the magnetic focusing source and the performance of the existing system was promising, further work on the electrostatic focusing source was reduced to a negligible level. The results of scaling the source and engine have been discussed in detail in Section 2.1.2 and will not be further discussed here.

2.3 Cathode Development

2.3.1 Introduction

The cathode development work begun and reported under Contract NAS8-42 has been continued and extended. The major activity in this area has centered on sintered nickel matrix cathodes. Before describing the specific results obtained, it is appropriate to review briefly some of the more general requirements, characteristics, and problems inherent in cathodes suitable for use in bombardment ion engines. Cathodes for both arc or ionization chamber and neutralization are of interest. The requirements for the former are considerably more stringent than for the latter; consequently, the major portion of the discussion to follow will deal primarily with cathodes for use in ionization (arc) chambers of electron-bombardment engines.

Simply stated, the essential purpose of the cathode in an electron-bombardment ion engine is to provide a supply of electrons to the ionization chamber where they collide with and ionize the propellant atoms. For this ionizatien process

to occur efficiently, the electron emission must have certain characteristics. In a slit aperture geometry, for example, the emission should be spatially uniform over the cathode area so that the corresponding ionization is uniform along the entire slit length of the source; this in turn insures uniform extracted ion current densities and minimizes locally excessive electrode current drains and undue extraction system wear.

Clearly then the cathode behavior is seen to exert a strong influence on the engine performance. This becomes even more obvious when it is remembered that the cathode consumes power and represents a limitation on engine efficiency. Suitable cathodes, therefore, combine a variety of characteristics, including:

1. Emitted current densities of several amperes/cm^2 at reasonable temperatures (near 1700°F).
2. Uniformly emitted current over the cathode area.
3. Constant emissive properties in time over extended periods of operation (i.e., long life).
4. Reliable, reproducible, and predictable operation.
5. Ease of activation.
6. Resistance to sputtering.
7. The attainment of all of the above characteristics in the environment of an operating engine.

The basic cathode emission process consists of freeing electrons from the surface of the cathode. To do this requires the expenditure of work, the measure of which is the "work function". This work function can to a large extent be controlled during the cathode fabrication process; that is, a properly fabricated cathode can be made to emit electrons with a minimum energy expenditure by having a low work function. This behavior is described by Richardson's equation, viz.,

$$j_s = A_R T^2 \exp\left(-\phi/kT\right) \qquad (5)$$

where j_s is the saturated (temperature limited) current density, A_R is Richardson's constant, ϕ is the work function, T is the absolute temperature and k is the Boltzmann constant. From the above equation, it is clear that for a fixed temperature which implies a fixed energy input to the cathode, the emitted current density may be increased for a decreased value of work function. The goal of the cathode program described herein, therefore, was to develop cathodes with sufficiently low work function and sufficiently high value of Richardson's constant so as to yield

adequately high emitted electron current densities with a sufficiently low investment of heating power; such performance was to be obtained while maintaining the other desired characteristics listed above.

The traditional method of lowering the work function of a metal so as to enhance electron emission for a given temperature has been to provide a surface layer coverage on the cathode, the coverage usually consisting of a thin layer of the oxides of barium, strontium, and calcium in appropriate ratios. Usually these oxides are introduced in the form of their carbonates which are subsequently dissociated as follows:

$$(Ba, Sr, Ca)\ CO_3 \rightleftharpoons (Ba, Sr, Ca)\ O + CO_2 \qquad (6)$$

This is followed by the reduction of a portion of the oxide by the addition of an appropriate reducing agent to yield the metal, since it has been found that a small admixture of the metal with its oxide yields the lowest value of work function. The carbonates may be introduced to the cathode base metal as a coating or may be impregnated into a porous matrix of the base cathode material; the cathodes resulting from the latter method are termed "porous matrix" cathodes. The work here reported has dealt exclusively with porous matrix cathodes in which a commercial emission carbonate mixture is distributed throughout a sintered nickel matrix. Relative to other proposed cathode types, the nickel matrix cathodes have been shown to recover better from sputtering damage and other accidental situations, can provide higher operational reliability, and can operate at high partial pressures of gases which would poison the emission of other types of cathodes (Reference 6). Furthermore, the matrix cathodes activate well and compare favorably on a current density at equal temperature basis.

2.3.2 Cathode Fabrication

The sintered nickel matrix cathodes studied under this program were fabricated using standard powder metallurgical techniques. With some minor variations, the fabrication procedure has been to thoroughly mix carbonyl nickel powder (4 to 7 micron particle size), a commercial mixture of alkaline earth carbonates (G.E. No. 118-5-2), and a reducing agent (if used) in a ball mill. The mixture is then hydrostatically pressed into slugs at 36,000 psi and then sintered. The sintering process forms the nickel matrix through the high temperature bonding of the individual particles and also serves to change much of the carbonates to oxides. The sintering process is a crucial step in the determination

of the properties of the resultant cathode. Because of this, variations in the sintering schedule were studied, including time and temperature effects and the environmental effects of vacuum versus a hydrogen atmosphere. These will be discussed in more detail below.

Initial consideration of the sintering process reveals that two important processes occur. The first is the sintering itself and the second is the decomposition of the Ba, Sr, Ca, carbonates to form the oxides upon releasing CO_2. The degree of sintering, which determines the structural properties and the porosity of the cathode structure, is determined by the sintering temperature and the time maintained at the sintering temperature. If the sintering has not proceeded to a sufficient degree then the cathode material is of high porosity, is soft, and breaks easily while machining. If the sintering is allowed to proceed too far then the machinability approaches that of solid nickel and the porosity of the material becomes so low that the cathode activation time becomes excessive. Thus, the degree of sintering determines the machinability as well as the porosity or the length of the activation time. On the other hand, the desired activation time depends on the use of the particular cathode. For example, the initial developmental testing of an ion engine system is expedited if the cathode activation time is short, while for engine lifetime testing a cathode having a long activation time is required since cathode lifetime is in the first approximation proportional to the activation time providing excessive sputtering is not encountered. Thus, the intended use of the particular cathode determines the necessary degree of sintering.

The second process occurring during sintering is the carbonate decomposition described in Equation (6). Not until these reactions proceed completely to the right is it possible for the cathode to have good emission characteristics, since the presence of the carbonate is poisonous to the emitting surface. This poisoning effect has been observed in this laboratory as well as in others.

Upon examining the processes of importance during sintering it becomes apparent that the sintering environment is unimportant as long as it is inert and capable of removing the CO_2 as fast as it is evolved. Thus, it was anticipated that the standard procedure of sintering in a hydrogen atmosphere should produce the same cathode characteristics as resulted by sintering in vacuum employing an induction furnace. Sintering was performed in a hydrogen atmosphere at atmospheric pressure and in a vacuum at 10^{-4} torr for various cathode compositions and the resulting emission characteristics investigated. The results indicated no difference in the resulting emission characteristics except that the hydrogen sintering resulted in

gassy cathodes compared to those fabricated by vacuum sintering. This was reasonably expected since the CO_2 evolution rate was readily detected in the vacuum sintering making it possible to determine the completion of the decomposition reaction. For the hydrogen sintering the completion of decomposition was determined by trial and error.

It is generally believed for oxide cathodes that the attainment of a surface of low work function requires that a small amount of free barium metal be present in the (Ba, Sr, Ca) O coating of the cathode. The decomposition of BaO may occur thermally, and calculation of the vapor pressure of the resulting barium from the reaction

$$BaO \longrightarrow Ba + \frac{1}{2}\ O_2 \qquad (7)$$

yields a vapor pressure on the order of 10^{-16} torr at 1450°F. On the other hand the reaction

$$2BaO + \frac{1}{3}\ W \longrightarrow \frac{1}{3}\ Ba_3WO_6 + Ba \qquad (8)$$

results in a barium vapor pressure on the order of 10^{-7} torr at the same temperature. Hence a substantial increase in the available free barium should be obtained by adding a reducing agent such as tungsten. Tests performed in this laboratory have indicated that the addition of up to four per cent by weight of tungsten resulted unexpectedly in cathodes of poor characterisitcs; however, one per cent by weight of ZrH_2 yielded more promising reuslts in agreement with the work reported by C. P. Hadley, et al, (Reference 7). The poor performance of the tungsten activated cathodes may possibly have been due to the reaction

$$BaCO_3 + \frac{1}{3}\ W \rightleftharpoons \frac{1}{3}\ Ba_3WO_6 + CO \qquad (9)$$

which is highly favorable at temperatures above 1000°C where the sintering was carried out. Below this temperature the decomposition reaction is favored; the reaction rate, however, is so slow that a time of 1000 mins. may be required to complete the reaction (Reference 8)..

2.3.3 Cathode Testing

Early in the program, improvement in cathode performance was obtained by using a commercially available triple carbonate emitter mix (G.E. No. 118-5-2)

instead of the double carbonate (G.E. No. 118-5-1) used previously in work done under NAS8-42. (Reference 1) The triple carbonate resulted in a cathode which could emit a current density up to 1.5 amp/cm^2 for a cathode temperature as low as 1520°F as compared to required temperatures between 1750°F to 1800°F for the double carbonate.

Further evaluations of the triple carbonate emitter mix followed employing three cathodes run simultaneously in an identical environment. The cathodes were composed of the triple carbonate emitter mix, twenty per cent by weight, and powdered nickel, eighty per cent by weight, and were tested continuously for nine days. All three demonstrated good emission, the ability to stop and start repeatedly, and the ability to withstand exposure to air. Minimum cathode temperatures for stable operation at various vapor pressures were determined; saturated emission and cathode emission curves for several vapor pressures also were obtained during the course of the tests. The cathodes including the heaters showed no sign of performance loss or any indication that long life could not be realized. The tests were concluded after nine days because it was felt that the maximum amount of useful information had been obtained and that time could be better spent in a redirection of effort and an improvement in the cathode test facility.

Figure 35 is a typical saturation emission curve for one of the triple carbonate cathodes after it had been operated continuously for a period of nine days. Replotting the data in the form of a Richardson's plot results in Figure 36. From the slope of the curve, the work function is found to be approximately 1.0 eV with a Richardson's constant on the order of 1 x 10^{-2} amp/cm^2 - (°K)^2. The data points of the cathode temperature as measured by thermocouples, and restarting the arc. The arc would start at about 11 VDC. The current would almost immediately reach the value shown and thereafter would not increase even though the voltage was raised as high as 60 volts momentarily. The parameter which had a large effect on the arc stability was the mercury pressure. Despite the fact that a precise control or measurement of the mercury vapor pressure was not possible, a rough measurement of a pressure (or at least a pressure range) was obtainable. A thermometer was used to determine the temperature of a mercury pool and hence the mercury vapor pressure, providing the system had no cold spots. A check was afforded with a thermocouple vacuum gauge. To establish conditions for stable arc operation, an experiment to establish the minimum cathode temperature as a function of mercury vapor pressure was performed; emission was maintained at 1.1 amperes and 25 volts. A plot of this minimum cathode temperature for stable operation

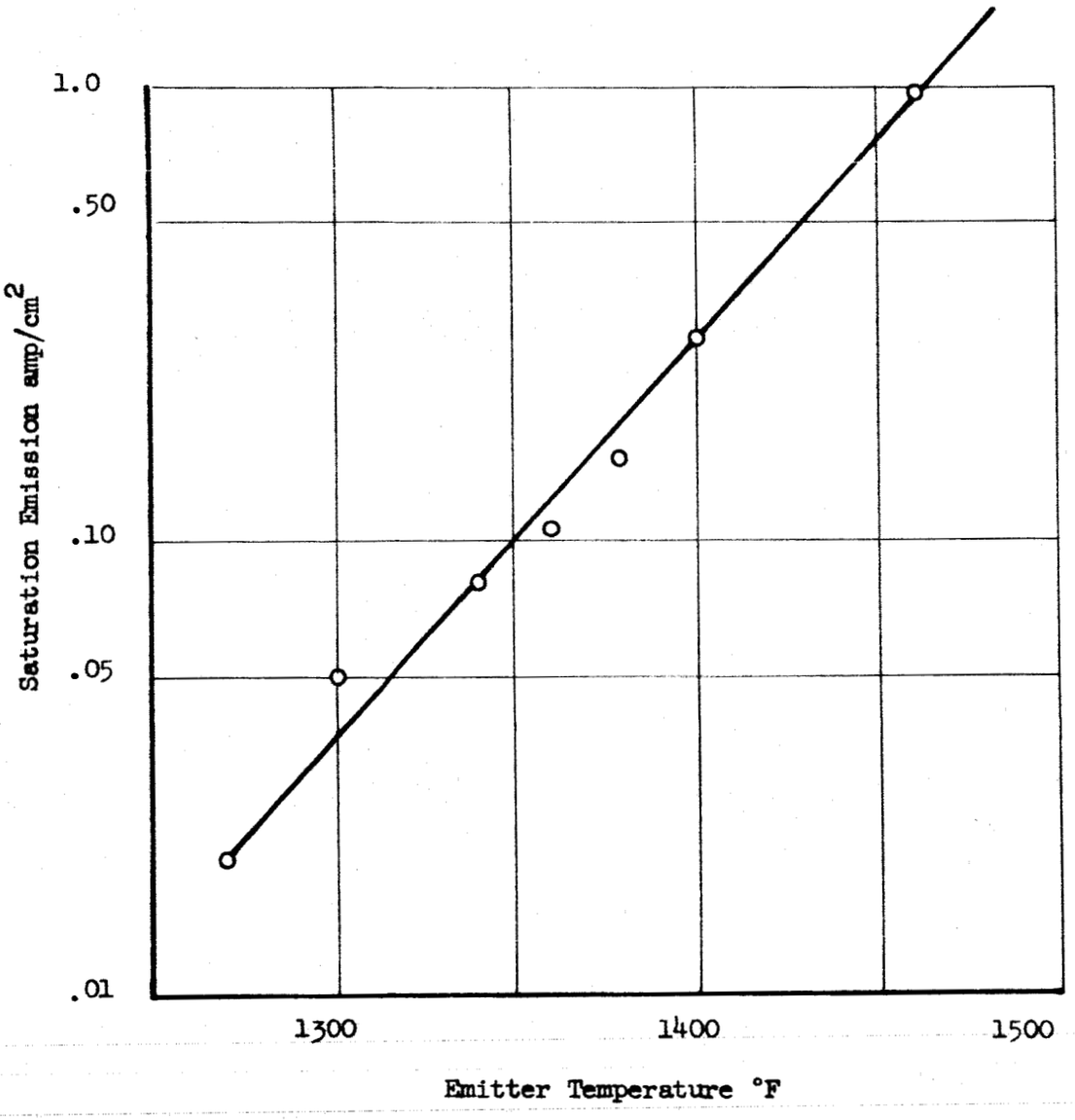

Figure 35

Saturation Emission as a Function of Temperature

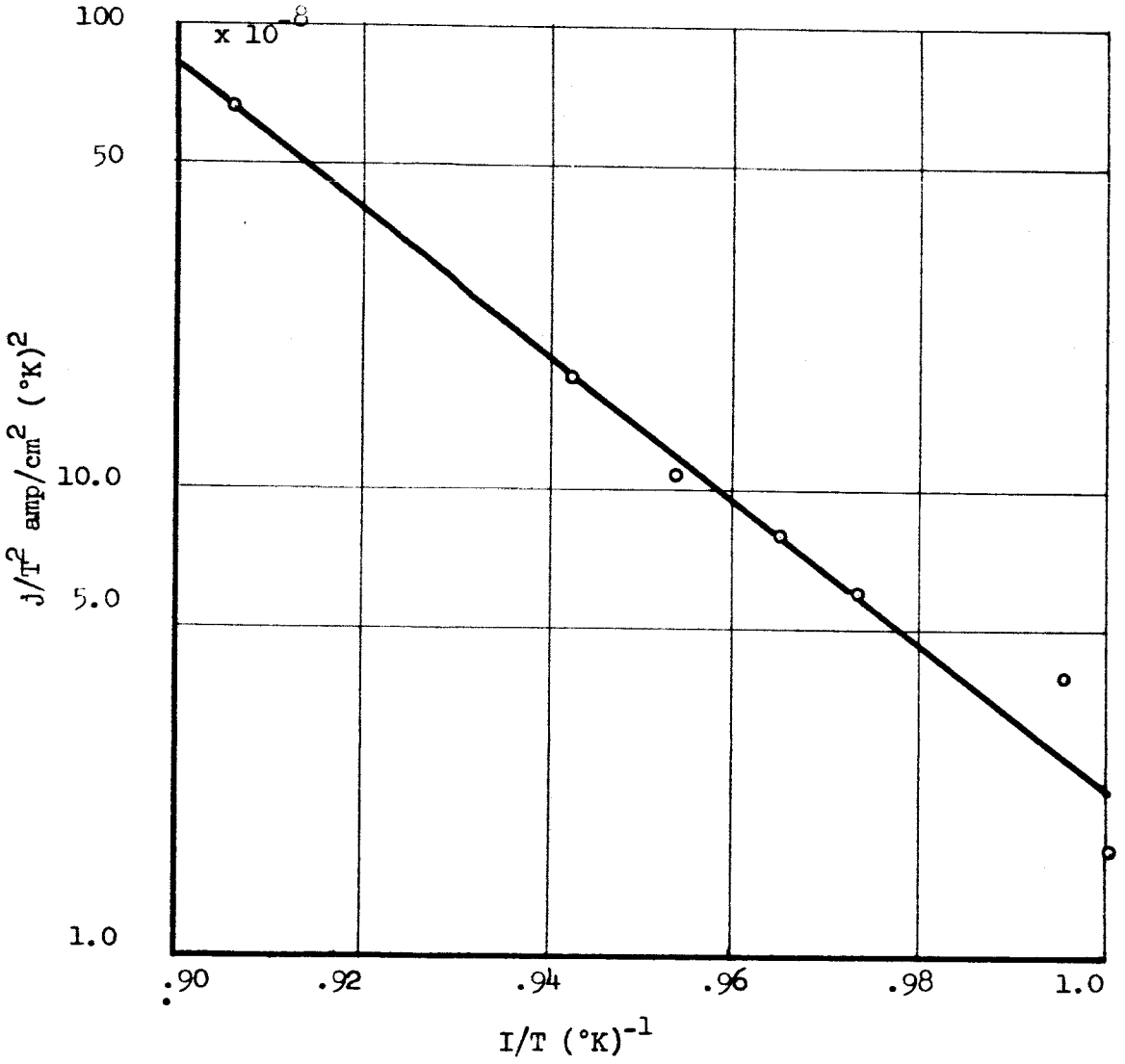

Figure 36

Richardson's Plot of the Data of Figure 35

is given in Figure 37. The actual vapor pressure was between the limits shown as determined by the liquid pool temperature and a thermocouple gauge, and is more likely to be near the temperature determination. The thermocouple gauge is believed to have been in error due to condensation of mercury in the neck of the gauge.

As work progressed, it became apparent that cathode emission characteristics were not as reproducible as had been anticipated. The initial change from the double to the triple carbonate, both 20 per cent carbonate by weight indeed had shown substantial improvement, viz., a drop in the required operating temperature from 1800°F to 1600°F for equal emitted current densities. To conclude, however, that suitable operating characteristics had been achieved was premature; subsequent cathodes containing the triple carbonate and fabricated "identically" yielded relatively poor emission properties.

The fundamental importance of dependable cathodes performance on meaningful ion source and extraction system testing made a concentrated cathode effort a paramount task. The first step was to use those cathode materials believed to the most promising in an experimental investigation of the effect of the sintering schedule on the emission properties. Prior schedules were suspected of being far too long, resulting in excessive sintering of the nickel and the attendent reduction of the pore size. The activation times may have been excessive because of the slow rate of migration of the oxides through the small pores. Possibly the pores had become disconnected and no migration at all occurred. It was planned, therefore, to determine the emission properties of several cathodes as a function of the sintering time for sintering times ranging from 0 to 60 minutes. In addition, the effect of adding a reducing agent (tungsten powder or zirconium hydride) was to be determined.

Relatively long term testing was undertaken in both a high vacuum and a mercury atmosphere. Specifically in a mercury atmosphere a test duration of 125 hours was accomplished for a 20 per cent triple carbonate, 80 per cent porous nickel cathode. During the test period the emission was maintained at approximately two amperes per square centimeter for temperatures in the vicinity of 1800°F and anode potentials from 10 to 15 volts. No degradation of performance was observed during the testing period. The termination of the test was not due to a failure but rather to initiate testing of other cathode materials.

Tests were conducted on two cathodes in the high vacuum (3×10^{-6} torr) diode test facility. The performance capability of the cathodes was investigated by bringing the cathodes to the desired operating temperature and applying a time varying

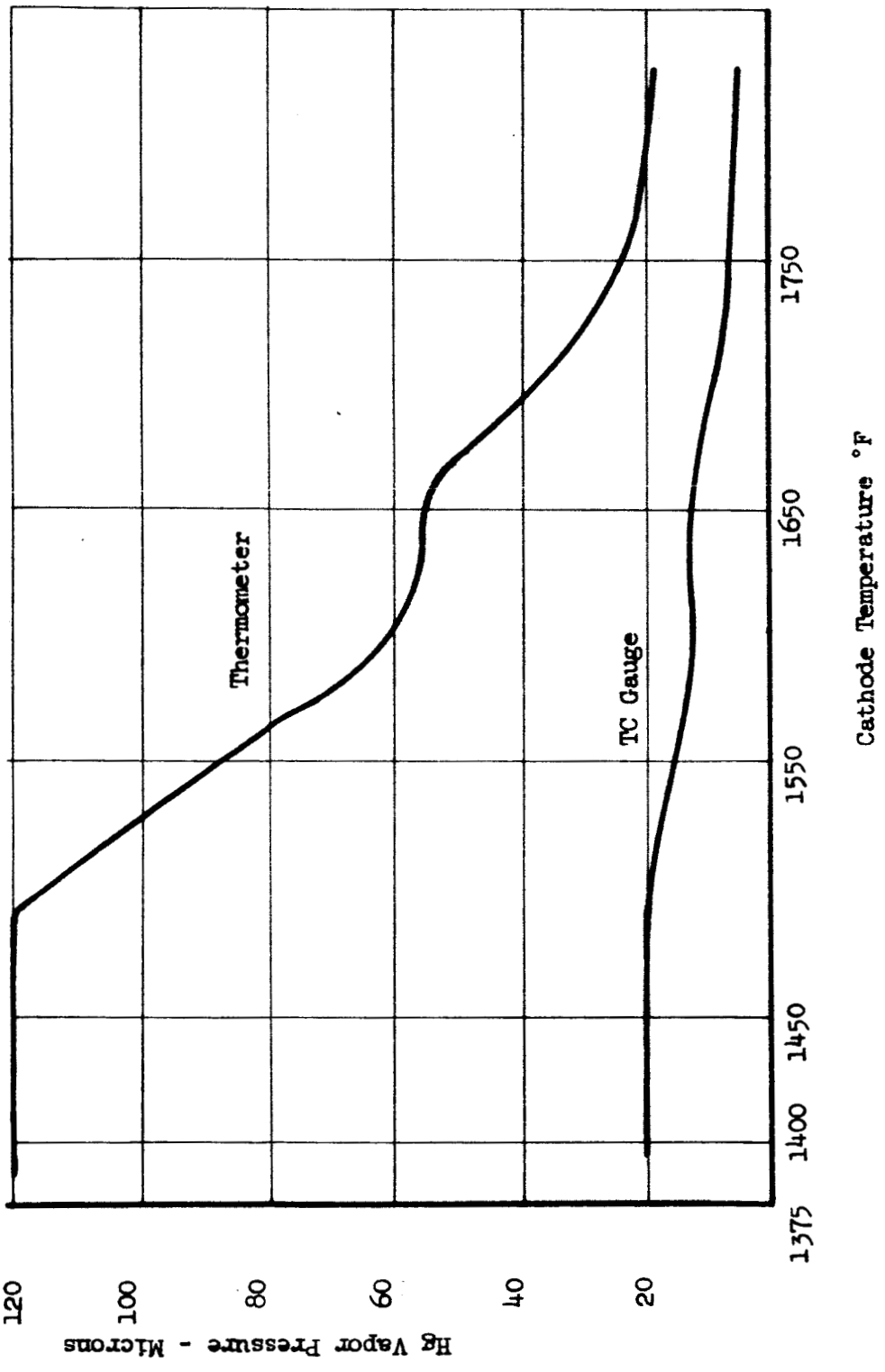

Figure 37

Minumum Vapor Pressure Versus Cathode Temperature

potential difference across the diode in order to display the current-voltage characteristics on a cathode ray oscilloscope. The typical anode to cathode separations were 0.030 inches and applied potential differences up to 1200 volts were used. The preliminary results of the two cathode tests are shown in Figures 38 and 39. The former shows the characteristics of a cathode which contains one per cent zirconium hydride activator with 20 per cent triple carbonate emitter mix and the remainder powdered nickel. The emission area of this cathode was 0.80 cm^2. The cathode shown in Figure 39 was identical in manufacturing technique but the hydride activator was eliminated and replaced by nickel. The area of this cathode was 0.94 cm^2. Comparison of the data indicated that the hydride-activated cathode had approximately 50 per cent greater emission capability than the unactivated unit. Furthermore, the performance obtained over a period of time generally indicated that the hydride activated cathode appeared to improve slightly in performance over a period of several days. The cathode without the activator appeared to decrease in performance after two days of operation. The performance level of the zirconium hydride cathodes, was entirely sufficient for use in the engine testing. Zero field current densities exceeding 1 amp per square centimeter could be obtained reliably at temperatures of approximately 1800°F. The lifetime of these cathodes including their swaged heaters appeared to be well in excess of 200 hours, the arbitrary limit of the initial test durations. Subsequently, tests of over 500 hours duration were conducted in a mercury vapor test facility. The test conditions were 2 amp/cm^2 at 1800°F. In addition, ion source tests were conducted with cathode emission currents in excess of 1.5 amp per cm^2 at a temperature of 1500°F. In the high vacuum test facility (2×10^{-6} torr) an emission current density of 1.5 amp/cm^2 required temperatures on the order of 1800°F. It is suspected that the presence of hydrocarbons in the high vacuum system even at pressures in the 10^{-6} range was sufficient to poison the cathode. In the engines and in the mercury vapor test facility it is suspected that the presence of the mercury vapor inhibited the influx of the hydrocarbons; hence little, if any, poisoning was experienced. The cathodes used in the ion engines also have been exposed to air for as many as three times (the cathode was cold when exposed to air) without observing any deterioration of its performance characteristics.

2.3.4 Conclusions and Recommendations

A substantial improvement in cathode performance was obtained initially through the use of triple carbonates in the cathode fabrication process. Subsequent efforts showed some discrepancies in cathode behavior; consequently a cathode development program was initiated in order to increase the cathode performance

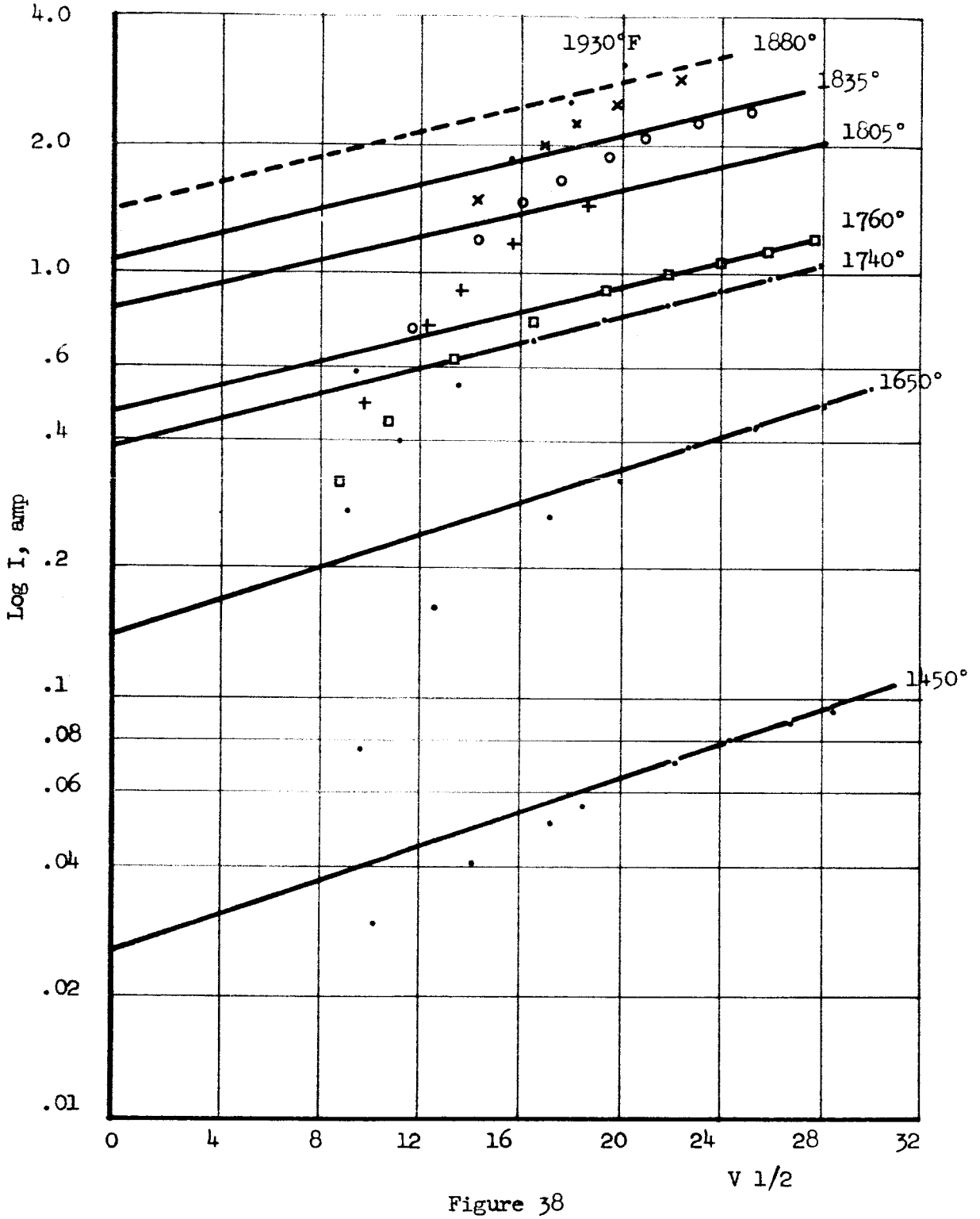

Figure 38

Schottky Plot for a Cathode of Composition 20% Triple Carbonate 79% Nickel, and 1% Zr H_2

Note: Symbols denote individual data points taken in sets while cathode is held at the constant temperature indicated.

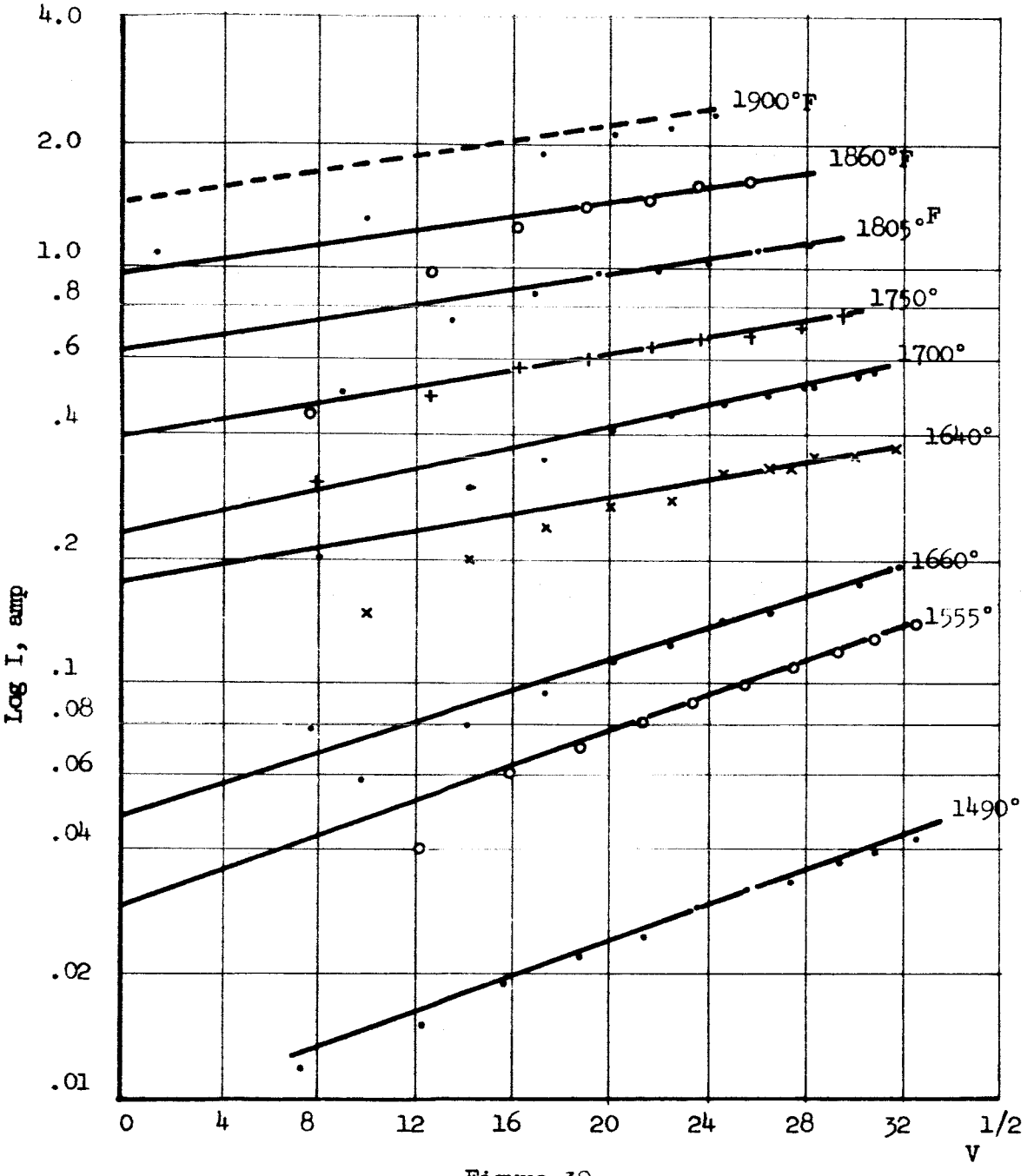

Figure 39

Schottky Plot Obtained for a Cathode Composition of 20% Triple Carbonate, 80% Nickel, and No Activator.

Note: Symbols denote individual data points taken in sets while cathode is held at the constant temperature indicated.

dependability. The program was directed towards two specific aspects of the cathode fabrication procedure; one was an evaluation of the sintering technique and the other was the use of reducing agents which serve as activators. In order to measure the resulting cathode properties without having the emission characteristics influenced by external conditions such as positive ion bombardment as present in an arc discharge, a vacuum diode test system was constructed. In addition, cathodes were tested in a low pressure mercury arc.

The results of the cathode testing program demonstrated the emission capability of the nickel matrix cathodes and suggested the superiority of the triple over the double carbonate. Furthermore, it was found that vacuum sintering was somewhat more convenient than sintering in a hydrogen atmosphere; the former method permitted the observation of the carbonate decomposition and the attendant carbon dioxide release. The optimum cathode sintering time was found to coincide with the termination of the carbonate decomposition process. A further cathode performance advantage was realized through the use of reducing agents in the activation process. Two such agents were investigated, zirconium hydride and tungsten powder, with the former yielding much better performance. In addition it was found that several factors must be incorporated into the cathode design for reliable operation in a bombardment engine. These are:

1. Operation at somewhat higher than the minimum emission temperatures to insure uniform arcs.
2. Design of the cathodes to be stabilized by heater input rather than by arc heating.
3. Keep the lead length short even at the expense of slightly higher power requirements.

The cathode work reported above was undertaken to provide cathodes suitable for use in experimental studies of an electron-bombardment ion engine. Although cathodes optimized with respect to emissive characteristics, life, and reliability did not constitute a specific goal of this program, a number of cathodes with excellent performance resulted. Subsequent efforts to improve or reproduce these cathodes showed a number of inconsistencies resulting in a somewhat less than ideal cathode reliability level. Nonetheless the nickel matrix cathode still appears to be the most suitable type, affording both performance and life potential. It is felt that additional development efforts are warranted. Further impetus stems from the requirement for cathodes of uniformly good quality to insure reliable and meaningful experimental comparisons and evaluations of engine performance.

The objectives of future cathode development programs should include:

1. Development of higher emission capabilities of cathode stock.
2. Development of materials and processing techniques to insure consistently high performance and uniformity.
3. Establishment of procedures for storage, handling, and machining of cathode stock.
4. Establishment of minimum standards of material quality and process control factors.
5. Development of more efficient cathode and heater configurations.
6. Development of more suitable, efficient, and reliable means of supporting and electrically connecting cathodes and heater elements in engine assemblies.

2.4 Life Testing

2.4.1 Introduction

The basic objective of this program was to determine the feasibility of attaining long extraction system lifetime at relatively high ion current density. Thus, upon design completion of an ion engine system, tests to enable the prediction of attainable lifetime were conducted. The object of the testing was to operate the ion engine system for sufficiently long periods to result in measurable extraction system erosion. It was decided that a test duration of 100 hours would be adequate for this purpose.

Two tests were accomplished, one of 70 hours and the other of 100 hours duration. Termination of the first test at 70 hours was due to electrical shorting of the extraction electrodes because of the build up of sputtered material on them. This shorting material resulted from sputtering in the beam catching area. Upon modifying the target area together with increasing the distance between the target and the source a second test of 100 hours duration was successfully completed.

2.4.2 Test Procedures

The testing was carried out continuously in that the tests were run for 24 hours per day. Interruption, however, was necessary approximately every twelve hours to refull the mercury feed system. The duration of this interruption was usually less than 15 minutes. The pressure in the vacuum test chamber was maintained at less than 5×10^{-6} torr and for approximately 90 per cent of the time the pressure was less than 2×10^{-6} torr. On several occasions, however, the pressure

went unintentionally up to the 10^{-5} range during replacement of the liquid nitrogen supply. No deleterious effects appear to have resulted from these short periods of high pressure.

The engine conditions that existed near the beginning, the middle, and near the end of the two tests are shown in Table 7. Throughout each test the mercury feed rate was held constant at 71.9 ma and 71.0 ma for the first and second tests, respectively. For both tests an attempt was made to maintain the source current above 50 ma while attempting to hold the arc current below 30 volts in order to reduce cathode sputtering and to restrict the production of doubly-ionized mercury. In order to accomplish this, it was found necessary throughout the tests to increase gradually the cathode temperature by increasing the cathode power. This in turn resulted in the gradual reduction of the engine power efficiency.

During the first test, data was taken periodically approximately every half hour while for the second test the data was taken every hour. The engine configurations used in the two tests are shown in Figures 40 and 41. Note that the two configurations are essentially identical except that the acceleration electrode length used in the 100 hour test is one half that used in the 70-hour test..

2.4.3 Results of Life Testing

Observations made during life testing have led to the suspicion that cathode sputtering is occurring at a significant rate for arc voltages as low as 25 volts. This suspicion is suggested by the observation that when the arc is turned off for a period of about five minutes and then reignited the cathode initially displays improved emission characteristics over that which existed before the arc interruption. About ten minutes after reignition, the performance regressed to that which existed before arc interruption. It is theorized that this effect is due to sputtering. While the arc was off, barium and/or barium oxide migrated to the cathode surface at a certain rate dependent upon the cathode temperature, this rate being greater than the loss of barium and/or barium oxide from the surface by evaporation. Thus, a good emission surface was built up during the arc-off period. This was suggested by the initial display of good cathode performance after reignition. However, associated with the arc is the bombardment of the cathode by positive ions producing a sputtering of the cathode surface. The sputtering rate at an arc voltage of 25 volts was apparently greater than the diffusion rate at 1950°F since upon initially igniting the arc a voltage of 25 volts was required to obtain an arc current of approximately one ampere.

TABLE 7

ENGINE CONDITIONS EXISTING NEAR THE BEGINNING, MIDDLE, AND END OF THE 70 HOUR AND 100 HOUR ENGINE TESTS

	70 Hour Test			100 Hour Test		
	10 Hours	35 Hours	55 Hours	10 Hours	50 Hours	90 Hours
Power Efficiency, %	75.5	74.4	71.1	74.8	73.4	71.5
Propellant Utilization, %	73.8	69.5	71.0	72.2	72.2	73.6
Rocket Efficiency, %	55.6	51.6	50.5	53.5	52.8	52.4
Source Current, ma	53	50	51	51	51	52
Target Current, ma	53.2	52	53	50.2	50.8	50.5
Accel Current, ma	0.8	0.9	1.05	0.7	0.99	1.1
Decel Current, ma	1.2	0.3	0.4	0.4	0.2	0.2
Arc Current, amp	1.0	1.2	1.5	0.8	0.92	0.88
Arc Voltage, volts	28	29	28.5	29	28	31
Cathode Power, watt	58.5	61.4	68.4	62.1	62.4	68.5
Cathode Temperature, °F	1960	1970	2030	1930	1930	1960
Accel Voltage, kv	13.8	14.5	15.4	12.5	12.5	12.5
Decel Voltage, kv	6.0	6.2	6.0	5.5	5.6	5.5
Specific Impulse, sec.	7750	7870	7750	7420	7590	7420

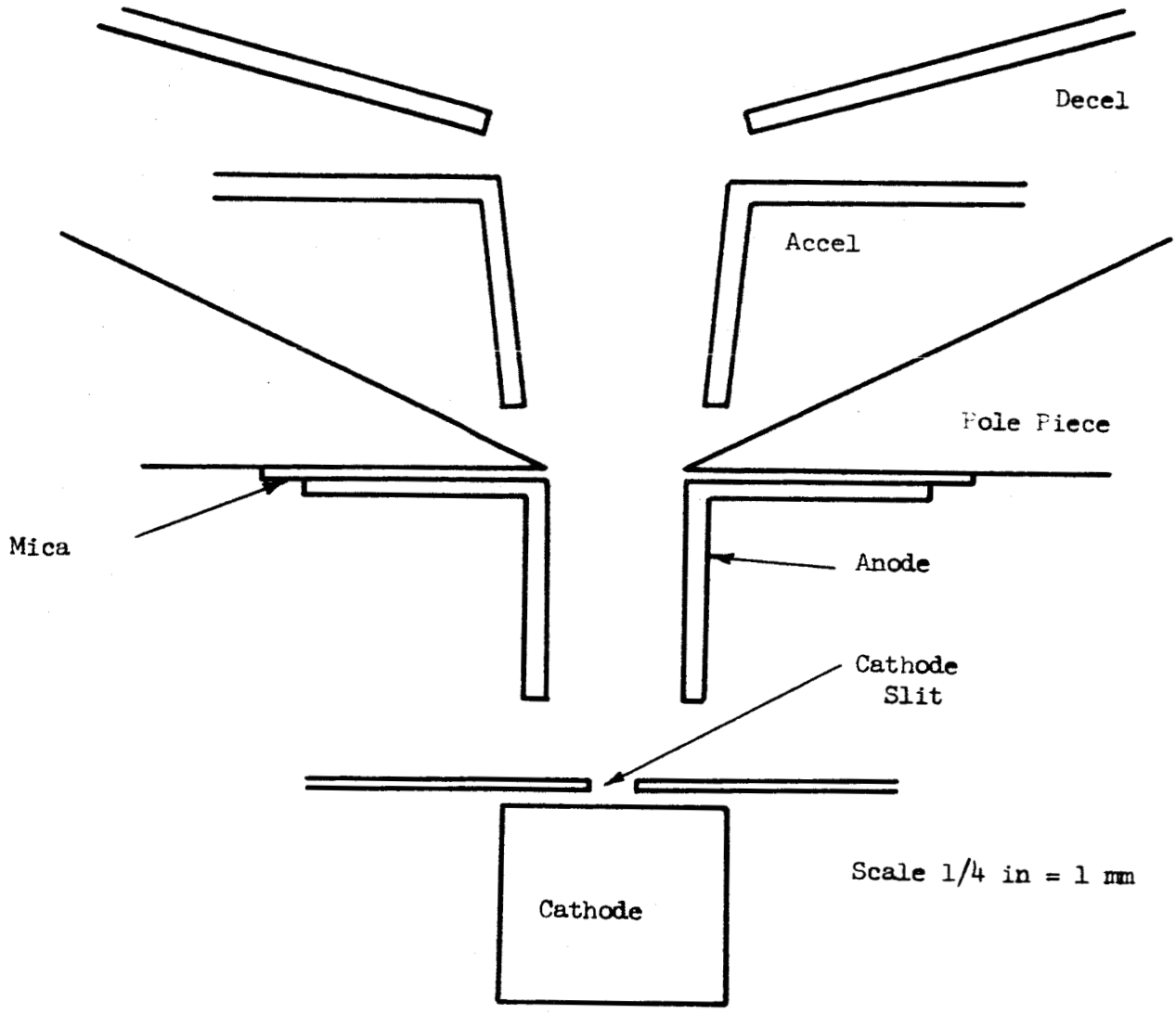

Figure 40

Engine Geometry Used During 70 Hour Life Test

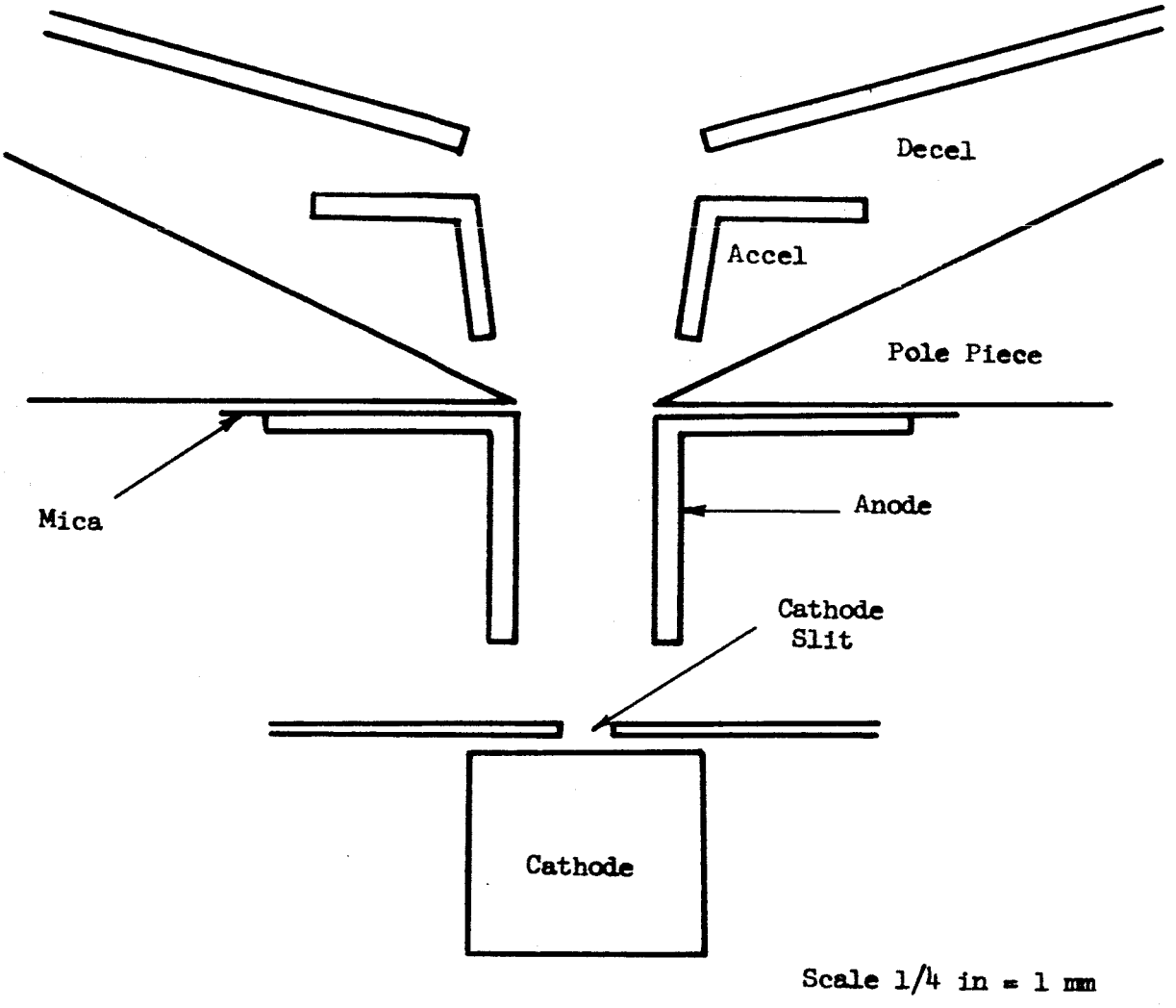

Figure 41

Engine Geometry Used During 100 Hour Life Test

The necessary arc voltage to obtain one ampere emission was observed to increase in a period of ten minutes from 25 volts to 30 volts. This suggests that sputtering which reduced the emission capability of the cathode took place. This emission capability reduction was offset, however, by increasing the applied voltage. It is assumed that the increased voltage enhanced the cathode emission from a poor cathode surface by field induced work function reduction or by increased heating of the cathode surface. It was concluded that the possibility exists that cathode sputtering does occur for arc voltages as low as 25 volts.

The extrapolated lifetime of the extraction system was calculated by determining theoretically the dependence of lifetime on the magnitude of the beam current and the propellant utilization, and then normalizing the resulting equation utilizing the experimentally determined erosion rate together with an estimate of the maximum total amount of erosion that can be tolerated. The details of this calculation are found in Appendix 2, while the results are plotted in Figure 42. It is seen that the extrapolated lifetime of a tantalum electrode approaches 10,000 hours for a 40 ma beam current at 95 per cent utilization. The use of graphite multiplies these curves by a factor of approximately five, yielding the possibility of extraction system lifetimes in excess of 10,000 hours for a 60 ma beam current and propellant utilization in excess of 90 per cent.

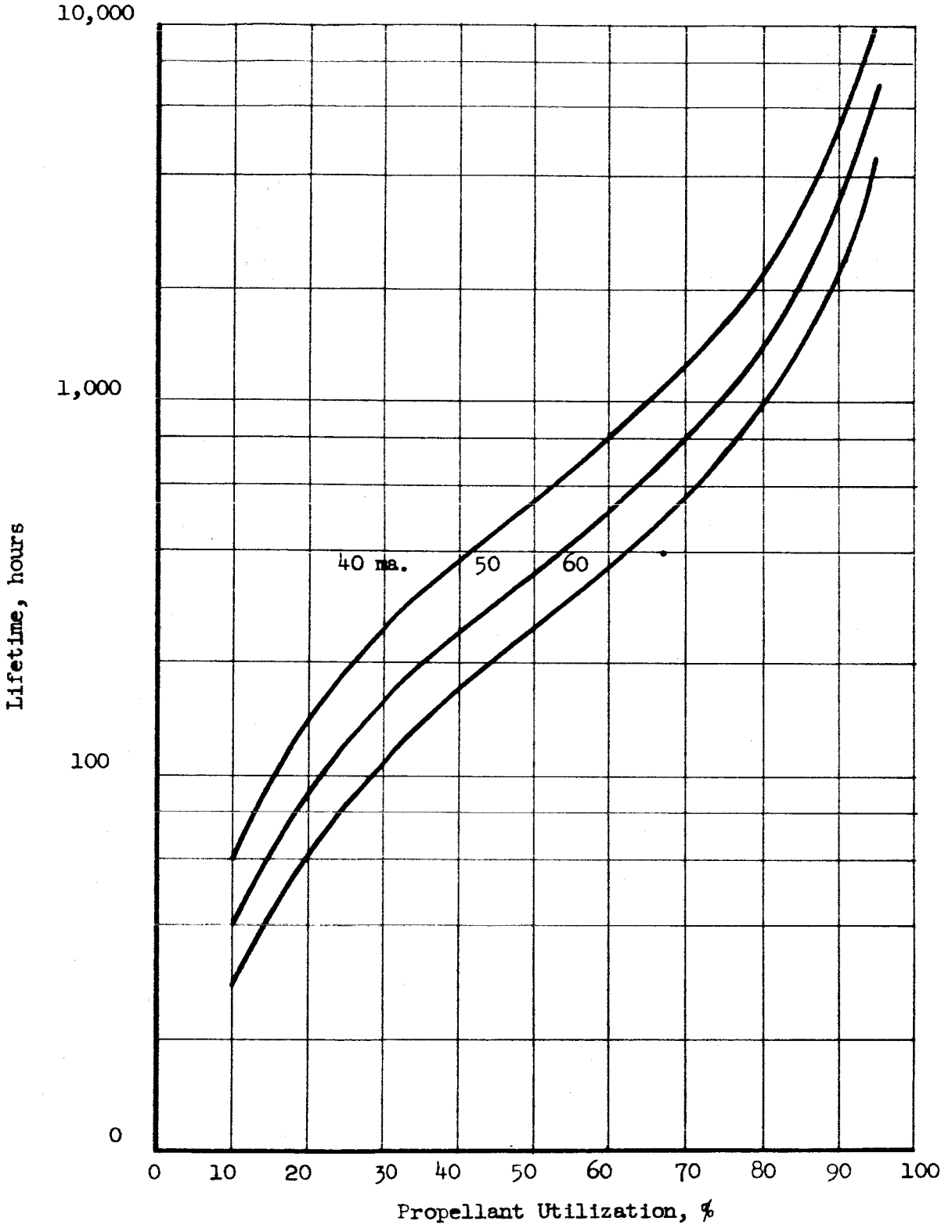

Figure 42

Predicted Extraction Electrode Lifetime vs Propellant Utilization for Three Values of Beam Current Using a Tantalum Accel Electrode

3.0 SUMMARY AND CONCLUSIONS

The results of this program may be best summarized by referring to Figures 42 and 43 which present the two most significant parameters in evaluating ion engine performance. Figure 42 presents the predicted extraction electrode lifetime, for several values of beam current, as a function of propellant utilization. The curves are based on measured erosion rates obtained by long term engine operation. It is seen that for a beam current of 40 ma, a lifetime in excess of 10,000 hours is predicted providing the propellant utilization is above 95 per cent. In Figure 43, the lower curve presents the extrapolated power efficiency, at 93 per cent propellant utilization, as a function of specific impulse. This curve has been generated from experimental data obtained at a specific impulse of 9,000 seconds which has then been extrapolated to lower impulse values by assuming the source performance is independent of specific impulse. The upper curve of Figure 43 represents a realistic goal to which future work should be directed. It is seen that at a specific impulse of 7,500 seconds a useful goal is 85 per cent efficiency at 95 per cent propellant utilization. Presently the THW engine can attain 74 per cent power efficiency at 7,500 seconds specific impulse and 93 per cent propellant utilization.

The simultaneous realization of long extraction system lifetime and high power efficiency for high propellant utilization has not been demonstrated. The requirements for long extraction system life are high propellant utilization coupled with low residual background mercury pressure. The requirements for high power efficiency at high propellant utilization are the attainment of sufficient cathode emission for low values of arc voltage and low values of cathode temperature. The situation at the end of the program is that for extended operation at high propellant utilization, high values of arc voltage are required; in order to counteract the sputtering rate associated with such high arc voltage, high values of cathode temperature are necessary. The high cathode temperature necessitates excessive power input to the cathode resulting in reduced engine efficiency. On the other hand, for short term testing the sputtering damage of the cathode does not proceed to the point where excessive arc voltages and cathode temperatures are required. Hence, for short term testing, the good emission characteristics of the cathode are maintained, and high propellant utilization and high power efficiency are achieved. Typical of this situation is the data presented in Figures 25 and 28 where it is seen that at 90 per cent utilization an arc inefficiency of 550 eV/ion is experienced and a power efficiency of 80 per cent is attained.

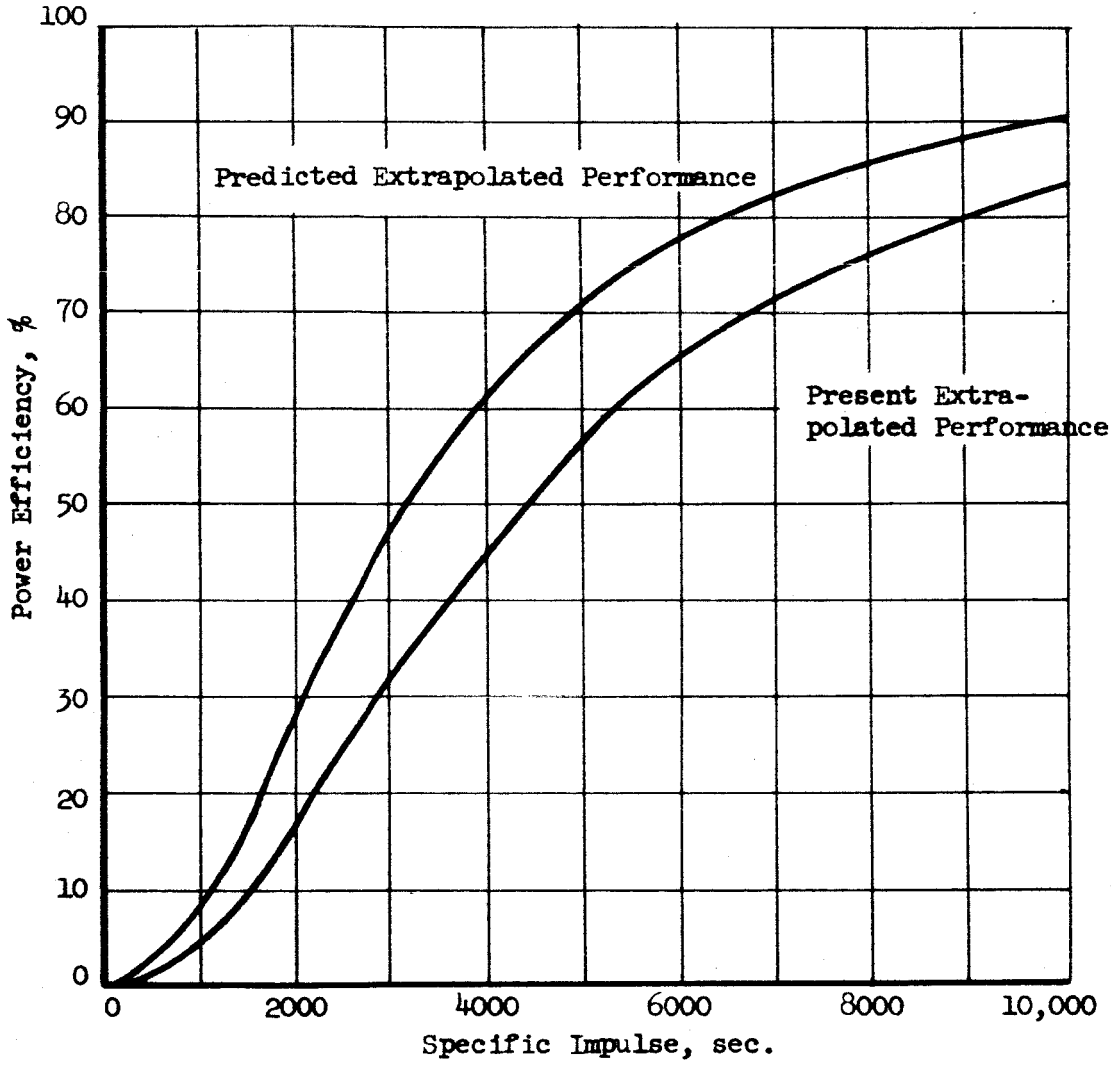

Figure 43

Power Efficiency vs. Specific Impulse

Also an arc voltage of 30 volts at a cathode temperature of approximately 1800°F is required to get 90 per cent propellant utilization. If the operation period is extended beyond that of a short term test, it is found, after four to five hours of operation, that setting a limit of 30 volts on the arc voltage and 2000°F on the cathode temperature results in a reduction of propellant utilization from 90 per cent to 70 per cent. After this initial cathode degradation, requiring four to five hours of operation, it is possible to rejuvenate the cathode by turning off the arc for periods of five to ten minutes. Upon arc reignition it is found that high utilization at lower arc voltage is possible; however, the degradation period is now about ten minutes instead of four to five hours. This rejuvenation process can be repeated many times producing the same results. The condition resulting in 70 per cent utilization at 30 volts of arc potential difference and a cathode temperature slightly under 2000°F is relatively stable; this is the condition which existed during the life testing portion of the program. It is clear, therefore, that the limitations imposed upon the arc voltage and cathode temperature limited the propellant utilization during the life testing. The temperature limitation was imposed to avoid the possibility of filament burn out; the arc voltage limitation was imposed to limit the cathode sputtering rate and to limit the double ionization probability. Thus, a demonstrated performance of extended testing at conditions commensurate with maximum lifetime could not be attained simultaneously with conditions of maximum power efficiency. Therefore, tests of short duration displayed conditions of maximum extraction system lifetime and high efficiency; extended testing produced degradation of the cathode performance resulting in the limiting of the propellant utilization to a value commensurate with short extraction system lifetime.

It is clear that at the heart of the inability to demonstrate simultaneity is the cathode and the related problem of cathode sputtering which occurs for arc voltages as low as 25 volts. This is due to the nature of the source geometry developed to date and because of the existing cathode performance characteristics. The problem is, therefore, a compound one in that the solution lies not only in the improvement of the cathode characteristics but also in the modification of the source geometry to yield more efficient ionization at lower arc voltages.

During this program period the groundwork for carrying out a source improvement program has been laid. The effect of varying the cathode slit width relative to the anode region width has been studied and a ratio less than 1:3 has been determined to be necessary. Scaling of the engine maintaining the 1:3 ratio has been

studied and it has been found that increasing the anode region width from 2 mm to 3 mm results in an improvement of overall engine performance for the same value of beam current. Fundamental to increasing the reliability of the engine system test results was the modification of the mercury feed system which decreased the response time and significantly reduced the error due to room temperature fluctuation. Thus, the indication of how to proceed in the development of the source geometry and the experience in designing and operating mercury feed systems can be combined to predict that the continuation of such a program would produce significant results.

REFERENCES

1. TRW Ion Engine Staff, "Summary Report on Bombardment Ion Engine Development", Final Report on Contract NAS8-42, TRW ER-5180, (October 1963).
2. R. C Speiser, "Ion Rocket Engine System Research and Development", Quarterly Report for Contract NAS3-2516, EOS Report 3670-Q-2 (17 July 1963).
3. G. K. Wehner, Phys. Rev., 108, 35 (1957).
4. W. R. Kerslake, "Charge Exchange Effects in the Accelerator Impingement of an Electron Bombardment Ion Engine", NASA TN D-1657, (May 1963).
5. N. L Milder, "Comparative Measurements of Singly and Doubly Ionized Mercury Produced by Electron Bombardment Ion Engine", NASA TN D-1219, (July 1962).
6. J. F. O'Leary, "Report on Cathode Development Studies", GHVA, Inc., Contract NAS8-858, (May 1962), (N63-22703).
7. C. P. Hadley, et al., Jl. Electrochem. Soc., 105, 395, (1958).
8. W. C. Rutledge and E. S. Rittner, Jl. Appl. Phys., 28, 167, (1957).
9. W. H. McAdams, "Heat Transmission", McGraw-Hill Book Co., Inc., New York, N. Y., 3rd Edition, p. 162, (1954).

APPENDIX 1

DESCRIPTION OF THE COMPUTER PROGRAM

This appendix gives some of the details of the digital computer program employed during this contract as an aid in the design and analysis of the ion acceleration system. The results that were obtained by means of the computer program are discussed in Section 2.1.3 of the body of this report.

The computer study began prior to the start of this contract and took as its starting point the analytical approach of Pierce's Theory and Design of Electron Beams. In this approach, certain properties of the charged particle beam are given or assumed, and an electrostatic potential field is sought which satisfies the beam properties. Pierce presents analytic solutions for a number of simple cases, but these do not apply directly to an optimized acceleration system for an ion engine. Consideration was given to approaching the practical problem from the same direction but by numerical methods; i.e., to assume a beam and solve for the potential. Stable numerical methods to do this, however, did not appear to be available.

The reverse of Pierce's approach then was tried. In this approach an electrode configuration and set of electrode potentials are given and a stable numerical method is made to yield the beam properties. If the solution is not a satisfactory beam then the given data are modified utilizing judgement and experimental information, and the calculation is repeated.

Under Contract NAS8-42 a computer program was written for the Burroughs 205 Electronic Data Processing System. Due to the relatively small memory size of the Burroughs 205, the accuracy obtainable with this program was not good enough for effective utilization of the results. The problem was, therefore reprogrammed for the IBM 7070 Data Processing System. The new program was in the testing stage when the present contract began.

This appendix provides, first, an overall picture of the computer program and, second, a closer look at certain features. Reference is occasionally made to the computer program by the name Ion Optics 3.

GENERAL DESCRIPTION

In applying the computing equipment available at TRW installations in the Cleveland area to the present research, exceptions to the standard practice necessarily had to be made. The accurate joint computation of electrostatic fields and ion beam characteristics demanded the use, for data storage, of a relatively large amount of memory capacity, and it was necessary to segment the program to fit the remaining storage space. The segmentation was done in two ways: the program was broken into a number of sequential phases, and one phase was subdivided into segments which are brought into the computer not sequentially but in an order determined during the running of the program. As was mentioned in Section 2.1.3, the computer operates upon values of electrostatic potential and charge density corresponding to the locations of mesh points which are the intersections formed in a two-dimensional grid of mesh lines.

The paragraphs which follow describe the applicable hardware and software facilities at TRW's Cleveland installation, the breakdown of the program into phases and segments, and a typical sequence of phases and segments as they might be involved in a computer run. Finally, this section is regarded as an appropriate place to insert the results of some timing studies that were performed with the program.

Hardware and Software Utilized. The makeup of the computer program was strongly influenced by the computational facilities that are available at the Data Processing Center of TRW Equipment Group. These include a tape-oriented configuration of the IBM 7070 Data Processing System, with two IBM 1401 Data Processing Systems standing nearby to perform auxiliary input-output operations. The IBM 7070 has approximately a 10,000 word (10K) magnetic core memory, a minimum add-time of 36 microseconds, and solid state modular design.

It is standard practice at this installation to write a research program in the FORTRAN compiler language, prepare a standard source-language card deck, and translate this on the IBM 7070 into a machine-language condensed object deck (and program listing), using an IBM 1401 to execute alphanumeric card-to-tape, tape-to-card, and tape-to-print functions. Certain control cards are then added to the object deck (a common option is to have this automatically done during the punching of the object dect), FORTRAN-style input cards are prepared and inserted, and the enlarged deck is processed by an IBM 7070 utility program called the PAT (Procedure for Automatic Testing) Compiler; this utility program produces on magnetic tape a PAT packet containing as card images, the object deck along with the necessary FORTRAN subroutines, input cards, loading routines and other utility routines.

The PAT packet is called into use by the operator of the computer. The (images of the) input cards are copied onto a separate tape from which they will be read under program control, the object program with its subroutines is loaded into the computer memory, and the program is executed. Customarily, one output tape is produced by the program during its execution and, optionally, a memory dump is written on the same tape; the output consists of print-line images. The IBM 1401 again is utilized for the card-to-tape and tape-to-print operations.

Phases of the Program. Since the Ion Optics 3 program and data would not all go into the 10K core storage of the IBM 7070, certain other features of the PAT system were brought into use. Sequential phases of the program were written in FORTRAN and translated separately into machine language (multiple FORTRAN processing is not regularly possible at this installation, since it would require special reallotment of tape drives). After testing, the object decks with control cards were arranged sequentially and PAT-compiled, producing a tape with several PAT packets on it, one for each object deck included. Input cards, instead of being PAT-compiled with the object decks, were arranged separately as an input deck which simply went card-to-tape on the different input decks. During a run, each PAT packet may be called into use by the computer operator. Whether a PAT packet is called manually by the operator or automatically by the program, the data portions of core memory are set to zero in the process; any data, to be saved, must be on magnetic tape. Besides restart tapes which are saved from run to run, there may be two output tapes produced by the program, the History tape and the Result tape. If a memory dump is obtained, it is written on the History tape.

The program consists at present of the following phases:

1. Solution phase.
2. Close phase.
3. List phase.
4. Equipotential phase.
5. Edit phase.
6. Restart phase.

The Solution phase of the program is itself too large for memory and is subdivided into segments, discussed at some length below. Neither the Solution phase nor its segments are included on the same PAT packet tape with the other program phases.

The repetitive computations that lead to a numerical solution are performed in the Solution phase, and a progress record is kept on the History tape. Certain other operations that are related to the numerical solution can also be performed by the Solution phase; such as, setting or changing the electrode voltages, and calculating charge exchange ion trajectories. At the end of the Solution phase the Close phase may be called into use automatically by the program; alternatively a memory dump may be obtained and the Close phase may be called by the operator.

The Close phase is associated with the generation of a restart tape. The Solution phase generates the first part of the restart tape as a series of restart data sets, each one being the latest approach to a solution at the time of its being written. The restart data sets are composed of values of electrostatic potentials and charge densities and identifying information. Further information is needed to actually restart a computation, and it is the Close phase that adds this information to the restart tape. Specifically, the restart tape is finalized by copying onto it: four segments of the Solution phase, two data arrays employed by the Solution phase, and all the input data not yet used by the Solution phase.

The List phase is capable of extracting from a restart tape any desired restart data set. The details of the intermediate or final solution that the data set represents are put on the Result tape for printing in an easily readable form. Some information that is useful for charge-exchange studies is calculated in the List phase and included in the output. This phase lists for each appropriate mesh point:

1. The coordinates of the point in units of the smallest mesh length (the distance between adjacent mesh points).
2. The electrostatic potential in volts.
3. The charge density in mks units, and a proportional quantity in volts.
4. The charge-exchange cross section for ions against neutral atoms in square meters.
5. The current density in mks units.
6. A charge-exchange collision frequency in reciprocal seconds.
7. The indices for locating the electrostatic potential and change density in core storage (during the Solution phase).

The Equipotential phase adds to the output of the List phase by writing on the same Result tape the coordinates of all the intersection points of an equipotential line with the mesh lines which cross it. The coordinates are given in units of the smallest mesh length. This may be done for any reasonable number of selected equipotential lines (not more than forty in the present version).

The Edit phase generates a new restart tape. It may select and modify information obtained from one, two, or three old restart tapes.

The Restart phase can be used to start a computation. Operating on a restart tape, it selects a restart data set to be placed in storage and places a record of its selection on the History tape. Then it copies the four segments of the Solution phase and the two data arrays onto other magnetic tapes. When all is in readiness the Restart phase, without a pause, copies one of the segments of the Solution phase over itself in core memory and begins to execute the segment, effecting a smooth transition into the Solution phase.

Segments of the Solution Phase. The Solution phase is the portion of the program that carries out the numerical solution. Basically, the method of solution involves an alternate modification of the electrostatic potential values on the one hand and the charge density values on the other hand. These two processes are very different in essence, one being based on a successive overrelaxation procedure and the other on ion trajectory calculations, so the program steps that do these jobs have been placed in different segments. In all, the Solution phase has five segments, four of which are stored on one magnetic tape, the Segment tape, and are brought into core memory one at a time under program control. The segments, although of different lengths, occupy overlapping regions of core beginning at a particular address (1287) and extending upward.

The five segments are:

1. Input segment.
2. Density segment.
3. Control segment.
4. Potential segment.
5. Start segment.

The Input segment reads and checks input data, which contains sets of parameters governing various actions of the Solution phase including criteria for exit. An input data set may also contain a trial solution for an arbitrary electrode geometry and the data arrays associated with that geometry. The Input segment may be called upon to read several input data sets at intervals during the Solution phase; normally the Solution phase continues until a blank card (image) is encountered on the input-deck tape. One portion of the Input segment initializes certain variables and arrays that are used by the Density segment; this portion is executed prior to every charge density calculation. The Input segment is the agency for reading the Density segment into core memory from the Segment tape.

The Density segment, as its name suggests, calculates charge density values, and its calculations are based on the current values of electrostatic potential. Two main steps are involved: calculations of trajectories of ions in the beam are based on the representation in the computer of the electrostatic field; the trajectories represent an ion beam configuration from which a charge density distribution is obtained. As an option, the Density segment may record the calculated trajectories on the History tape. Occasionally, the Density segment may serve merely as a link between the Input segment and the Control segment, and may perform no computations at all. At the completion of its function the Density segment reads the Control segment from the Segment tape.

The Control segment is entered from (read from tape by) either the Density segment or the Potential segment. It first writes a restart data set on the restart tape; then it controls the path which the program will follow. If the exit criteria included in the current set of input parameters are not yet satisfied, then the alternate modification of potential and density values will be continued; i.e., if the Density segment has just been executed then the Potential segment will be entered next, but if the Potential segment has just been executed then the Input segment will be entered next in order to initialize the variables and arrays that are used by the Density segment. On the contrary, if the exit criteria are satisfied then the alternate execution of the Potential and Density segments will be interrupted; in this case, if there is more input data to be read then the Input segment will be entered, but if there is not then the Solution phase will be ended and the computer will halt before going into the Close phase. Whenever the Restart phase is used, the first segment to be executed in the Solution phase is always the Control segment.

The Potential segment calculates electrostatic potential values, and its calculations are based on the current values of charge density. At each interior mesh point a potential value is calculated, using the current value of charge density at the point and the current values of electrostatic potential in the neighborhood of the point, and an overrelaxation factor is applied before the new value is stored. This is done for all interior mesh points in sequence, thus accomplishing a <u>sweep</u> of the electrostatic potential field. The Potential segment performs one or more field sweeps recording the effect of each sweep on the History tape, and then exits, the exit criteria being included among the input parameters. At the completion of its function the Potential segment reads the Control segment from the Segment tape.

The Start segment was originally used as an agency for entering the Solution phase. The five segments were originally written and translated separately and PAT compiled together, as has been described above for sequential phases. During a run the PAT packets were called into use in sequence. Each of the first four segments wrote itself onto tape, thereby generating a Segment tape. But the Start segment did nothing except read the Input segment from the Segment tape. In this way the program was started. After a restart tape had been generated, however, the Solution phase was regularly entered by first executing the Restart phase. As long as an acceptable restart tape is available there is no occasion to use the Start segment again.

A Representative Example. The relationship between the various phases and segments and the way in which these are applied to achieve a solution may be made clear by an example. Suppose that it is desired to study a new geometry, and assume that the restart tape is available from a previous solution of some other geometry. In planning for the computer run the geometry must first be defined; this includes establishing the mesh in relation to the electrodes, delineating the inter-electrode boundaries, and assigning relative storage locations to the values of electrostatic potential and charge density. Then the trial solution (starting values of the above field quantities) and the two constant data arrays employed by the Solution phase are developed. The conduct of the computer run is planned and the input data sets are developed; the two constant arrays and the trial solution are included in the first input data set. The input data sets are key-punched, verified, and put card-to-tape. A tape-to-printer listing at this time is useful as a check. A deck of cards is also prepared that will call the sequential phases from the PAT packet tape.

To start the computer run the PAT packet tape and the old restart tape are mounted on the IBM 7070 and the deck of call cards is inserted in the console card reader. The Restart phase is first to be called. It selects the last restart data set - the one containing the final solution for the old geometry - from the restart tape, copies the segments of the Solution phase onto the Segment tape and the two old data arrays onto a different tape, the Array tape, and enters the Control segment of the Solution phase. Here, the computer is in very nearly the same condition as when the Control segment was entered for the last time when the previous run was performed. It is ready to read input data. Now the machine operator substitutes the new tape of input data sets for the old restart tape; thus the input data that the computer will read will be the first new input data set. A new restart tape is begun by the Control segment, and the first restart data set written is a duplicate of the selected restart data set containing the old final solution.

The Input segment reads an input data set. This will happen as many times during the Solution phase as there are input data sets to be read. The first set contains the two new constant data arrays and the trial solution for the new geometry. The Input segment erases the old data arrays from the Array tape and writes the two new arrays in their place. (The first of these arrays correlates the coordinates of mesh points with the relative storage locations of the potential and density values. The second array defines the steps to be executed during each field sweep. The arrays share a portion of core memory analogous to the way the segments do. The first array is always in core during the execution of the Density segment, while the second array is in core during the Potential segment.) The trial solution is put in core memory by the Input segment in place of the final solution from the previous run. The remaining parameters in the first input data set cause the Density segment not to compute and cause the Control segment, after it writes another restart data set (this time containing the trial solution), to enter the Input segment again.

The second input data set contains the electrode voltages. Of course, these might have been included as part of the trial solution, but setting them separately like this permits different values to be inserted. Again the Density segment does not compute. The Control segment this time enters the Potential segment where one field sweep is performed; an appropriate portion of the second constant data array controls this special field sweep, letting the Potential segment calculate boundary values, with no overrelaxation, instead of interior values. After this sweep, program control passes again through the Control segment and into the Input segment. A restart data set is invariably written each time the Control segment is entered.

The third input data set allows the iterative computation to begin, but sets up moderate criteria for exit from the Potential segment and from the alternate modification of potential and density values. In each iteration the segments are used in this order:

1. Density segment (for computation, not as a link).
2. Control segment.
3. Potential segment (for an arbitrary number of sweeps).
4. Control segment.

After an unspecified number of such iterations, the exit conditons become satisfied and the Control segment (at Step 4 above) directs the Input segment (at Step 5) to read more input. The solution thus far obtained is not intended to be accurate, and is regarded as the rough solution.

The fine solution is sought by the next to the last input data set, whose exit criteria are as stringent as may be required by the solution's intended use. This may be the fourth input data set; alternatively, there may be any number of intermediate sets to control the avenue of approach by which the fine solution is reached from the rough solution. The purpose of including intermediate sets of data is usually to reduce the computing time needed to arrive at the fine solution. The computation proceeds iteratively as described above for the third data set.

The last data set selects the trajectory recording option in the Density segment. The Density segment performs its usual computations and additionally records on the History tape the trajectories that it calculates. The Control segment then terminates the Solution phase since there is no more tape input. The computer halts.

As there is no need for a core dump, the operator presses the START button and the Close phase is called from the PAT packet tape. This copies onto the new restart tape the four Solution phase segments from the Segment tape, the two constant arrays from the Array tape (duplicates, in content if not in form, of these same arrays in the first input data set), and whatever trailer card images still remain on the input data set tape unread by the Input segment.

The last two phases to be called are the List phase and the Equipotential phase. Their present action is to generate the Result tape from which can be printed in legible form the final potential and density for each mesh point of interest (some mesh points where the charge density is always zero can be omitted from the list), the coordinates of a convenient set of points lying on each equipotential line for which they are desired, and other information useful for charge exchange study and for checking.

The IBM 7070 computer run being over, the History tape and the Result tape are printed by the IBM 1401. Significant information from the printed listings either is plotted, as for example in Figures 31 and 32, or is interpreted directly.

Timing. Of all the phases of the program the Solution phase is, naturally, the most time-consuming. It usually takes several hours, while all other activities involved in a run ordinarily add up to less than thirty minutes. There follow some typical running times:

1. The Edit phase takes about five minutes, when used.
2. The Restart phase and Close phase combined take about five to ten minutes, depending on the amount of tape searching that is needed to find the desired restart data set.
3. The List phase takes a little less than five minutes to do a thousand mesh points.
4. The Equipotential phase takes a little more than one minute to read in all the data for a thousand mesh points. After the data has been read, it takes about twenty seconds to do each equipotential line (up to forty lines may be called for).
5. The time taken by the Solution phase is very roughly proportional to the square of the number of mesh points, and depends also on the degree of precision demanded of the solution and on the avenue along which the solution is approached. The problems to which the program has been applied have typically treated about a thousand mesh points and have typically used one to three hours of computer time in the Solution phase. For these problems the several segments have been timed separately.
6. The Potential segment takes a little more than twelve seconds to execute each field sweep; the number of sweeps is typically limited by an input parameter to fifteen, so the Potential segment typically runs about three minutes.
7. Cycling through the four segments (including the output of the two restart data sets) at the behest of the Control segment takes about one minute exclusive of calculating and input of new data.
8. The Density segment timing depends on the number of particles that represent the beam (the maximum is ten particles), on how far they go before being intercepted or nuetralized, and on whether the trajectories are recorded. For each particle that traverses both the accel and decel channels (see Figure 30) about forty seconds must be added to the cycling time if the trajectories are not recorded, and about seventy seconds if they are recorded. Particles that are intercepted take less time.
9. The Input segment reads a typical input data set in from two to twenty seconds, except that the insertions for a new geometry (as in the first input data set of the Example given previously) take approximagely fifteen minutes to be read; each of the two constant arrays and the trial solution takes about five minutes.

10. A core dump taken at the end of the Solution phase requires a little more than three minutes.
11. Getting on and off the machine, mounting and dismounting tape reels, plus the time between phases often comes to about five minutes.

FEATURES OF THE NUMERICAL COMPUTATION

The numerical computation portion of the program, comprising the Density and Potential segments of the Solution phase, is characterized by a number of general features, most of which are held in common with a number of other programs written to solve similar problems on other computers. The following list is representative:

1. A square mesh is employed to represent the geometry.
2. The mesh may double in linear size from one region to another.
3. Symmetrically located regions of the geometry are represented only once in the mesh.
4. Boundaries of the geometry are not restricted to lie on mesh points.
5. Boundary conditions may be Dirichlet or Neumann or mixed.
6. Electrostatic potential calculations are performed in fixed point arithmetic.
7. Overrelaxation is utilized to speed convergence in potential calculations.
8. Ion trajectories calculated in order to obtain charge densities are terminated if they intersect any electrode.
9. Charge densities are correctly calculated if beam ion trajectories cross the symmetry axis or each other.
10. Trajectories of charge exchange ions are calculated as equally well as those of beam ions.
11. Trajectories and charge densities are calculated without the extraction of square roots.

Together with the above general features, none of which are thought to advance in any way the state of the art, the program has one feature which may conceivably be unique in the realm of numerical methods applied to the solution of problems involving charged particle beams. This is the feature that allows the program to calculate roughly the shape and position of the plasma-ion interface (meniscus) from which the ion beam emerges.

Meniscus Location Feature. A persistent question that, until recently, was raised each time a new geometry was proposed for computer solution was the question of where to lay the boundary representing the source meniscus. The usual answer was to start with it flat (a straight-line meniscus) across the mouth of the source and after solving for the flat meniscus to try other shapes. Unfortunately, the shape of the ion beam may depend strongly on the meniscus shape assumed. The program feature described here automatically locates the meniscus and eliminates the need to guess at a numerical boundary condition at the source.

The numerical method for doing this fits very naturally into the Potential segment. If anything can be said a priori about the value of electrostatic potential at a locality in the ion beam close to the plasma ion interface (or anywhere else in the ion beam), it is that the value is not appreciably more positive than the source potential, for if it were more positive, ions would be repelled from that locality and no ion beam would exist there (contrary to the premise that the locality is in the beam). If a numerical solution is obtained for a relatively low beam current (emission limited case) with a fixed boundary representing the meniscus, the computed potential values close to the meniscus invariably come out negative, considering the source as being at zero or reference potential. As the current is increased, the positive charge density of the ion beam tends to make these computed potential values less and less negative. At some point a current (space charge limited current) is reached that is the maximum obtainable physically with a meniscus of the assumed shape. Any attempt to get a numerical solution with the same fixed boundary for an appreciably larger current than the space charge limited current results in failure, because certain of the potential values close to the meniscus are computed to be not only less negative, but actually positive, if Poisson's equation is assumed to hold in this region; such potential values, as is argued above, violate physical principles. The concept on which the meniscus locating feature is based is that, for an ion engine whose meniscus is a free interface between a gaseous neutral plasma and an ion beam, the region where these positive values are computed belongs properly to the neutral plasma - not to the ion beam. Since the plasma is a conductor approximately at source potential, the computer is programmed to set these positive values immediately to zero whenever they occur. The computation thereafter proceeds as if the edge of the zero potential region were the meniscus, with one exception; namely, the zero potential values at the computed meniscus may become negative again if the positive charge density (a nominal value is assigned at the mesh points where the potential has been set to zero) is not great enough to prevent it.

Thus, in principle, the computed meniscus moves either way until a final solution is reached in which the position and shape of the meniscus is appropriate to the emission of a space charge limited current. It is maintained that this position and shape approximates the position and shape that the meniscus takes on physically in the ion engine.

APPENDIX 2

POROUS DIFFUSER STUDIES

Introduction. As a portion of the program, mercury wetting tests were conducted with a porous graphite plug to investigate the potential suitability of such a unit as the phase separator in a zero-gravity propellant feed system. In concept, such a system would work as follows. Liquid mercury would be stored under vacuum in a spherical tank. A porous element not wetted by the liquid mercury would be carefully located near the center and fitted to the discharge tube of the tank. Under zero gravity conditions the liquid would wet and adhere to the tank walls forming a void in the vicinity of the porous element, providing the liquid does not completely fill the tank. Liquid would not permeate the porous element. Upon heating the vessel, a vapor bubble would form around the porous element, through which mercury vapor would pass as the temperature of the fluid reservoir was raised. The porous element would thus function as a phase separator, permitting vapor, but not liquid, to pass through it. The vapor flow rate through the porous separator would be dependent upon the reservoir temperature and could be controlled by the heat input to the reservoir.

The critical component in such a system would be the porous element. Since practical flight feed systems demand long-term, unattended operation, the practicality of a system of the type described depends upon the development of a porous diffuser which is not wet after long periods of exposure to mercury. This wetting determination was the basic purpose of the tests described below. A secondary objective was a rough calibration of a porous diffuser in terms of its vapor deliver rate.

Apparatus and Procedure. The apparatus described below was set up specifically to study the wettability of porous materials over long periods and to determine a preliminary correlation between the temperatures (and pressures) set up in a liquid tank or reservoir and the rate of mercury vapor transfer across a porous plug. A schematic drawing of the essential components of the test apparatus is shown in Figure 44. A photograph of the entire test rig is shown in Figure 45.

Mercury from the feed tank was allowed to flow into the reservoir at the base of the porous element (a graphite crucible with a 30 micron average pore size with 80 per cent porosity). Heating was accomplished by means of a ring heater at the base of the reservoir, a heating element on the porous element itself, and an externally applied radiant heater. Thermocouples were suitably located within the

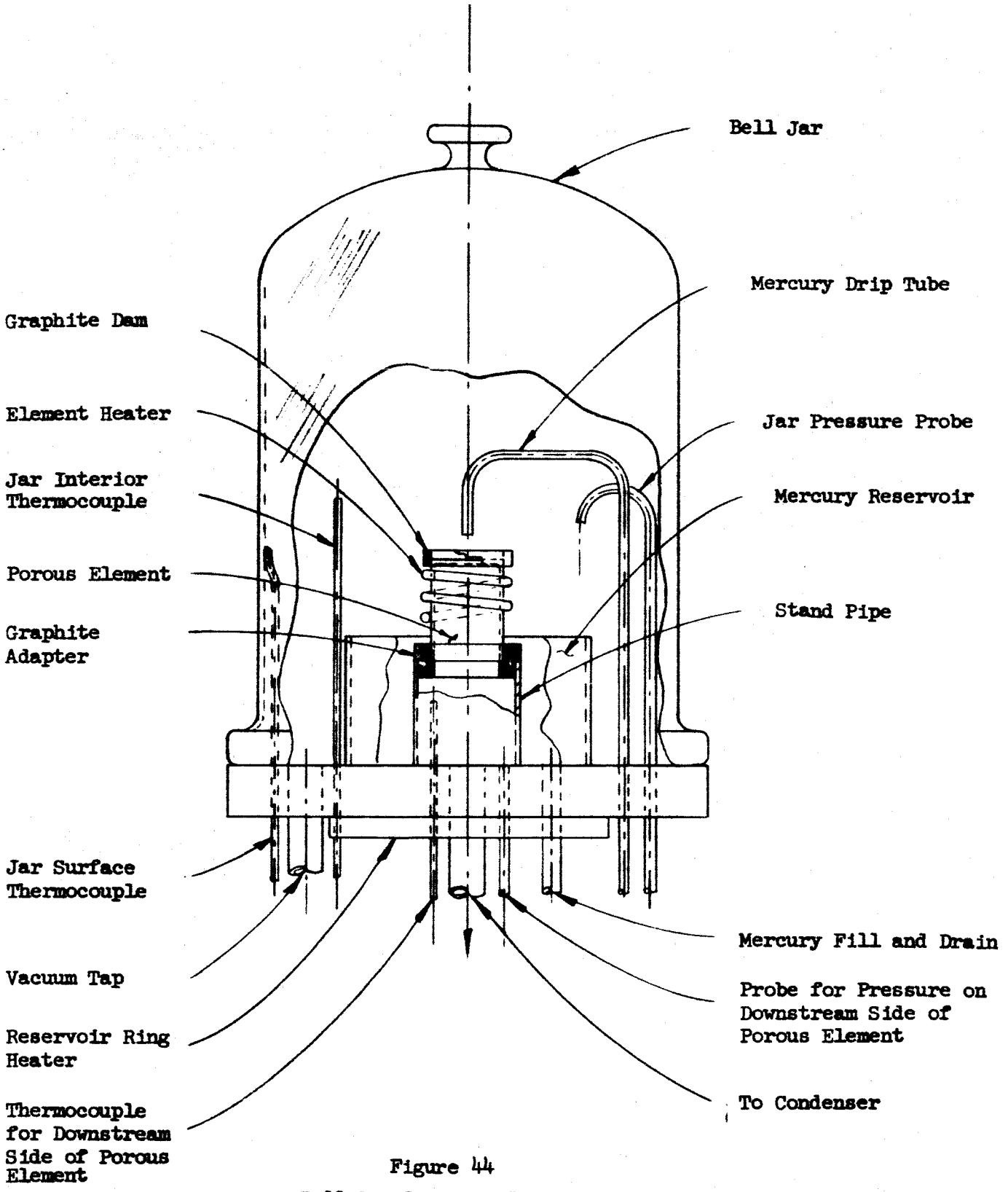

Figure 44

Bell Jar Capsule, General Arrangement

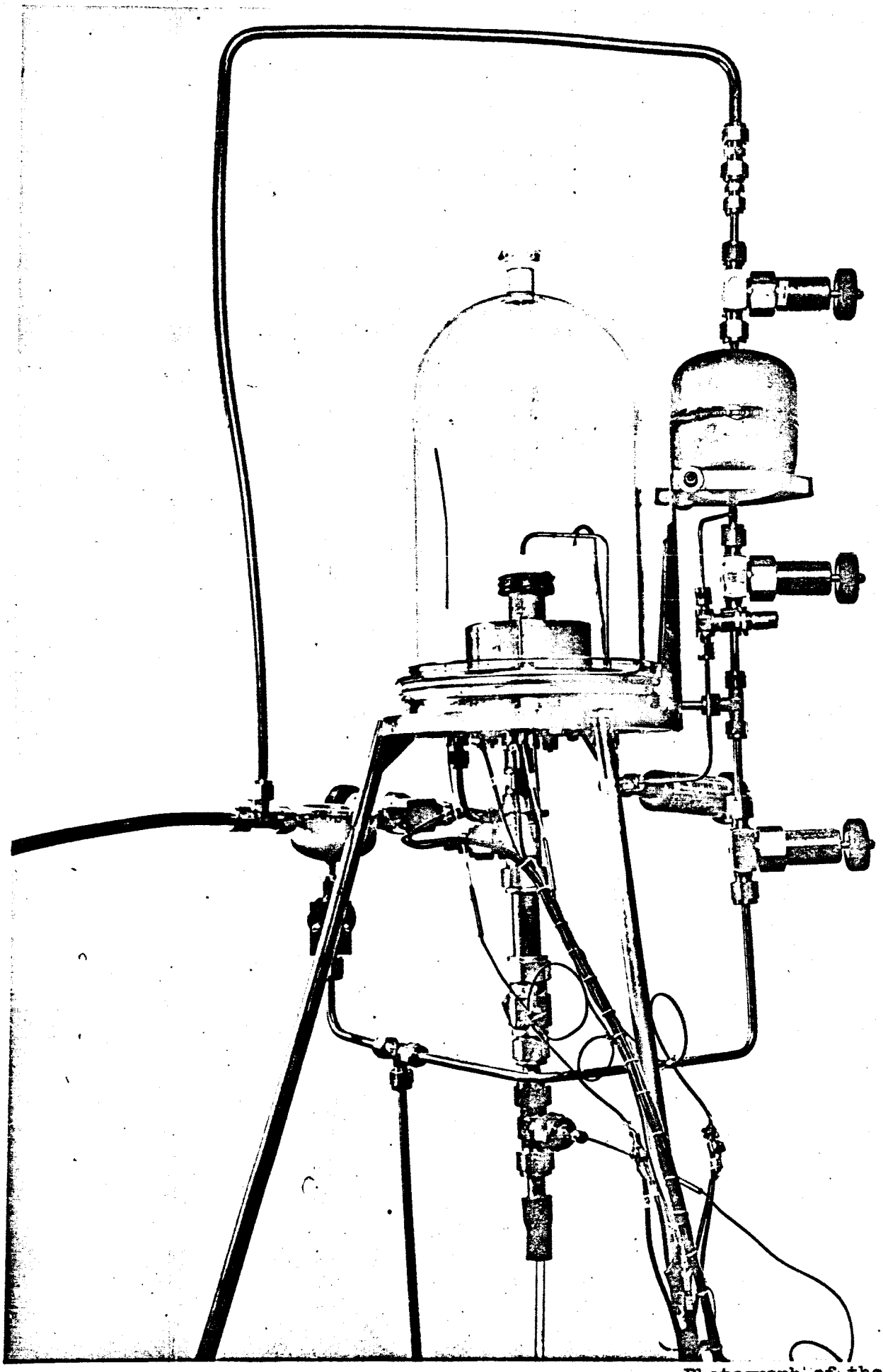

Figure 45

Photograph of the Porous Diffuser Test Facility

system in order to assure that a uniform temperature was maintained on all test components. A second mercury feed line (the drip tube) was also included in the set up in order to allow a droplet of mercury to collect on the surface of the porous element. This permitted the wetting angle between the mercury and the graphite to be observed at any time during the tests.

A water cooled condenser was placed in series with the graphite vaporizer. Also connected to the condenser was a graduated burrette tube capable of indicating changes in collected volume of 0.01 cubic centimeters.

To operate the test rig, the condenser water was first turned on. After evacuating the system to a pressure level of 50 microns or less, the system was heated to its operating temperature (116°C). This corresponds to a vapor pressure of 670 microns which was theoretically sufficient to dirve mercury at a 4.5×10^{-4} gm/sec. flow rate through a porous bed of a 30 micron pore size and 80 per cent porosity. These design calculations were performed using McAdams (Reference 9) relations for pressure drop in packed tubes. Since this is not an exact representation of the mercury vaporizer system, true flow rates could only be determined experimentally.

An average flow rate was observed by determining the change in mercury collection height in the burrette over a several hour period. Wetting characteristics were determined by visually observing any change in wetting angle of a drop of mercury on the top of the vaporizer section.

Results. The collection rates and temperatures, shown in Table 8, are representative data taken over an approximate 100 hour period.

During the test interval there was no change in the wetting angle between the mercury and the graphite. When this test was extended from 100 to 500 hours the same wetting results were found. The average flow rate over the 100 hour test period was 0.008 cc/hr corresponding to approximately 14 ma of equivalent singly-ionized mercury flow. Because of the magnitude of the flow rate the absolute values could only be determined by an averaging technique over several hour test periods. Instantaneous flow rates (over a few minutes time interval) could not be determined.

At the end of the 500 hour test period neither deterioration of the graphite, nor of the bonding agents used to cement portions of the graphite together, nor change of the wettability characteristics of the material was observed.

Table 8

Elapsed Time (hrs)	Thermocouple Reading[1] 1	2	3	4	Hg volume in collection tube (cm^3)	Flow rate (cm^3/hr)
-	-	-	-	-	3.53	-
3	-	-	-	-	3.51	0.00667
16	27°C	107°C	106°C	104°C	3.35	0.0100
6	27	112	110	119	3.305	0.0075
-	27	113	112	110	3.688	-
18	24	116	114	106	3.445	0.0135
8	27	117	114	117	3.395	0.00625
16	27	114	114	114	3.300	0.00593
8	28	118	116	119	3.2500	0.00625

[1]Thermocouple junction locations were:

(1) Water condenser temperature.

(2) Base of graphite porous element.

(3) Bell jar vapor temperature.

(4) Bell jar glass temperature.

Conclusions and Recommendations. As a result of these mercury wettability tests it was concluded that porous graphite may be a suitable material for use as a phase separator for periods up to 500 hours in the type of mercury feed system described above. Preliminary measurements of mercury flow rates versus pressure indicate reasonable flow rates for reasonable vapor pressures. The time stability of vapor flow has not yet been established.

To completely evaluate the process there are additional areas which require further investigation. These are:

1. The long term wetting effects exhibited by mercury on vaporizer materials other than graphite.
2. The change in rate of vaporization as the system temperature changes.
3. Methods of measuring instantaneous vapor flow rates generated within the feed system.

APPENDIX 3

CALCULATION OF THE EXTRAPOLATED EXTRACTION SYSTEM LIFETIME

It is presently generally accepted that charge exchange ion production is unavoidable because of the inability of ion sources to ionize all of the propellant provided to the source. The fraction of the propellant which is ionized, called the propellant utilization and designated by the symbol, η_m, determines the charge exchange current, I_{Ac}, which is collected by the accel electrodes. An expression for I_{Ac} sufficiently accurate for the present purposes can easily be shown to be

$$I_{Ac} = \frac{1 - \eta_m}{\eta_m} \quad \frac{I_S^2}{e} \quad \left(\frac{L}{A}\right) \quad \frac{\sigma}{v_n} \tag{A-1}$$

where σ = average value of charge exchange cross section

v_n = average speed of the neutral atoms undergoing charge exchange

L = effective length of the potential well region

A = effective cross section of the accel electrode region

I_S = beam current

e = electronic charge

and where all the quantities are expressed in a consistent set of units.

The lifetime of an extraction system is determined by the number of ampere hours required to erode away a critical amount of electrode material. This amount will be assumed to be that contained in two parallelapipeds of dimensions 0.2 x 0.2 x 5 cm^3, one parallelapiped located in each accel electrode. For tantalum electrodes this corresponds to a total weight loss of 6.62 grams. The measured weight loss occurring for the 70 hour and 100 hour tests resulted in a determined erosion rate of 11.3 gm/amp-hr and 13.5 gm/amp-hr, respectively. In order to obtain a pessimistic value of extrapolated lifetime the larger value of erosion rate will be used in the following calculations. Thus, the following working relationship between lifetime and charge exchange current is obtained:

$$t = \frac{492}{I_{Ac}} \tag{A-2}$$

where t is the electrode lifetime in units of hours and I_{Ac} is the charge exchange current in units of milliamperes. The units of the constant are obvious. Thus, for a charge exchange current of 1 ma, an electrode lifetime of 492 hours is predicted.

The use of Equation (A-1) permits the extrapolation to other values of propellant utilization. This is accomplished by evaluating the constants of Equation (A-1) for the conditions I_{Ac} = 0.6 ma, I_S = 50 ma, η_m = 0.70 which are sufficiently representative of the conditions which existed during the life testing. Upon substituting into Equation (A-2) there results

$$t = 880 \times 10^3 \left(\frac{\eta_m}{1 - \eta_m}\right) \frac{1}{I_S^2} \left(\frac{R_{Ta}}{R}\right) \qquad \text{(A-3)}$$

where I_S is the source current expressed in milliamperes and R_{Ta}/R is the linear erosion rate of tantalum relative to that of another material, R being proportional to the rate at which the sputtered surface recedes per incident ion. It is Equation (A-3) which is plotted in Figure 42.

It is easily shown that the ratio of the linear erosion rates is given by

$$\frac{R_{Ta}}{R} = \frac{S_{Ta}}{S} \cdot \frac{\rho}{\rho_{Ta}} \cdot \frac{M_{Ta}}{M}$$

where S is the sputtering rate expressed in atoms per ion

ρ is the density of the electrode material

M is the atomic weight of the elctrode material

The linear erosion rate ratio of tantalum relative to graphite is obtained using S_{Ta} = 0.5 atom/ion and S_c = 0.19 atom/ion at an incident mercury ion energy of 500 eV (Reference 3) and is found to be R_{Ta}/R_c = 4.5. Thus, it si possible that graphite accel electrodes could exhibit approximately five times the lifetime of tantalum electrodes.

APPENDIX 4

PROPELLANT FEED SYSTEM

During the testing phases of the program, several laboratory-type mercury feed systems were employed. They differed mainly in the details of their respective vaporizers, rather than in the manner of liquid supply or metering and were designed and constructed to function primarily as experimentally flexible laboratory units. Of primary interest, therefore, were considerations such as flow variability, flow metering, regulation, control and response, rapid refill capability, ease of usage, and minimum maintenance. The mercury propellant feed systems used in this program may logically be divided into two essential elements, the liquid driver and the vaporizer. Both have their unique problems and will be discussed in turn.

The initial source and extraction work was carried out using mercury feed systems built under NAS8-42 and described in detail in Reference 1. In essence these systems consisted of a mercury storage reservoir and a motor-driven positive displacement plunger which slowly drove liquid mercury to a heated vaporizer. The vaporizer consisted of an electrically heated stainless steel porous plug matrix, two inches long and one-quarter inch in diameter, vertically mounted directly in the engine propellant supply line. Liquid mercury was fed into the bottom at a constant rate. This end of the matrix was held at a constant temperature of about 20°C, while the top end was maintained at a fixed temperature near 300°C. At equilibrium, a definite interface was formed within the matrix above which the mercury was vaporized and below which the mercury remained a liquid. Under these equilibrium conditions, mercury vapor exited from the matrix at the same flow rate at which liquid mercury entered. The remainder of the mercury feed system served to supply this heated porous matrix with liquid mercury at a constant metered rate.

To accomplish this, a neoprene plunger was pushed through a 2 mm precision bore capillary tubing at a constant speed, driving liquid mercury into the vaporizer at the same rate at which it was displaced from the tubing. The linear displacement rate of this plunger was indirectly measured and served as the basis upon which the mercury vapor flow rate was calculated. The use of a T-bore stopcock in conjunction with the precision bore tubing allowed rapid refilling of the tubing with a new charge of mercury from the supply seservoir. The neoprene plunger was driven through the capillary tubing by a tungsten rod which in turn was coupled to a feed screw. The plunger travel up the capillary tubing was quite slow, about 0.003 cm per minute for an equivalent mercury delivery rate of 60 ma. This in turn permitted a single filling of mercury (about twelve inches of column length) to serve

for many hours of source testing. Initially a stepping motor and gear system were used to turn the feed screw at constant speed. Periodic monitoring of the plunger displacement rate verified the constancy of propellant feed during ion source testing.

Such was the basic mercury feed system developed under Contract NAS8-42. In general, its performance was satisfactory. The entire system appeared to have only one major limitation and this involved the time response of the porous matrix vaporizer. To shift from one vaporization equilibrium condition to another at flow rates greater than 100 ma required of the order of five minutes. However, at flow rates corresponding to about 40 ma of beam current, it frequently required of the order of thirty minutes or more for stabilization, the time increasing even more if the flow change was from high to low. What were thought to be adequate equilibration times were allowed to elapse prior to data recording at a new flow rate.

As work progressed under NAS3-2522 the mercury feed system was more closely investigated with respect to calibration and time stability. The calibration consisted of displacing the plunger of the positive displacement drive by a measurable amount and weighing the amount of mercury that would be delivered to the vaporizer. The stability test consisted of measuring the rate at which mercury was delivered as a function of time for time durations up to eight hours. It was found that the long term accuracy was approximately $\pm$ 1/2 per cent and the short term accuracy $\pm$ 1 per cent, providing the laboratory temperature held reasonably constant. When the laboratory temperature changed significantly, larger derivations were experienced. It was evident that the system was responding to room temperature changes, the feed rate increasing gradually during the day as the ambient temperature increased and rapidly decreasing on occasion because of sudden drafts. In order to eliminate the room temperature dependence the engine feed line was enclosed in a water jacket maintained at tap water temperature; preliminary measurements indicated that the tap water temperature remained constant within 1/2°C throughout the day.

Additional stability measurements were made periodically by determining the maximum output source current as well as periodically monitoring the arc characteristics. This investigation revealed a propellant utilization in excess of 100 per cent, in some instances, and showed the influence of the vaporizer (as distinquished from the liquid driver portion of the feed system). The basic problem was that the very slow response of the capillary vaporizer made true "equilibrium" vaporization conditions somewhat difficult to verify, despite the standard practice of waiting before recording data.

In order to reduce the time required for the vaporizer portion of the feed system to come to equilibrium the vaporizer was completely redesigned. The redesign was based on the results of a first order transient analysis of the dynamics of the vaporizer. If it is assumed that the vaporizer consists of a long capillary through a thick walled tube, the wall being thick enough that a temperature gradient along the length of the tube is independent of the presence or absence of mercury in the capillary, then it can be shown that for small disturbances about the equilibrium position the mercury liquid-vapor interface will move exponentially towards the equilibrium position having a characteristic time, τ, given by

$$\tau = \frac{\rho_{Hg} A_c N_o}{M \dot{n}_o \left(\frac{B}{T(s)} - \frac{1}{2}\right) \frac{T'}{T(s)}}$$

where ρ_{Hg} = the density of mercury

A_c = the cross section area of the capillary

N_o = Avogadro's number

M = gram atomic weight of mercury

$\dot{n}_o$ = rate at which mercury is fed into the vaporizer

s = the equilibrium position of the interface

$T(s)$ = the temperature at the equilibrium position

T' = the temperature gradient along the length of the capillary

B = the constant in the equation $P = P_o \; e^{-B(1/T - 1/T_o)}$ where P is the vapor pressure at temperature T and P_o is the vapor pressure at temperature T_o.

Thus it is seen that the characteristic time depends directly on the cross sectional area of the capillary and inversely on the product of the mercury feed rate and the temperature gradient.

The most obvious method of reducing the response time of the vaporizer was thus to decrease its effective cross-sectional area. A capillary vaporizer was built having a cross-sectional area of 5×10^{-4} cm^2 (some 600 times smaller than the effective area of the porous plug units). For a feed rate equivalent to 60 ma and a temperature gradient of 70°C/cm a theoretical characteristic time of 15 seconds was obtained (using Equation (A-4)) which compared favorably with a measured characteristic time of six seconds. This constituted an obvious improvement over

the porous plug units which, under similar circumstances, showed characteristic times on the order of hours and consequently demanded long waiting periods to insure the existence of vaporization equilibrium. The capillary vaporizer design resulted in a considerable saving of time and allowed more extensive engine testing over a wide range of feed rates.

These capillary vaporizers more than met expectations. They turned out to be extremely convenient and flexible for laboratory usage; their response time, for example, could be varied somewhat for a particular flow rate by increasing or decreasing the temperature gradient. The sensitivity of the capillary vaporizer was such that the pulses from the stepping motor (used to turn the feed screw and liquid mercury feed plunger) were manifested in the mercury arc as voltage and current pulsations. This led in turn to the elimination of the stepping motor arrangement and the substitution of a synchronous motor whose output was coupled through a transmission so that the rotational speed could be continuously varied. This modification resulted in very good short term stability (<30 sec.) of the feed system and arc characteristics.

A recalibration and redetermination of the feed system's stability was carried out. The basic calibration was found to be accurate to better than one per cent. Two sources of instability were revealed, however; the first depended on room temperature variations and the second was mechanical in nature having a periodicity equal to that of the drive screw. The instability induced by room temperature variations had been reduced to less than one per cent by inclosing the mercury feed line in a water jacket as previously described. Despite this precaution, additional fluctuations were still encountered when the feed system was exposed to sudden cold (or hot) drafts, since the capillary tubing had not been water-jacketed. The periodic instability was related to poor alignment of the reduction gears and amounted to the superposition of a linear and a periodic displacement on the motion of the drive piston. For the two feed systems which were used one was found to have a maximum deviation of seven per cent while the other was stable to one per cent. These per cent deviations correspond to peak to peak gear displacements of 0.0007 in. and 0.0001 in. respectively.

The determination of the various causes of feed system fluctuations facilitated the attainment of improved accuracy of data. For example, by taking readings at the proper angular position of the liquid drive system, the associated error could be reduced to less than one-half of the maximum possible error. It was felt that the basic characteristics of the mercury feed systems were well understood and consequently reliable data obtained.

REPORT DISTRIBUTION LIST FOR CONTRACT NO. NAS3-2522

NASA Lewis Research Center (1)
Spacecraft Technology Procurement Section
21000 Brookpark Road
Cleveland, Ohio 44135
Attention: John H. DeFord

NASA Lewis Research Center (1)
Technology Utilization Office
21000 Brookpark Road
Cleveland, Ohio 44135
Attention: John Weber

NASA Marshall Space Flight Center (1)
Huntsville, Alabama
Attention: M-RP-DIR/Dr. E. Stuhlinger

NASA Headquarters (2)
FOB-10B
600 Independence Avenue, Southwest
Washington, D. C. 20546
Attention: RNT/James Lazar

Commander (1)
Aeronautical Systems Division
Wright-Patterson Air Force Base, Ohio
Attention: AFAPL (APIE)/Lt. Robt. Supp

Jet Propulsion Laboratory (1)
4800 Oak Grove Drive
Pasadena, California
Attention: J. J. Paulson

Electro-Optical Systems, Inc. (1)
125 North Vinedo Avenue
Pasadena, California
Attention: R. C. Speiser

General Electric Company (1)
Flight Propulsion Laboratory
Cincinnati, Ohio 45215
Attention: M. L. Bromberg

Ion Physics Corporation (1)
Burlington, Massachusetts
Attention: Dr. S. V. Nablo

Space Technology Laboratories (1)
8433 Fallbrook Avenue
Canoga Park, California
Attention: Dr. D. Langmuir

AFWL (1)
WLPC/Capt. C. F. Ellis
Kirtland Air Force Base
New Mexico

NASA Lewis Research Center (1)
21000 Brookpark Road
Cleveland, Ohio 44135
Attention: Reports Control Office

North American Aviation, Inc. (1)
12214 Lakewood Avenue
Downey, California
Attention: Technical Information Office
Department 4096-314

NASA Lewis Research Center (2)
21000 Brookpark Road
Cleveland, Ohio 44135
Attention: Library

Aerojet-General (1)
Nucleonics Division
San Ramon, California
Attention: Mr. J. S. Luce

Hughes Research Laboratories (1)
Malibu Canyon Road
Malibur, California
Attention: Dr. G. R. Brewer

NASA Lewis Research Center
Spacecraft Technology Division
21000 Brookpark Road
Cleveland, Ohio 44135
Attention: J. H. Childs (2)
D. L. Lockwood (1)
R. D. Shattuck (1)
J. A. Wolters (7)

United Aircraft Corporation (1)
Research Laboratories
East Hartford 8, Connecticut
Attention: R. J. Meyerand, Jr.

NASA Lewis Research Center
Electromagnetic Propulsion Division
21000 Brookpark Road
Cleveland, Ohio 44135
Attention: W. R. Mickelsen (1)
W. Moeckel (1)

Westinghouse Astronuclear Laboratories (1)
Pittsburgh, Pennsylvania 15234
Attention: Electric Propulsion Lab.
Mr. W. H. Szymanowski

NASA Scientific and Technical Information
Facility (6 + 1 Reproducible Master)
Box 5700
Bethesda, Maryland 20014
Attention: NASA Representative RQT-2448

Aerospace Corporation (1)
P. O. Box 95085
Los Angeles, California 90045
Attention: Library Technical Documents
Group